Gold Mineralization in the Kyaikhto District, Mon State, Southern Myanmar

ミョー, ジョウ, ライン

Gold Mineralization in the Kyaikhto District, Mon State, Southern Myanmar

A thesis submitted in partial fulfilment of the requirements for the degree of

Doctor of Engineering

by

Myo Kyaw Hlaing

Department of Earth Resources Engineering,

Kyushu University, Fukuoka

Japan

January 2019

This work is dedicated to my beloved parents,

U Kyaw Shay and Daw Hla Thein Nu,

For a lifetime of love

With love and respect.....

ABSTRACT

The Kyaikhto gold district is located within the Slate Belt and Mogok Metamorphic Belt of southern Myanmar. The study area is covered by Carboniferous to Lower Permian metasedimentary rocks consisting of slate, phyllite, and schist of the Mergui Group, intruded by later igneous rocks. Four gold occurrences have been identified in the Kyaikhto district: the Kunzeik in the north, Zibyaung, and Thae Phyu Chaung in the center and Meyon in the south. Gold mineralization in the Kyaikhto district is associated with sheeted, stockwork, dissemination, and sulfide-bearing quartz veins and is structurally controlled by the NNE or NNW-trending faults systems. The main purpose of this study is to determine the genesis of ore-forming fluid and to constrain the formation of gold mineralization in the Kyaikhto district.

This dissertation consists of five chapters that describes and interprets the Kyaikhto gold district.

Chapter I describes the significance of this dissertation, general introduction, problem statement, aims and objectives, explains the methodology, gives the motivation and new contributions of the thesis dissertation.

Chapter II reviews the regional geology and tectonic setting of the Kyaikhto gold district. It reviews the geology of mineralized zones, presents whole-rock geochemical data and including classification of the igneous rocks in the Kyaikhto gold district.

Chapter III discusses the mineralization styles in the Kyaikhto gold district and fluid inclusion studies on the Kunzeik prospect and Zibyaung deposit. Ore minerals recognized include sphalerite, galena, chalcopyrite, molybdenite and pyrite with minor native gold and electrum in the Kyaikhto gold district. Based on a combination of petrography and microthermometry, two types of fluid inclusions were identified in the Kunzeik prospect and Zibyaung deposit; Type A: aqueous carbonic inclusions consisting of three phases with two components (liquid-liquid-vapor or L-L-V) and Type B: aqueous liquid and vapor inclusions consisting of two phases (liquid-vapor or L-V). At the Kunzeik prospect, Type A fluid inclusions homogenize at temperatures from 296 to 376 °C and salinities are low (1.6–4.6 wt.% NaCl equivalent). The homogenization temperatures of Type B fluid inclusions in vein quartz range from 246 to 312 °C, with salinities between 1.2 and 10.7 wt.% NaCl equivalent. In the Zibyaung deposit, the homogenization temperatures of Type A inclusions vary from 305 to 378 °C, with salinities from 4.6 to 9.6 wt.% NaCl equivalent. The homogenization temperatures of Type B fluid inclusions mainly range from 242 to 298 °C, with salinities from 0.9 to 11.8 wt.% NaCl equivalent. The relationship between Type A and Type B of fluid inclusions suggests that two types of fluids were present during the precipitation of quartz-sulfide vein in the Kunzeik prospect and Zibyaung deposit. In the Kunzeik prospect and Zibyaung deposit, the characteristics of fluid inclusions are similar to those of orogenic gold mineralization systems.

Chapter IV presents a detailed description of the Thae Phyu Chaung gold deposit, including the variable styles of precious and base-metal occurrences. A detailed paragenetic sequence for mineralization and alteration is provided, together with the interpretation of fluid inclusion studies. The Thae Phyu Chaung deposit is covered by the Carboniferous to Lower Permian metasedimentary rocks such as black slate and slaty phyllite of Mergui Group and later intrusive rocks. Black slate and slaty phyllite that were metamorphosed to greenschist facies and are composed of epidote, muscovite, chlorite and sericite. The most common alteration in the Thae Phyu Chaung deposit is argillic and propylitic alteration adjacent to mineralized veins. Three distinct types of gold occurrences were distinguished. Type-I is native gold which was deposited in microscopic veinlets in chalcopyrite, galena, sphalerite, pyrite-II, and telluride minerals and type-II is coarse-grained (up to 200 μm) high fineness native gold which was deposited both in sulfides or gangue minerals as free grains. Type-III is electrum which is closely associated with chalcopyrite, galena, sphalerite, and altaite. The tellurium-bearing minerals are 20-300 μm and commonly form euhedral to subhedral grains of hessite, tellurobismuthite, hedleyite, altaite, cervelleite, tetradymite, and petzite. Four paragenetic stages of ore formation are recognized in the Thae Phyu Chaung gold deposit; the Stage I (Fe-As), the Stage II (Cu-Pb-Zn) (the base metal stage), the Stage III (Au-Ag-Te-Bi-Sb) (the main ore stage) and the Stage IV (Fe-O). Three stages of quartz generation (Stage I, II and III quartz) recognized in gold-bearing quartz veins correspond to the paragenetic stage I, II and III, respectively. Three types of fluid inclusions are distinguished in Stage I, II and III quartz. Fluid inclusions are classified into aqueous carbonic fluid inclusions (Type I), aqueous fluid inclusions (Type II) and carbonic fluid inclusions (Type III). Type I inclusions in Stage I quartz homogenize completely at temperatures between 345 and 384 °C, have salinities from 0.4 to 2.8 wt.% NaCl equivalent. Type II inclusions in Stage I quartz homogenize at temperatures between 312 and 371°C, have moderate-low salinities (1.9 to 8.3 wt.% NaCl equivalent). The homogenization temperatures of Type II inclusions in Stage II quartz vary from 250 to 335 °C, with salinities from 1.4 to 7.2 wt.% NaCl equivalent. The homogenization temperatures of the Type II inclusions in Stage III quartz mainly range from 213 to 280°C, with salinities from 0.5 to 5.4 wt.% NaCl equivalent. These characteristics of fluid inclusions data indicate that the ore-forming system transformed from a CO_2-rich mesothermal fluid into CO_2-poor meteoric water during fluid evolution.

Finally, Chapter V concludes this thesis by general conclusions and recommendations for further research on the Kyaikhto gold district.

ACKNOWLEDGEMENTS

This PhD dissertation presented in this research would never have been completed without the help of many people from whom I received contributions, support, and encouragement.

Sincere thanks are due to the Japan International Cooperation Agency (JICA) SHIGEN NO KIZUNA program, Japan for the PhD scholarship and financial support.

I wish to express my special thanks to Professor Koichiro Watanabe, Department of Earth Resources Engineering, Kyushu University in Japan for his kind permission to carried out this research work and good advice and reading the thesis and giving facilities in varies ways.

I respectfully special thanks to Professor Akira Imai, Department of Earth Resources Engineering, Kyushu University in Japan for his closely supervision, suggestions, practical guidance and critical reading during the preparation of this paper manuscript, excellent, valuable references and your patience while correcting thesis written in English.

I would like to express special thanks to my supervisor to Associate Professor Kotaro Yonezu, Department of Earth Resources Engineering, Kyushu University in Japan and giving me the opportunity to travel the world and work with excellent geologists. Thanks for your constant encouragement, guidance, advice, critical reading during the preparation of this advice thesis, and valuable references. I am especially grateful for keeping me motivated during over the years when the brain was particularly resistant.

I would like to special thanks to Assistant Professor Thomas Tindell, Department of Earth Resources Engineering, Kyushu University in Japan for his suggestion and constant encouragement, guidance, advice, critical reading during the preparation of this thesis, and valuable references.

I deeply grateful to Professor Day Wa Aung, Department of Geology, University of Yangon in Myanmar for his kind permission to carried out this research work and good advice and giving facilities in varies ways.

I would like to express thanks to Associate Professor May Thwe Aye, Department of Geology, University of Yangon in Myanmar for her carried out this research work and good advice, suggestions, practical guidance and valuable references.

I special thanks to Lecturer Dr. Aung Zaw Myint, Department of Geology, University of Yangon in Myanmar for his valuable advice, guidance and critical reading during the preparation of this thesis manuscript and kind helps.

To all my fellow Economic Geology Laboratory students, too many to list here, but you've all provided inspirational insights into my research, much needed mental escapes, and plenty of unforgettable moments. Thanks to you all for sharing this unique experience of happiness and frustration that comes with the PhD.

Last but not least, my greatest appreciation and sincere thanks to my beloved father U Kyaw Shay and my mother Daw Hla Thein Nu who stayed away during my study in Japan, my sister and brother for their heartfelt support, endless encouragement and patience during my stay away from them.

CONTENTS

		Page
ABSTRACT		i
ACKNOWLEDGEMENTS		iii
CONTENTS		v
LIST OF FIGURES		ix
LIST OF TABLES		xvii
CHAPTER I	GENERAL INTRODUCTION	1
	1.1 Background	1
	1.2 Location and Accessibilities	5
	1.3 Problem Statements	5
	1.4 Research Methodology	5
	1.4.1 Literature reviews	5
	1.5 Thesis aims and objectives	6
	1.6 Expected Benefits of the Research	7
	1.7 Field Work and Sample Collection	7
	1.8 Laboratory Works	8
	1.8.1 Petrography	8
	1.8.2 X-ray Diffractometry	8
	1.8.3 X-ray fluorescence spectroscopy	9
	1.8.4 Fluid inclusion studies	9

1.8.4.1 Fluid Inclusion Microthermometry 9

1.9 Thesis organization 10

References 12

CHAPTER II 2.1 General Statement 16

2.2 Regional geology 16

2.3 Deposit geology 20

2.4 Metasedimentary rocks 22

2.5 Granitic rocks 24

2.5.1 Biotite granite 24

2.5.2 Biotite granodiorite 24

2.6 Modal composition 26

2.7 Geochemistry 26

2.7.1 Major and trace element 26

2.8 Discussion and Conclusions 30

References 31

CHAPTER III Gold mineralization in the Kyaikhto district, Mon State, southern Myanmar 34

3.1 General Statement 34

3.2 Mineralization 34

3.2.1 Kunzeik 34

3.2.2 Zibyaung 34

3.2.3 Thae Phyu Chaung 35

3.2.4 Meyon 35

3.3 Fluid inclusions studies 37

3.3.1 Fluid inclusion petrography 37

3.4 Microthermometry 38

3.4.1 Kunzeik 38

3.4.2 Zibyaung 38

3.5 Discussion and Conclusions 42

References 45

CHAPTER IV Geology, mineral chemistry and fluid inclusion microthermometry of the Thae Phyu Chaung Au-Ag-Te-Bi deposit in Slate-Belt, Kyaikhto district, Mon State, southern Myanmar 47

4.1 General Statement 47

4.2 Deposit geology 47

4.3 Petrography of gold-bearing quartz veins 51

4.4 Hydrothermal alteration 54

4.4.1 Propylitic alteration 55

4.4.2 Argillic alteration 55

4.5 Mineral parageneses 58

4.5.1 Stage I (Fe-As) 58

4.5.2 Stage II (Cu-Pb-Zn) 58

4.5.3 Stage III (Au-Ag-Te-Bi-Sb) 59

4.5.4 Stage IV (Fe-O) 60

4.6 Ore mineralogy and mineral chemistry 62

4.6.1 Sulfide minerals 62

4.6.2 Telluride minerals 63

4.6.3 Gold-silver minerals 64

4.7 Fluid inclusions studies 74

4.7.1 Fluid inclusions petrography 74

4.8 Microthermometry 76

4.8.1 Stage I (Fe-As) 76

4.8.2 Stage II (Cu-Pb-Zn) 77

4.8.3 Stage III (Au-Ag-Te-Bi-Sb) 77

4.9 Discussion 82

4.10 Conclusions 85

References 87

CHAPTER V GENERAL CONCLUSIONS 89

5.1 General statement 89

5.2 Comparison of orogenic gold deposits worldwide 89

5.3 General Conclusions 94

5.4 Recommendations for further research 94

References 96

LIST OF FIGURES

		Page
Figure (1.1)	Location, major structural belts and location of major gold deposits and prospects in Myanmar (Modified after, Mitchell *et al*., 1999 and Swe *et al*., 2017), PFZ, Papun Fault Zone, TPFZ, Three Pagodas Pass Fault	3
Figure (2.1)	Regional tectonic setting of Myanmar and its surrounding area (Modified after Mitchell *et al*., 2018). EHS, Eastern Himalayan Syntaxes; MBT, Main Boundary Thrust; RRF, Red River Fault; PFZ, Papun Fault Zone, TPFZ, Three Pagodas Pass Fault	17
Figure (2.2)	Geological map of the southern part of the Slate Belt and Mogok Metamorphic Belt in which the Kyaikhto gold district is located (Modified after Myanmar Geosciences Society (MGS), 2014). Abbreviations: Q = Quaternary, M_1-P_1 = Lower Miocene to Lower Pliocene, J = Jurassic, Tr =Triassic, P_2-T_2 = Middle Permian to Middle Triassic, C-P_1 = Carboniferous to Lower Permian, O = Ordovician, PƐ-J = Precambrian to partly Jurassic, Mz=Mesozoic	18
Figure (2.3)	Regional Tectonic Setting of the Kyaikhto gold district (Modified after Mitchell *et al*., 2004). Abbreviations: Al = Alluvium, KS = Cretaceous Clastics, SF = Sagaing Fault, STF = Sakan Taung Fault, SBF = Slate Boundary Fault, M = Mogok Metamorphic Belt, MG = Mergui group (or) Slate Belt, $J_{2,3}$ = Middle - Upper Jurassic, $T_{2,3}$ = Middle – Upper Triassic, T_3 J_1 = Upper Triassic-Lower Jurassic, K_1= Lower Cretaceous, P_2-T_3 = Middle Permian to Upper Triassic, C-P_1 = Carboniferous to Lower Permian, O_1-D_2 = Lower Ordovician- Middle Devonian, PƐ-J = Precambrian to partly Jurassic, Ɛ-J_1 = Cambrian – Lower Jurassic, $Ɛ_2$-T_2= Middle Cambrian-Middle Triassic, $Ɛ_3$-P_1=	19

Upper Cambrian- Lower Permian, $Ɛ_{2,3}$ = Middle-Lower Cambrian

Figure (2.4) Geological map of the Kyaikhto gold district. Red lines are faults (Modified after Mackenzie, (1999), Mitchell *et al*., (2012). Abbreviations: Q = Quaternary, P_1-Q = Lower Pliocene to Quaternary, K-Pg = Cretaceous to Paleogene, Mz = Mesozoic, C-P_1=Carboniferous to Lower Permian, PƐ-J = Precambrian to partly Jurassic 21

Figure (2.5) (a) Hand specimen of black slate from the Thae Phyu Chaung deposit, (b) Photomicrograph of black slate from the Thae Phyu Chaung deposit consisting of quartz (qz), chlorite (chl), sericite (ser) that show nearly parallel alignment, (c) Hand specimen of slaty phyllite from the Thae Phyu Chaung deposit, (d) Photomicrograph of slaty phyllite from the Thae Phyu Chaung deposit showing phyllitic texture, (e) Hand specimen of schist from Zibyaung deposit and (f) Photomicrograph of schist from the Zibyaung deposit consisting of quartz (qz) , chlorite (chl), biotite (bt) and sericite (ser) 23

Figure (2.6) (a) Photograph of hand specimen of biotite granite at the Thae Phyu Chaung deposit, (b) Photomicrograph of biotite granite at the Thae Phyu Chaung deposit consisting of quartz (qz), orthoclase (or), and biotite (bt), (c) Hand specimen of biotite granodiorite at the Kunzeik prospect, and (d) Photomicrograph of biotite granodiorite at the Kunzeik prospect consisting of quartz (qz), orthoclase (or), plagioclase(pgl) and biotite (bt). 25

Figure (2.7) (a) Modal classification diagram of the Kyaikhto granitoids after (Streckeisen, 1976) (b) Classification diagram based on total alkali versus SiO_2 (Middlemost, 1985), (c) K_2O versus SiO_2 discrimination diagram (Maniar and Piccoli, 1989), (d) A/NK versus A/CNK (Peccerillo and Taylor, 1976) , (e) [R_1= 4Si - 28

11(Na + K) - 2(Fe + Ti)] Vs [R_2= 6Ca + 2Mg + Al] diagram of the Kyaikhto granitoids (Batchelor and Bowden,1985).

Figure (3.1) (a) Photograph (a, d, g, j) and photomicrographs (b, c, e, f, h, i, k, l) showing ore and ore minerals from the Kyaikhto gold district: (a) quartz-sulfide vein from the Kunzeik, (b) fractured pyrite replaced by chalcopyrite in quartz vein from the Kunzeik, (c) molybdenite dispersed in biotite granite from the Kunzeik, (d) quartz-sulfide vein from the Zibyaung, (e,f) electrum associated with galena, sphalerite and euhedral pyrite in the quartz-sulfide vein from the Zibyaung, (g) quartz-sulfide vein from the Thae Phyu Chaung, (h) native gold associated with chalcopyrite in the quartz-sulfide vein from the Thae Phyu Chaung, (i) sphalerite and chalcopyrite enclosed within galena in the quartz-sulfide vein from the Thae Phyu Chaung, (j) quartz-sulfide vein from the Meyon, (k) pyrite and chalcopyrite enclosed within covellite in the quartz-sulfide vein from the Meyon, and (l) pyrite associated with chalcopyrite in the quartz-sulfide vein from the Meyon. Abbreviations: py = pyrite, gn = galena, cv = covellite, ccp = chalcopyrite, sph = sphalerite, mo = molybdenite, qz = quartz, el = electrum and Au = native gold 36

Figure (3.2) Photomicrographs of fluid inclusions in quartz-sulfide veins at room temperature in plane-polarized light. (a, b) Type A and B fluid inclusions coexisting together within same quartz gain in quartz-sulfide veins from the Kunzeik, (c) Type A and B fluid inclusions in the quartz-sulfide vein from the Zibyaung, and (d) Type B fluid inclusions in quartz-sulfide veins from the Zibyaung 39

Figure (3.3) Histograms of total homogenization temperatures (T_h) of primary inclusions and salinities of fluid inclusions in quartz-sulfide vein from the Kunzeik and Zibyaung. (a) Histograms of T_h of primary inclusions in quartz-sulfide vein from the Kunzeik, (b) salinities of fluid inclusions in quartz-sulfide vein from the 40

Kunzeik, (c) Histograms of T_h of primary inclusions in quartz-sulfide vein from the Zibyaung, and (d) salinities of fluid inclusions in quartz-sulfide vein from the Zibyaung. Note: N = total number of fluid inclusions

Figure (3.4) Total homogenization temperature versus salinity diagram for the fluid inclusions of in the quartz-sulfide vein from the Kunzeik and Zibyaung. 43

Figure (4.1) (A) Geological map of the Thae Phyu Chaung gold deposit (B) Mineralization map of the Thae Phyu Chaung gold deposit, and (C) Cross section along the A to B of the Thae Phyu Chaung gold deposit 49

Figure (4.2) (a) Photographs showing nature of gold-bearing quartz vein hosted by black slate with argillic alteration zone at the Shaft I of the Thae Phyu Chaung gold deposit, (b) gold-bearing quartz vein about 1m thickness at the Shaft I of the Thae Phyu Chaung gold deposit, (c) nature of bended and sheeted gold-bearing quartz vein at the Shaft III of the Thae Phyu Chaung gold deposit, (d) distorted vein by the effects of shear at the Shaft III of the Thae Phyu Chaung gold deposit 50

Figure (4.3) (a) Hand specimen of gold-bearing quatz veins of paragenitic stage I, II and III with chlorite (ch), kaolinite (kao) and sericite (ser) alteration, (b and c) Gold-bearing quartz veins of paragenitic stage I, II and III with sulfide and alteration minerals. Note bands enriched in gold (Au) white arrow and red arrow. ccp: chalcopyrite, py:pyrite,gn:galena, sph:sphalerite 52

Figure (4.4) Photomicrographs of quartz under crossed polars (a) fine to medium-grained quartz formed in late stage with chlorite (chl) in gold-bearing quartz veins, (b) coarse-grained quartz formed in paragenitic stage I quartz (Q_1) with stage II quartz (Q_2) and paragenitic stage I, II and III in gold-bearing quartz veins, (c,d) fine to medium-grained paragenitic stage II quartz (Q_2) quartz 53

associated sulfide minerals and paragenitic stage III quartz (Q_3) in the gold-bearing quartz vein, (e) different paragenitic stages I-III quartz (Q_1-Q_3) with chlorite (chl), sericite alterration in gold-bearing quartz veins and (f) paragenitic stages II-III quartz (Q_2-Q_3) which was filled by late sulfide that was formed by alteration of fine-grain sericite (ser), chlorite (chl) in the gold-bearing quartz vein.

Figure (4.5) (a,d and g) hand specimen in paragenetic stage I-III of gold-bearing quartz veins. Photomicrograph showing (b and c) native gold (Au) associated with paragenetic stage I (Q_1),II (Q_2) and III (Q_3) quartz, galena (gn), chalcopyrite (ccp) ,chlorite (chl) and sericite(ser) of gold-bearing quartz vein, (e and f) chalcopyrite (ccp) associated with paragenetic stage I (Q_1),II (Q_2) and III (Q_3) quartz, pyrite (py), chlorite (chl) and sericite(ser) in gold-bearing quartz vein, (h and i) chalcopyrite (ccp) associated with paragenetic stage I (Q_1),II (Q_2) and III (Q_3) quartz, pyrite (py) chlorite (chl) and sericite(ser) of gold-bearing quartz vein. 56

Figure (4.6) Paragenetic sequence of mineral deposition at the Thae Phyu Chaung gold deposit 61

Figure (4.7) (a) Photomicrographs showing native gold (Au) associated with galena(gn), tellurobismuthite (tb), hessite (hs), pezite (pz) and chalcopyrite (ccp) in paragenetic stage II and III of the gold bearing quartz vein, (b) native gold (au) associated with altaite (alt) (PbTe), tellurobismuthite (tb) (Bi_2Te_3), galena (gn), hessite (hs), pezite (pz) in paragenetic stage II and III of the gold bearing quartz vein, (c) chalcopyrite associated with altaite (alt) (PbTe), tellurobismuthite (tb) (Bi_2Te_3) and galena (gn) in paragenetic stage II and III of the gold bearing quartz vein 66

Figure (4.8) (a) Photomicrographs of chalcopyrite (ccp) associated with early pyrite (py I) in paragenetic stage I of the gold bearing quartz vein, (b) native gold (Au) inclusions in galena (gn) associated with 67

chalcopyrite (ccp) and sphalerite (sph) in paragenetic stage II and III of the gold bearing quartz vein, (c) sphalerite (sph) associated with late pyrite (py II), early chalcopyrite (ccp) and galena (gn) in paragenetic stage II and III of the gold bearing quartz vein, (d) pyrite (py II) fracture fillings within chalcopyrite (ccp), (e) chalcopyrite (ccp) inclusions in sphalerite (sph) filling cracks, (f) pyrrhotite (po) associated with chalcopyrite, (g) the famatinite (fn) associated with gudmundite (gud) and chalcopyrite in paragenetic stage II and III of the gold bearing quartz vein, (h) chalcopyrite is also in contact to sphalerite (sph) and pyrite (pyII) and it is surrounded by hematite (hem) in paragenetic stage III and IV of the gold bearing quartz vein

Figure (4.9) (a) Photomicrographs showing native gold (Au) in late pyrite (py II) in paragenetic stage II and III of the gold bearing quartz vein, (b) native gold (Au) associated with (Au+Sb) unnamed mineral in paragenetic stage II and III of the gold bearing quartz vein, (c) chalcopyrite (ccp) in native gold (Au) in paragenetic stage III and IV of the gold bearing quartz vein, (d) electrum (el) associated with sphalerite (sph) and chalcopyrite (ccp) in paragenetic stage II and III of the gold bearing quartz vein, (e) native gold (Au) associated with galena (gn), sphalerite (sph) and chalcopyrite (ccp) in paragenetic stage II and III of the gold bearing quartz vein, (f) electrum (el) associated with native silver (Ag), native bismuth (Bi) and chalcopyrite (ccp), famatinite (fn) and gudmundite (gud) in paragenetic stage II and III of the gold bearing quartz vein, and (g) native gold (Au) associated with chalcopyrite (ccp), (h) free native gold (Au) in paragenetic stage II and III of the gold bearing quartz vein 68

Figure (4.10) (a) Photomicrographs showing native bismuth (Bi) associated with galena (gn), arsenopyrite (Asp) and Bi+Te minerals in paragenetic stage II and III of the gold bearing quartz vein (b) arsenopyrite associated with galena (gn), native bismuth (Bi) and 69

Bi+Te minerals in paragenetic stage II and III of the gold bearing quartz vein (c) chalcopyrite (ccp) associated with galena (gn) and Bi+Te minerals in paragenetic stage II and III of the gold bearing quartz vein

Figure (4.11) (a) Hand specimen of native free gold (Au) in paragenetic stage II and III of the gold- bearing quartz vein, (b) Photomicrographs showing free grains of native gold (Au) in paragenetic stage II and III of the gold bearing quartz vein (c) free grains of native gold (Au) in paragenetic stage II and III of gold-bearing quartz vein 70

Figure (4.12) (a)Phase relations in the system Au–Ag–Te at 120 and 300 °C, whereas solid lines indicate compositions of coexisting phases, modified after Afifi (1988). The Type-I gold-rich assemblage (shaded area) preceded deposition of the more silver-rich assemblages (b) The Type-II silver-rich assemblage (c) The Type-III bismuth-rich assemblage 73

Figure (4.13) Photomicrographs of typical fluid inclusion assemblage from different mineralization stages at the Thae Phyu Chaung gold deposit. (a) Primary, pseudosecondary and secondary fluid inclusions in same sample; (b) Aqueous-carbonic fluid inclusions (Type I) (liquid+liquid+vapor) fluid inclusions in Stage I quartz , (c) Aqueous fluid inclusions (Type IIa) (vapor-rich) fluid inclusions in Stage II quartz , (d) Aqueous fluid inclusions (Type IIb) (liquid-rich) fluid inclusions in Stage III quartz, and (e) Carbonic fluid (Type III) (vapor or liqiud) fluid inclusions in Stage I quartz of gold-bearing quartz vein 78

Figure (4.14) Photomicrographs of fluid inclusion assemblage from different mineralization stages at the Thae Phyu Chaung gold deposit. (a , b) Primary Type I and Type IIa, IIb, and Type III fluid inclusions in Stage I quartz of gold-bearing quartz veins from different 79

samples; (c ,d) Primary Type IIa and IIb fluid inclusions in Stage II quartz of gold-bearing quartz veins from different samples; (e , f) Primary Type IIb fluid inclusions in Stage III quartz of gold-bearing quartz veins from different samples

Figure (4.15) Histograms of total homogenization temperatures (T_h) of primary inclusions and salinities of fluid inclusions in different stages at the Thae Phyu Chaung deposit. Note: N= total number of fluid inclusions 80

Figure (4.16) Plots of total homogenization temperatures (T_h) vs salinities of fluid inclusions in different stages quartz in the Thae Phyu Chaung deposit. Three pink arrows marked as (1), (2) and (3) represent the fluid evolution from Stage I quartz to Stage III quartz. The arrows (1) and (2) mean that the fluids have wider salinities range from Stage I quartz to Stage II quartz due to the fluid immiscibility. The arrow (3) represents that the temperature and salinities both decrease from Stage II quartz to Stage III quartz 84

Figure (5.1) World distribution of greenstone-hosted quartz-carbonate vein deposits or orogenic gold deposits containing at least 30 tons of Au. (from Dubé et al., 2007) 91

Figure (5.2) Schematic diagram showing the setting and nature of orogenic lode–gold deposits. (A). Plate tectonic environments of formation of orogenic lode–gold deposits and other largely syn-volcanic or syn-intrusive gold-rich deposit styles. (B). Depth profile of orogenic lode–gold deposit (from Groves et al.,1998) 93

LIST OF TABLES

			Page
Table	(1.1)	Gold districts in Myanmar (Modified after Mitchell *et al*., 1999 and Swe *et al*., 2017)	4
Table	(2.1)	The modal composition of the Kyaikhto granitoids	29
Table	(2.2)	Representative major elements analyses of intrusive rocks of Kyaikhto gold district	29
Table	(2.3)	Representative trace element analyses of intrusive rocks of Kyaikhto gold district	30
Table	(3.1)	Summary of fluid inclusion types and microthermometric data for fluid inclusions of the Kunzeik and Zibyaung.	41
Table	(4.1)	Summary of hydrothermal alteration from orientated samples analyzed by XRD and thin section	57
Table	(4.2)	Representative chemical compositions of sulfide minerals from the Thae Phyu Chaung gold deposit	71
Table	(4.3)	Representative chemical compositions of Au-Ag-Te-Bi bearing minerals from the Thae Phyu Chaung gold deposit	72
Table	(4.4)	Summary of fluid inclusion types and microthermometric data for fluid inclusions of the different stage in the Thae Phyu Chaung deposit	81
Table	(5.1)	Comparative table with other orogenic gold deposits Myanmar and worldwide	92

CHAPTER I

GENERAL INTRODUCTION

1.1 Background

Mesothermal gold-quartz vein, porphyry type Cu-Au and related epithermal Au deposits in Myanmar are distributed along the Central Magmatic Arc, sediment-hosted epithermal Au deposits are distributed along the Sagaing Fault Zone, mesothermal to epithermal Au deposits are distributed in Tagaung Myitkyina Belt, Au-Cu skarn and mesothermal veins deposits in marble, gneiss and granite are distributed within the Mogok Metamorphic Belt in the north and mesothermal gold-quartz veins deposits are distributed within the Slate Belt in the south (Mitchell *et al.,* 1999) (Figure 1.1). Gold occurrences in Myanmar are known in the form of auriferous quartz veins throughout the Phayaung Taung, Modi Taung, Nankwe, Shwekyin, and Kyaiktho areas in the Slate Belt southwestern part of the Eastern Highland (Figure 1.1 and Table 1.1). The Kyaikhto gold district is situated at the southern end of the Slate Belt and Mogok Metamorphic Belt where gold deposits are hosted by the granitic rocks and Carboniferous to Lower Permian metasedimentary rocks of the Mergui Group metamorphosed to greenschist facies (Mitchell *et al.,* 1999) (Figure 1.1 and Table 1.1). The Slate Belt was intruded by numerous granitic rocks that host tin and tungsten deposits of the Western Granite Province, part of the Southeast Asian Granitoid Tin Belt (Cobbing *et al*.,1992). This belt of gold mineralization was first reported by Mitchell *et al.* 1999 as gold deposits of slate-hosted mesothermal quartz-gold veins (orogenic gold deposit) (Figure. 1.1). Orogenic gold deposits are associated with regionally metamorphosed terranes (Groves *et al.,* 1998, 2003; Goldfarb *et al.,* 2001, 2005,2015) and the mineralization displays strong structural controls at a variety of scales. Metamorphic grade of host rocks range from

sub greenschist to granulite facies, although mainly greenschist facies (Goldfarb *et al.*, 2004). This deposit type has also been referred to as shear-zone-related, quartz-carbonate, mesothermal, greenstone- hosted, orogenic and metamorphic deposit (Dubé and Gosselin, 2007 and *references therein*). The mineralizing events typically involved hydrothermal fluids depositing gold, quartz, and sulfides in structurally controlled fractures formed after the metamorphic belt had undergone some uplift into brittle regions of the crust (Craw *et al.*, 1999; Bierlein *et al.*, 2004, 2006; Aliyari *et al.*, 2007). The orogenic gold deposits usually show the following characteristics: (1) Orebodies are structurally controlled by the faults or brittle to ductile zones, and host rocks are deformed and variably metamorphosed. (2) Hydrothermal alteration assemblages mainly consist of quartz, sericite, sulfide, carbonate, and chlorite. (3) Ore-forming fluids have low salinities (up to 12 wt.% NaCl equivalent) and are mixtures of H_2O and CO_2, with fewer amounts of CH_4 and N_2, and near-neutral pH. (4) The mineralized lodes formed over a broad upper to middle-crustal P-T conditions, between about 100–500 MPa and 200–650^{o}C (Groves *et al.*, 1993,1998, Goldfarb *et al.*, 2001, Chen *et al.*, 2006, Ma *et al.*, 2017). Mackenzie *et al*., (1999) suggested that gold and sulfide-bearing veins in the Kyaikhto gold district were "metamorphic-mesothermal vein deposits". Four mineralized zones have been identified from south to north as the Kunzeik prospect, the Zibyaung deposit, the Thae Phyu Chaung deposit and the Meyon deposit within the Kyaikhto gold district (Figure 1.1). However, there is no detailed research work about gold mineralization in the Kyaikhto district and ore genesis is poorly understood.

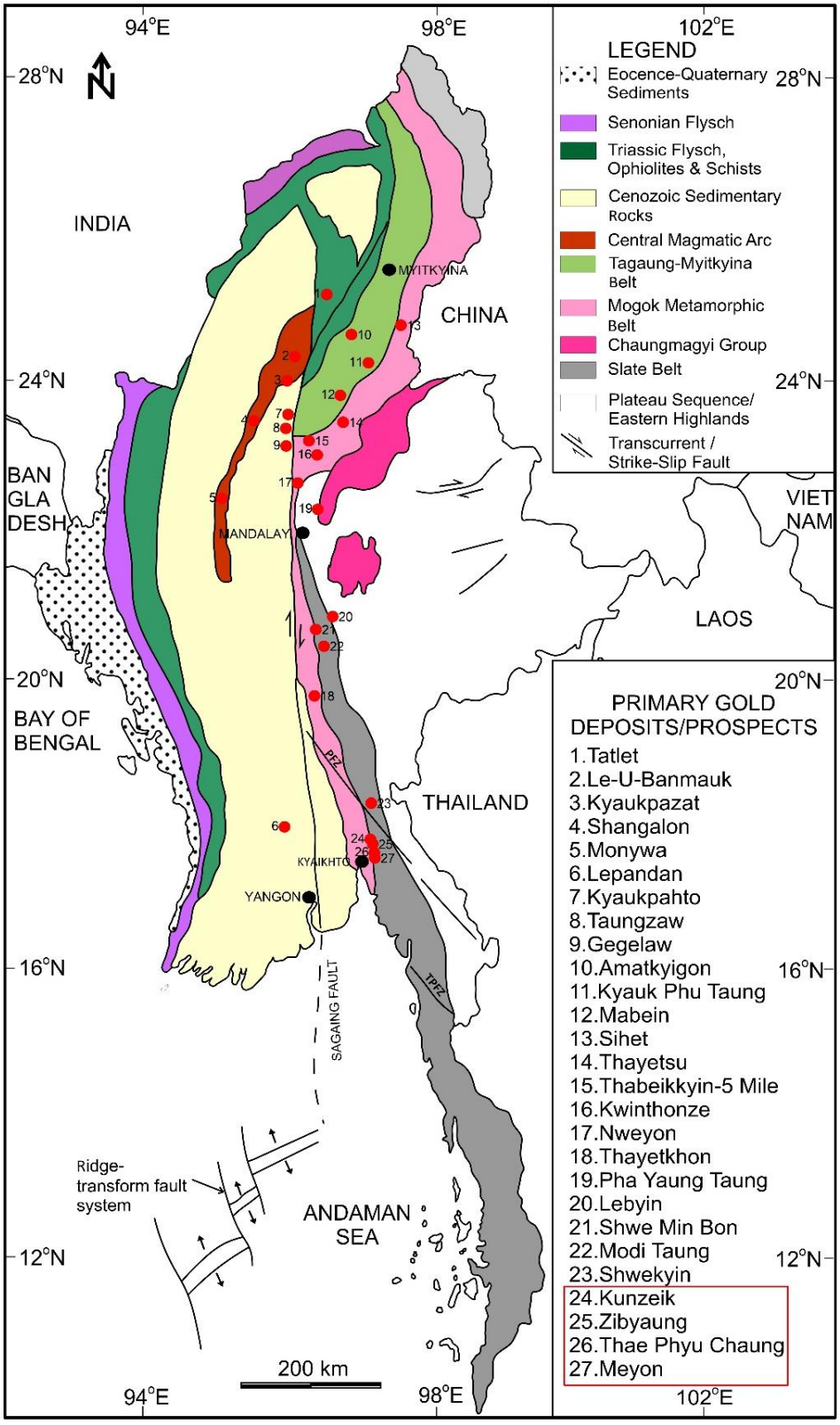

Figure. 1.1 Location, major structural belts and location of major gold deposits and prospects in Myanmar (Modified after Mitchell *et al.*, 1999 and Swe *et al.*, 2017), PFZ, Papun Fault Zone, TPFZ, Three Pagodas Pass Fault.

Table.1.1 Gold districts in Myanmar (Modified after Mitchell *et al.*, 1999 and Swe *et al.*, 2017)

District	Setting	Type	Age
Le-U-Banmauk- Monywa	Central Magmatic arc	Mesothermal, Porphyry style Cu, Au, and Epithermal Au	Upper Cretaceous?
Lepandan -Gegalaw	Sagaing Fault	Sediment-hosted Au (Sb, As)	Upper Eocene to Miocene?
Amatkyigon- Mabein	Tagaung Myitkyina Belt	Mesothermal to Epithermal gold Au (Cu)	Miocene?
Sihet- Thayetkhon	Mogok Metamorphic Belt	Mesothermal Au Zn, Pb, and Au	Post-Cretaceous?
Phayaung Taung -Kyaikhto	Slate belt	Mesothermal Au-Ag-Te-Bi (Cu)	Jurassic to Paleocene?

1.2 Location and accessibilities

The Kyaikhto gold district is located in southern Myanmar, approximately 80 km north east of Yangon. The district is located about 10 km north of Kyaikhto city in the northeastern part of Mon State at latitude between 17 ° 40' N and 17° 20' N, and longitude between 96°52' E and 97° 06' (Fig.1.1). It can be accessed by car or by train from Yangon to Kyaikhto city, Mon state; it can also be reached by motorcycle from Kyaikhto city. Figure 1.1 shows the location map of the Kyaikhto gold district.

1.3 Problem statements

There have not been researched in detail for gold mineralization in the Kyaikhto gold district. Therefore, a detailed study on gold mineralization is a major need to be researched in the Kyaikhto gold district. The main theme is to clarify genesis though mineralogical and geochemical studies, to investigate the nature of ore mineralization style and to identify the type of ore deposit.

1.4 Research methodology

A detailed geochemical analysis has been conducted to evaluate the alteration, mineralization, and origin of ore-forming fluid. The methodology includes three sections: literature reviews, field investigation and laboratory analysis. The laboratory works of mineralogical and geochemical analyses have been carried out.

1.4.1 Literature reviews

The present research was started by a review of literature. The literatures reviewed include on the exploration history of the Kyaikhto gold district; the regional geology and tectonic setting; the geology of the deposit, including the nature of geological structures as the

faults distribution pattern and their deposit character; the nature of mineralization style, references include the published, unpublished papers, reports and geological maps of the deposits; including regional scale, the cross-sectional profiles of the deposit scale of controlling in the several structural directions. Additionally, literatures were surveyed on the theoretical background of general characteristics, distinctive features of mineralization in Slate Belt (orogenic type), mode of their formation and alteration/ gold mineralization associated with characteristics of the host rocks.

1.5 Thesis aims and objectives

The principal aim of this PhD dissertation is the genesis of ore-forming fluid and to constrain the formation of gold mineralization within the Kyaikhto district. This will be achieved by:

1. To make detail geological map,
2. To investigate the petrological characteristics of host rock and related ore minerals,
3. To explore the geochemical characteristics of the gold mineralization,
4. To determine the gold mineralization style and evolution of hydrothermal fluids and to provide the origin of ore mineralization,
5. To established models for orogenic (mesothermal) gold mineralization systems and comparing the results with orogenic gold mineralization systems occurrences worldwide.

1.6 Expected Benefits of the Research

This thesis has a number of benefits not only for the production of more economical mineral resource but also for state and national exploratory development of gold mineralization related as follows:

1. The mineralization style in the Kyaikhto gold district and the geochemical patterns of related with the ore mineralization which plays a vital role in exploitation.
2. The petrographical characteristics of host rock and associated ores.
3. The structural control of ore formation and exploration style of mineralization.

1. 7 Field Work and Sample Collection

Most of the data presented in this thesis were collected by the author over four field seasons (October 2015; April-May 2016; May-June 2017; May-June 2018). During the field work, geological data were collected to make detail for the geological map, to explore the genetic relationship of the host rocks and associated gold mineralization, to collect the representative samples from host rock and characteristics of gold mineralization. Over 200 samples were selected for mineralogical analyses. 40 samples were tested by X-ray diffraction analysis. 35 rock samples for geochemical analyses were prepared by crushing to small pieces with a hammer and then by powdering to 200-mesh using an agate ball mill. The concentration of major and trace elements was determined by X-ray fluorescence spectroscopy. 65 thin sections for petrographic study and 95 polished sections were analyzed for ore mineralogy and 35 samples in doubly polished thin sections for fluid inclusion studies.

1.8 Laboratory Works

The laboratory work includes mineralogical analysis as a petrographic study, ore microscopy and XRD (X-ray diffraction spectroscopy), XRF (X-ray fluorescence spectroscopy). Polished sections were analyzed for ore mineralogy using a scanning electron microscope (SEM) with energy-dispersive X-ray spectroscopy (EDS) of HITACHI-SU3500 at the Center of Advanced Instrumental Analysis, Kyushu University, to provide elemental identification and quantitative compositional information. All analyses were undertaken at the Department of Earth Resources Engineering, Kyushu University in Japan.

1.8.1 Petrography

Petrography analyses were undertaken on thin sections and polished sections using transmitted and reflected light optical microscope. Uncertain minerals are also detected by X-ray diffraction analysis. 95 polished sections for ore and gangue minerals from the Kunzeik prospect, the Zibyaung deposit, the Thae Phyu Chaung deposit, and Meyon deposit were investigated with a NIKON ECLIPSE LV100N POL petrographic microscope. This analysis was necessary in order to identify both altered and ore minerals as well as their textural relationships. Moreover, diagnostic hydrothermal minerals are recognized which typically occur in the alteration zone.

1.8.2 X-ray Diffractometry

X-Ray diffraction spectroscopy (XRD) is one of the non-destructive analysis methods. The first stage of the preparation, the samples were crushed manually in an agate mortar. Then the powder was hardened on an aluminum plate which had a square hole to put it in. The samples were then scanned using the XRD spectrometer. The intensity of the diffracted X-ray

is measured as a function of the diffraction angle (2θ). These diffraction patterns are used to identify the mineral species. An approximate sample size of the size of 1cm^3 (powder, 10μm) is required. XRD was conducted using an X-ray diffractometer of RIGAKU RINT-2000 under the condition of 40kV and 40 mA.

1.8.3 X-ray fluorescence spectroscopy

35 rock samples for geochemical analyses were prepared by crushing to small pieces with a hammer and then by powdering to 200-mesh using an agate ball mill. Concentrations of major and trace elements were determined by X-ray fluorescence spectroscopy (XRF) of RIGAKU RIX-3100 under the condition of 30 kV and 70mA. Loss-on-ignition (LOI) at 1000 °C was measured for each sample, and elemental concentrations were calculated from the results of both analyses. The standard JA-3 was repeatedly analyzed to monitor precision, yielding an error of less than ± 5%.

1.8.4 Fluid inclusion studies

1.8.4.1 Fluid inclusion microthermometry

Thirty-five doubly polished thin sections for fluid inclusion study were selected from the Kunzeik prospect, the Zibyaung deposit and the Thae Phyu Chaung gold deposit. Microthermometric measurements were carried out using a Linkam-THMS600 heating-freezing stage equipped on a NIKON ECLIPSE LV100N POL petrographic microscope. The heating/freezing rate was generally 0.2–5.0^{o}C/min but was <0.2^{o}C/min near the phase transformation. The uncertainties for the measurements are ±0.5, ±0.2 and ±2.0^{o}C for runs in the range of -120 to -70^{o}C, -70 to 100^{o}C, and 100 to 600^{o}C, respectively. Ice melting temperatures were observed at a heating rate of less than 0.1^{o}C/min and homogenization

temperatures at the rate of ≤1°C/min. The fluid inclusions were classified by the criteria of (Roedder, 1984). Total salinities of NaCl-H_2O inclusions were calculated by the equation of wt% NaCl = 1.78 T - 0.0442 T^2 + 0.000557 T^3 where T is depression temperature in °C (Bodnar, 1993). The salinities of CO_2-bearing fluid inclusions were calculated using the melting temperatures of clathrate and had standard errors of ±1.0° and ±0.2°C, (in presence of CO_2 vapor and CO_2 liquid) is a function of salinity according to the following mathematical expression (Collins, 1979): wt% NaCl = 15.52022 - 1.02342T - 0.05286T^2 where T is the clathrate melting temperature expressed in °C.

1.9 Thesis organization

The dissertation consists of five chapters:

Chapter II discusses the regional geology and tectonic setting and reviews other significant occurrences of the Kyaikhto gold district. It briefly reviews the geology of the Kyaikhto gold district mineralized zones and discusses whole-rock geochemical data of granitic rocks, including classification of the igneous rocks as alkalic or calc-alkalic, tectonic and magmatic evolution. In addition, the Kyaikhto gold district constraints integrated into district framework conclude the chapter.

Chapter III discusses the varying styles of precious and base-metal occurrences and fluid inclusion studies on Kunzeik prospect and Zibyaung deposit. In addition, this chapter is to determine the genesis of the gold mineralization in the Kyaikhto district based on the mineralogical and fluid inclusion studies.

Chapter IV presents a detailed description of the Thae Phyu Chaung gold deposit, including the varying styles of precious and base-metal occurrences. A detailed paragenetic

sequence for mineralization and alteration is provided, together with the interpretation of alteration zonation patterns and to determine the genesis of the gold mineralization in the Thae Phyu Chaung gold deposit based on mineralogical, alteration and fluid inclusion studies.

Chapter V concludes this thesis by comparisons with worldwide, general conclusions, and recommendations for further research of the Kyaikhto gold district.

References

Aliyari, F., Rastad, E. and Zengqian, H. (2007) Orogenic gold mineralization in the Qolqoleh Deposit, Northwestern Iran. *Resource Geology.*, 57, 269-282.

Bierlein, F. P., Groves, D. I., Goldfarb, R. J. and Dube, B. (2006) Lithospheric controls on the formation of provinces hosting giant orogenic gold deposits. *Mineralium Deposita*, 40, 874 - 886.

Bodnar, R. J. (1993) Revised equation and table for determining the freezing point depression of H_2O-NaCl solutions. *Geochimica et Cosmochimica Acta*, 57, 683-684.

Cobbing, E. J., Pitfield, P. E. J., Darbyshire, D. P. F. and Mallick, D. I. J. (1992) The Granites of the South-East Asian Tin Belt. *Overseas Memoir 10, British Geological Survey*, 369 p.

Chen, Y.J. (2006) Orogenic-type deposits and their metallogenic model and exploration potential, *Geology in China*, 33, 1181–1196.

Craw, D., Windle S. J. and Angus, P. V. (1999) Gold mineralization without quartz veins in a ductile-brittle shear zone, Macraes Mine, Otago Schist, New Zealand. *Mineralium. Deposita.*, 34, 382-394.

Collins, P. L. F. (1979) Gas hydrates in CO_2–bearing fluid inclusions and use freezing data for estimation of salinity. *Economic Geology*, 74, 1435-1444.

Dubé, B. and Gosselin, P. (2007) Greenstone-hosted quartz-carbonate vein deposits: in Good fellow, W.D., ed., Mineral Deposits of Canada: A Synthesis of Major Deposit-Types, District Metallogeny, the Evolution of Geological Provinces, and Exploration Methods: *Geological Association of Canada, Mineral Deposits Division, Spec. Publ.*, 5, 49-73.

Goldfarb, R. J. Groves, D. I. and Gardoll, S. (2001) Orogenic gold and geologic time: a global synthesis, *Ore Geology Reviews.,* 18, 1-2, 1–75.

Goldfarb, R. J., Ayuso, R., Miller, M. L., Ebert, S. W., Marsh, E. E., Petsel, S. A., Miller, L. D., Bradley, D., Johnson, C. and McClelland, W. (2004) The late Cretaceous Donlin Creek gold deposit, Southwestern Alaska: Controls on epizonal ore-forming. *Economic Geology.,* 99, 643 – 671.

Goldfarb, R. J., Baker, T., Dube, B., Groves, D. I., Hart, C. J. R. and Gosselin, P. (2005) Distribution, character, and genesis of gold deposits in metamorphic terranes. In Hedenquist, J. W., Thompson, J. F. H., Goldfarb, R. J. and Richards, J. P. (eds.) *Economic Geology 100th Anniversary Volume. Society of Economic Geologists Inc., Littleton,* 407-450.

Groves, D. I. (1993) The crustal continuum model for late-Archaean lode-gold deposits of the Yilgarn Block, Western Australia, *Mineralium Deposita.,* 28, 366–374.

Groves, D. I. Goldfarb, R. J. Gebre-Mariam, M. Hagemann, S. G. and Robert, F. (1998) Orogenic gold deposits: a proposed classification in the context of their crustal distribution and relationship to other gold deposit types, *Ore Geology Reviews.,* 13, 1–5, 7–27.

Groves, D. I., Goldfarb, R. J., Robert, F., and Hart, C. J. R. (2003) Gold deposits in metamorphic belts: Overview of current understanding, outstanding problems, future research, and exploration significance. *Economic Geology*, 98, 1-29.

Hlaing, M.K., Yonezu, K., Aye, M.T., Myint, A.Z. and Watanabe, K. (2016) Geology and Mineralogical characteristics of Zibyaung Gold Deposit at Kyaikhto area, Southern Myanmar. *Proceedings of International Symposium on Earth Science and Technology,* 403-407.

Ma, Y. Xiong, S.F. Li, H.L. and Jiang, S.Y. (2017) Origin and Evolution of the Ore-Forming Fluids in the Liyuan Gold Deposit, Central North China Craton: Constraints from Fluid Inclusions and H-O-C Isotopic Compositions, *Geofluids.*, 2017, 1-21

Mackenzie, M.J. (1999) Report on the Exploration Progress in block 3/13 for the Period January 1998 to December 1998. Palmer Resources Ltd. Myanmar (Burma) Project, (Unpublished), 1-67p.

Mitchell, A. H. G., Htay, N., Ausa, C., Deiparine, L., Khine, A and Po, S. (1999) Geological settings of gold districts in Myanmar. In Weber, G. (eds.) PACRIM 99, Proceedings International Congress on Earth Science, Exploration and Mining around the Pacific Rim. *Australasian Institute of Mining and Metallurgy, Bali, Indonesia*., 303–309.

Mitchell, A.H.G., Ausa, C., Deiparine, L., Hlaing, T., Htay, N. and Khine, A. (2004) The Modi Taung-Nankwe gold district, Slate Belt, Central Myanmar: mesothermal veins in a Mesozoic orogen. *Journal Asian Earth Science.,* 23, 321–341.

Mitchell, A.H.G. (eds.). (2018) Geological Belts, Plate Boundaries and Mineral Deposits in Myanmar. Myanmar Precious Resources Group, Myanmar and Oxford, United Kingdom, 1, 3-15.

Oo, Z.N. and Zaw, K. (2009) Geology and mineralization characteristics of Meyon gold deposit, Mon State, Southern Myanmar. *Proceedings of 11th Regional Congress on Geology, Mineral and Energy Resources of Southeast Asia (GEOSEA)*, 8–10 June, Kuala Lumpur, Malaysia., 32.

Oo, Z.N., Zaw, K. and Mernagh, T. (2010) Geological setting and nature of mineralization at Meyon gold deposit, Mon State, Myanmar. *13th Quadrennial International*

Association on Genesis of Ore Deposits (IAGOD) Symposium., Adelaide, 6-9 April 2010 CD-ROM.

Oo, Z.N. and Zaw, K. (2015) Geology and mineralization characteristics of Meyon gold deposit, Mon State, Southern Myanmar. *Poster no. 105, presented at the Society of Economic Geologists Conference.,* 27–30, Hobart, 2015 CD-ROM.

Roedder, E. (1984) Fluid Inclusions. *Reviews in Mineralogy.,* 12, 644p.

Swe, Y.M., Aye, C.C. and Zaw, K. (2017) Gold deposits of Myanmar. In: Barber, A.J., Khin Zaw and Crow, M.J. (Eds)Myanmar: Geology, Resources, and Tectonics. *Geological Society, London, Memoirs.,* 48, 557–572.

CHAPTER II

2.1 General statement

This chapter reviews the key geological features, from continental to regional scales, that allows the tectonic setting of the Kyaikhto gold district to be interpreted. This includes a review of the Slate Belt and a description of the Kyaikhto gold district. It discusses whole-rock geochemical data and including classification of the igneous rocks.

2.2 Regional geology

The Kyaikhto gold district is located between the southeastern part of the Indo-Burma Ranges (Burma Plate) and the southwestern part of the Indo-China Block (the southern part the Eastern Highlands) (Figure 2.1). Geological structures at the southwestern margin of the Eastern Highlands are complicated due to the presence of older and some young active strike-slip faults (Oo *et al.,* 2009, 2010, 2015). The Kyaikhto district is located close to the Sagaing Fault, a major young active strike-slip fault trending N-S about 32-40 km to the west (Figure 2.2). The Kyaikhto gold district is underlain by metasedimentary rocks and later granitic rocks. The metasedimentary rocks belong to the Mergui Group of Carboniferous to Lower Permian age (Mitchell *et al.,* 2004), which strikes N-S, along with the southwestern part of the Eastern Highlands.

The Kyaikhto gold district seems to have been subjected to dynamic deformation and conjugate local faulting in addition to a large amount of heat from the batholiths to the east (Mackenzie, 1999). The age of gold mineralization is suggested to be Late Cretaceous to Paleogene and may have been associated with deformation and metamorphism along the Papun Fault Zone (Figures 2.2 and 2.3) (Zaw *et al.,* 2014a, Barber *et al.,* 2017).

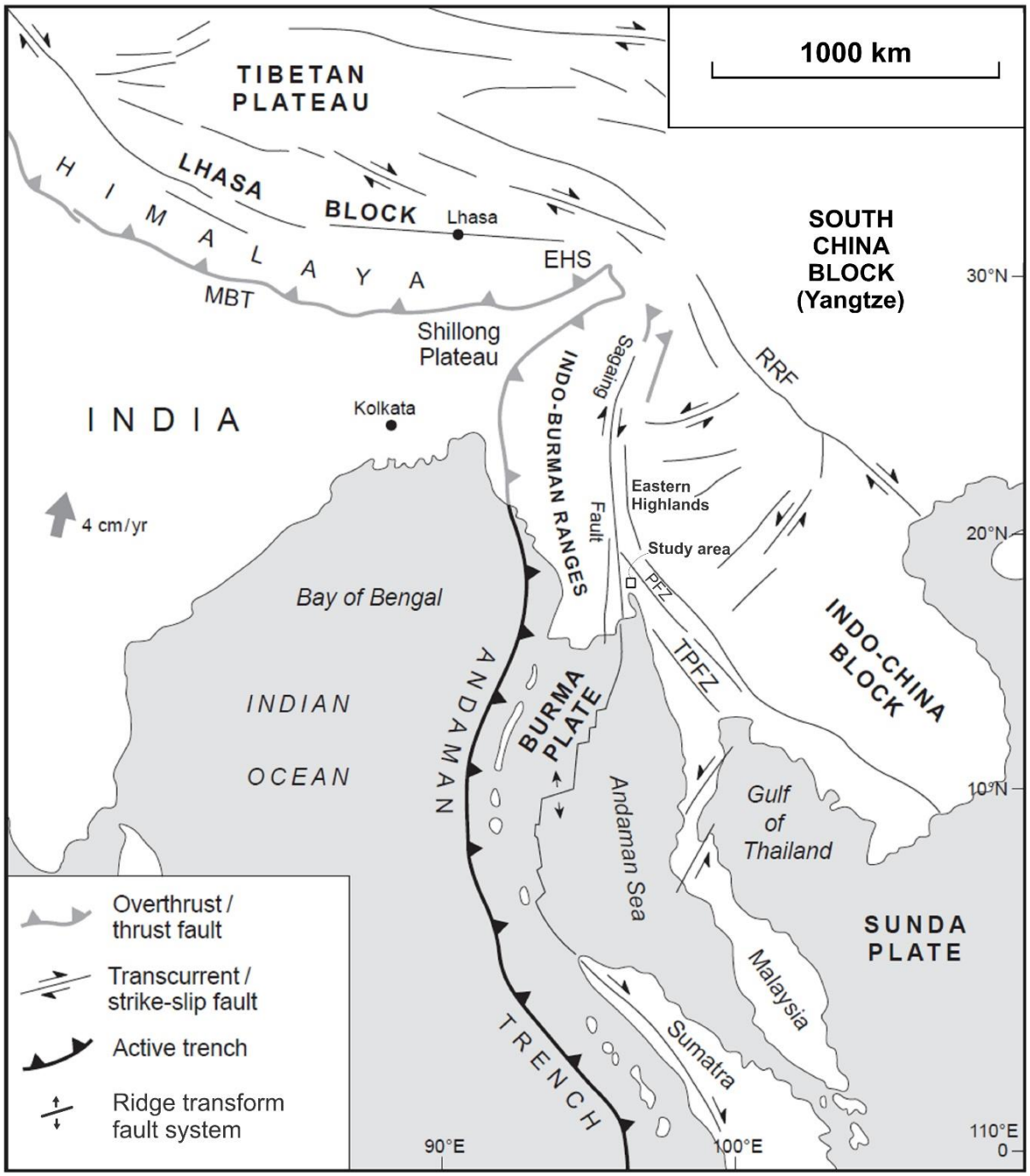

Figure 2.1. Regional tectonic setting of Myanmar and its surrounding area (Modified after Mitchell *et al.*, 2018). EHS, Eastern Himalayan Syntaxes; MBT, Main Boundary Thrust; RRF, Red River Fault; PFZ, Papun Fault Zone, TPFZ, Three Pagodas Pass Fault.

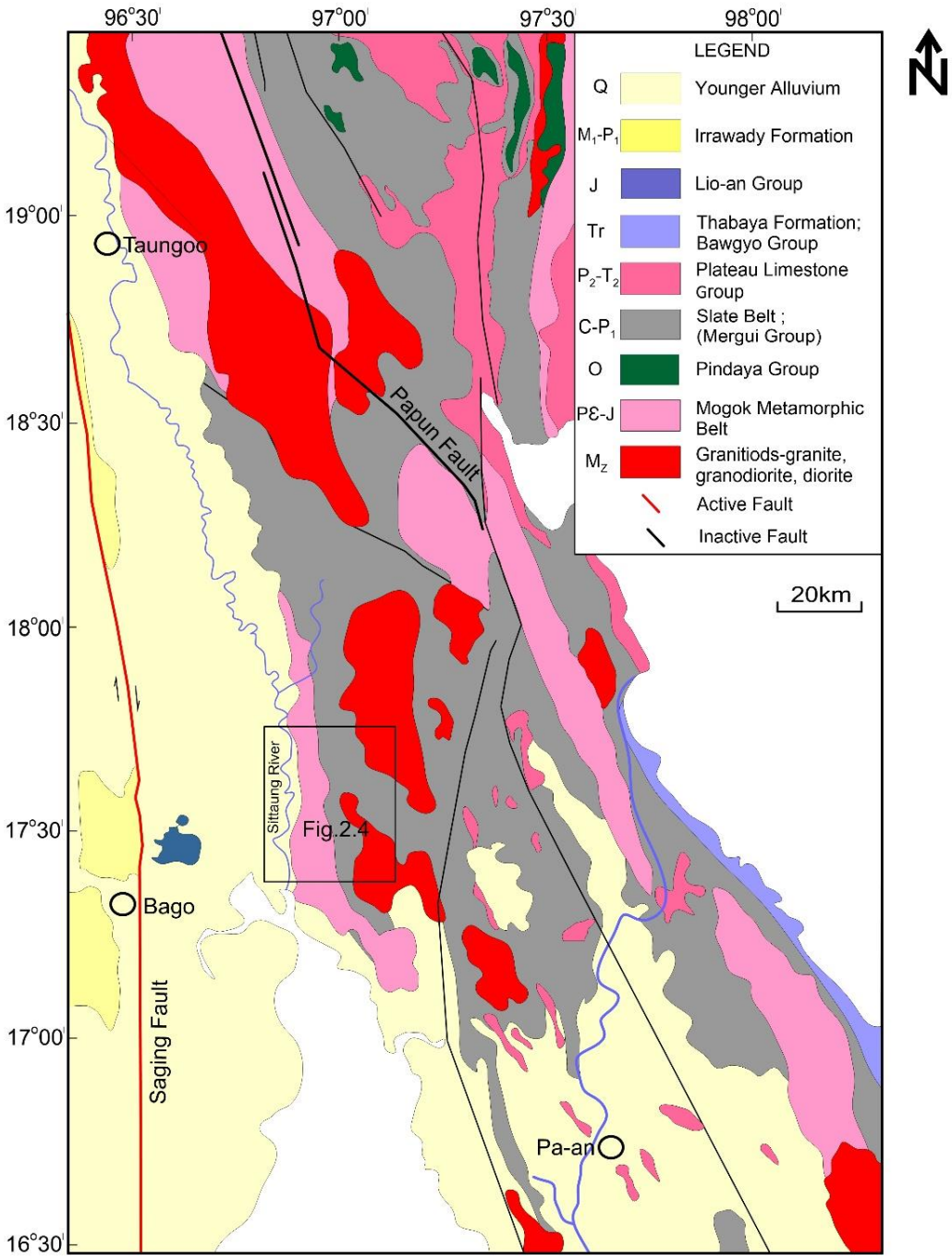

Figure 2.2. Geological map of the southern part of the Slate Belt and Mogok Metamorphic Belt in which the Kyaikhto gold district is located (Modified after Myanmar Geosciences Society (MGS), 2014). Abbreviations: Q = Quaternary, M_1-P_1 = Lower Miocene to Lower Pliocene, J = Jurassic, Tr =Triassic, P_2-T_2 = Middle Permian to Middle Triassic, C-P_1 = Carboniferous to Lower Permian, O = Ordovician, PЄ-J = Precambrian to partly Jurassic, Mz=Mesozoic.

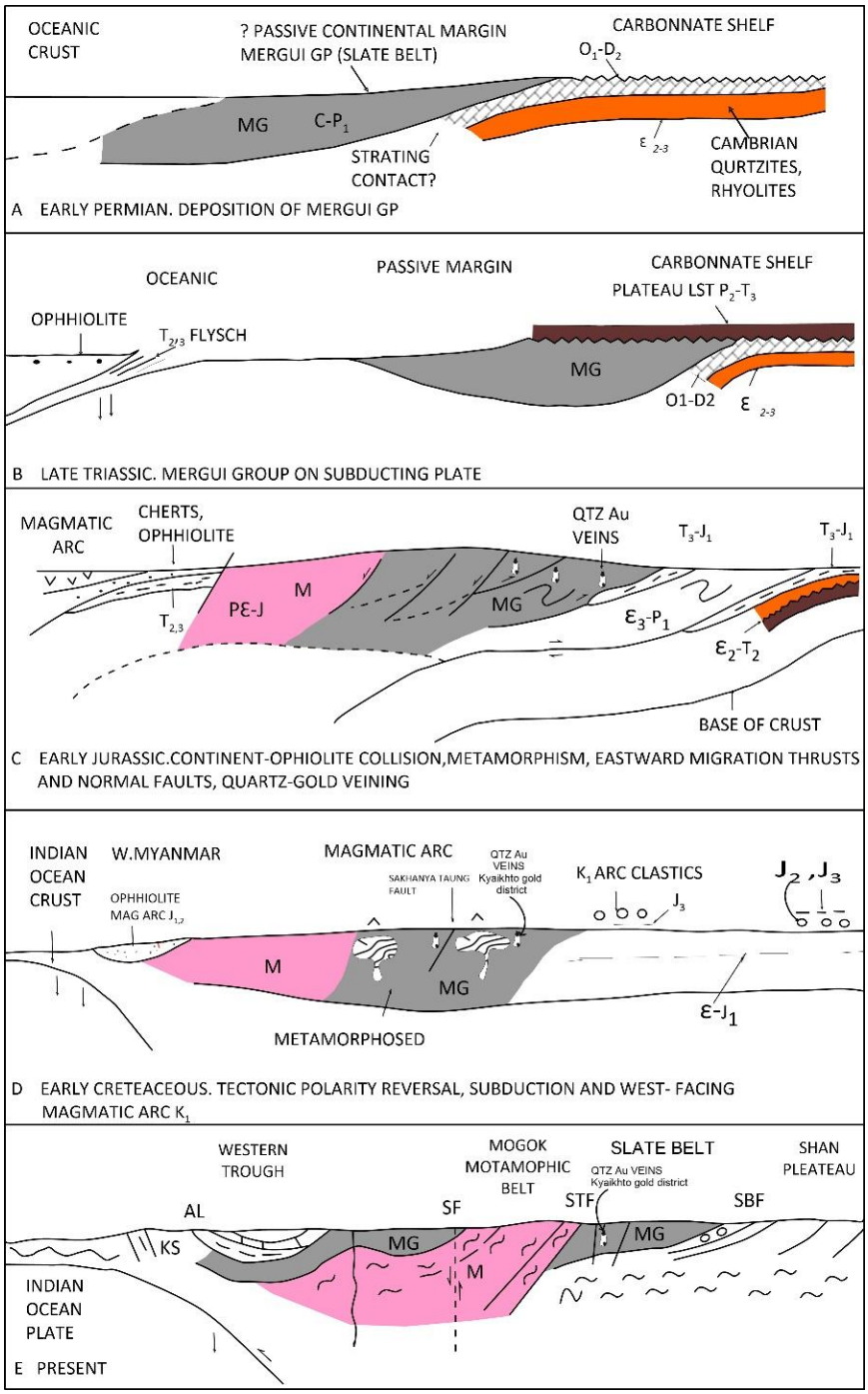

Figure 2.3. Regional Tectonic Setting of the Kyaikhto gold district (Modified after Mitchell *et al.*, 2004). Abbreviations: Al = Alluvium, KS = Cretaceous Clastics, SF = Sagaing Fault, STF = Sakan Taung Fault, SBF = Slate Boundary Fault, M = Mogok Metamorphic Belt, MG = Mergui group (or) Slate Belt, $J_{2,3}$ = Middle - Upper Jurassic, $T_{2,3}$ = Middle – Upper Triassic, T_3 J_1 = Upper Triassic-Lower Jurassic, K_1= Lower Cretaceous, P_2-T_3 = Middle Permian to Upper Triassic, C-P_1 = Carboniferous to Lower Permian, O_1-D_2 = Lower Ordovician- Middle Devonian, PƐ-J = Precambrian to partly Jurassic, Ɛ-J_1 = Cambrian – Lower Jurassic, $Ɛ_2$-T_2= Middle Cambrian-Middle Triassic, $Ɛ_3$-P_1= Upper Cambrian- Lower Permian, $Ɛ_{2,3}$= Middle-Lower Cambrian.

2.3 Deposit geology

Four mineralized zones have been identified from south to north as the Kunzeik prospect, the Zibyaung deposit, the Thae Phyu Chaung deposit and the Meyon deposit (Figure 2.4). Gold mineralization in the Kyaikhto district occurred as massive veins, network veinlets, stockworks, and dissemination. The general trend of quartz veins is NNE-SSW with some veins trending NW-SE.

The gold mineralization in the Kyaikhto district is predominately hosted by biotite granite, biotite granodiorite and metasedimentary rocks of Mergui Group (Figure 2.4). The Mergui Group consists of slate, phyllite, and schist. The metamorphic grade of these rocks is greenschist facies characterized by a mineral assemblage of epidote, biotite, muscovite and chlorite. Locally, fine-grained pyrite crystals are disseminated in the slate, phyllite, and schist.

The granitic rocks in this district can be correlated to the Mokpalin Quartz Diorite and the Kyaikhtiyo Granite that have the LA-ICP-MS zircon U–Pb ages of 90.8 ± 0.8 Ma and 63.3 ± 0.6 Ma, respectively (Mitchell *et al.*, 2012) (Figure 2.4). A 2 km^2 pyroxenite within sericite schist assigned to the Slate Belt and intruded by the granitic rocks was mapped in the study area (Mackenzie, 1999). Some 10 km to the southwest, several primary and alluvial gold workings are operated in the serpentinite that is exposed beneath the lateritic cover.

.

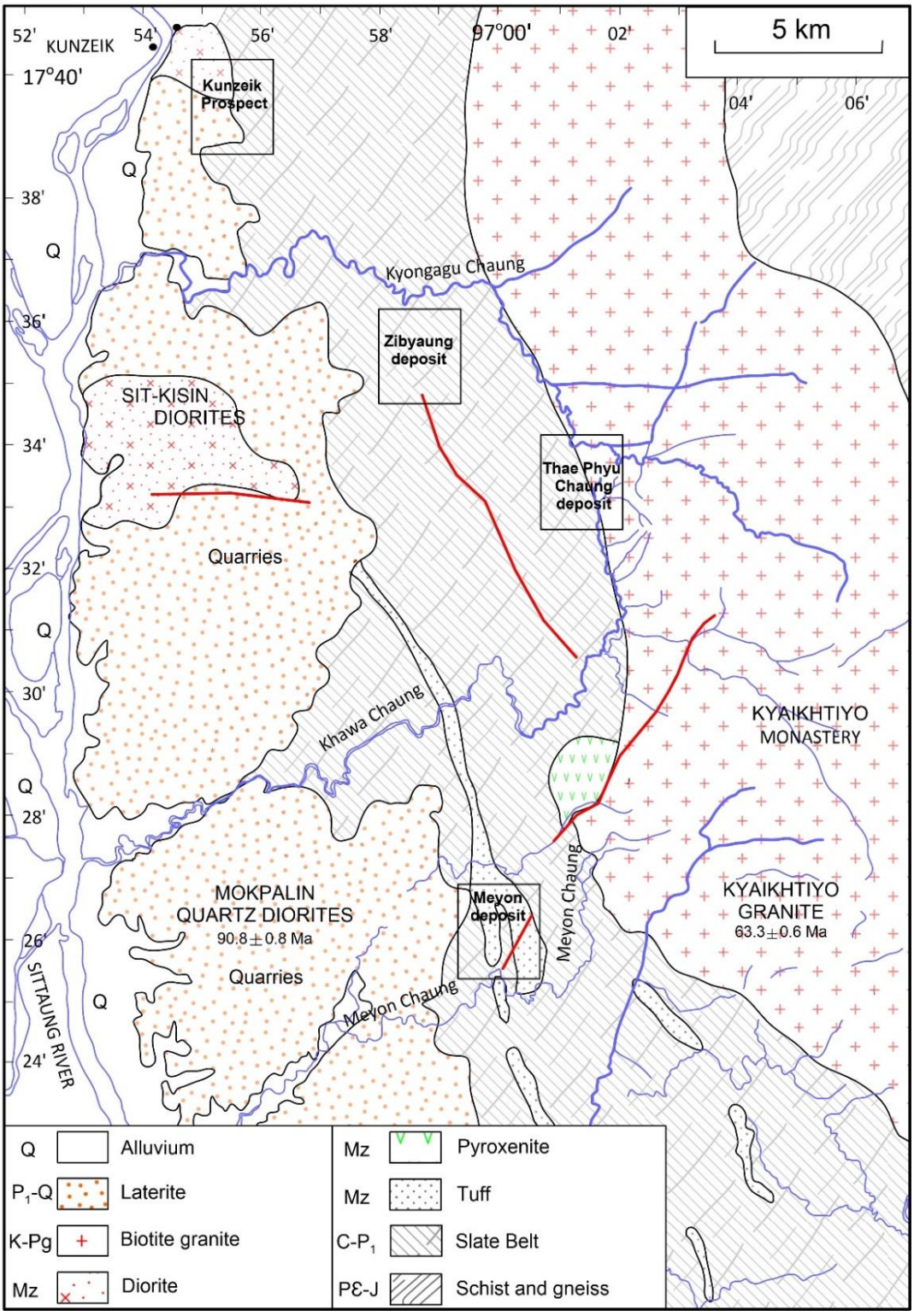

Figure 2.4. Geological map of the Kyaikhto gold district. Red lines are faults (Modified after Mackenzie, 1999, Mitchell *et al.*, 2012). Abbreviations: Q = Quaternary, P_1-Q = Lower Pliocene to Quaternary, K-Pg = Cretaceous to Paleogene, Mz = Mesozoic, C-P_1=Carboniferous to Lower Permian, PƐ-J = Precambrian to partly Jurassic.

2.4 Metasedimentary rocks

The metasedimentary rocks of the Mergui Group covered throughout the Kyaikhto district and consist of black slate, slaty phyllite, and schist. The black slate of Mergui Group shows lepidoblastic to granolepidoblastic textures, which are defined by the orientation of biotite and chlorite. Black slate and phyllite with a blocky form in outcrop are very fine-grained with black to pale green color (Figure 2.5a, b, c, d). Black slate is dominated by sericite, and chlorite (Figure 2.5 a, b).

Black slate and phyllite are characterized by the mineral assemblage of greenschist facies such as epidote, chlorite, and sericite. Locally, the black slate is interbedded with and/or gradationally changes to slaty phyllite. The grains are up to 10 μm in size with varying amounts of sericite and chlorite. Schist is mainly composed of quartz, biotite, and chlorite (Figure 2.5e, f). Mineral grains are typically affected by chloritization that modified the shapes of minerals and obscure their primary character in some cases. The matrix of black slate comprises 30 to 70% carbonaceous materials (graphite) and very fine quartz particles.

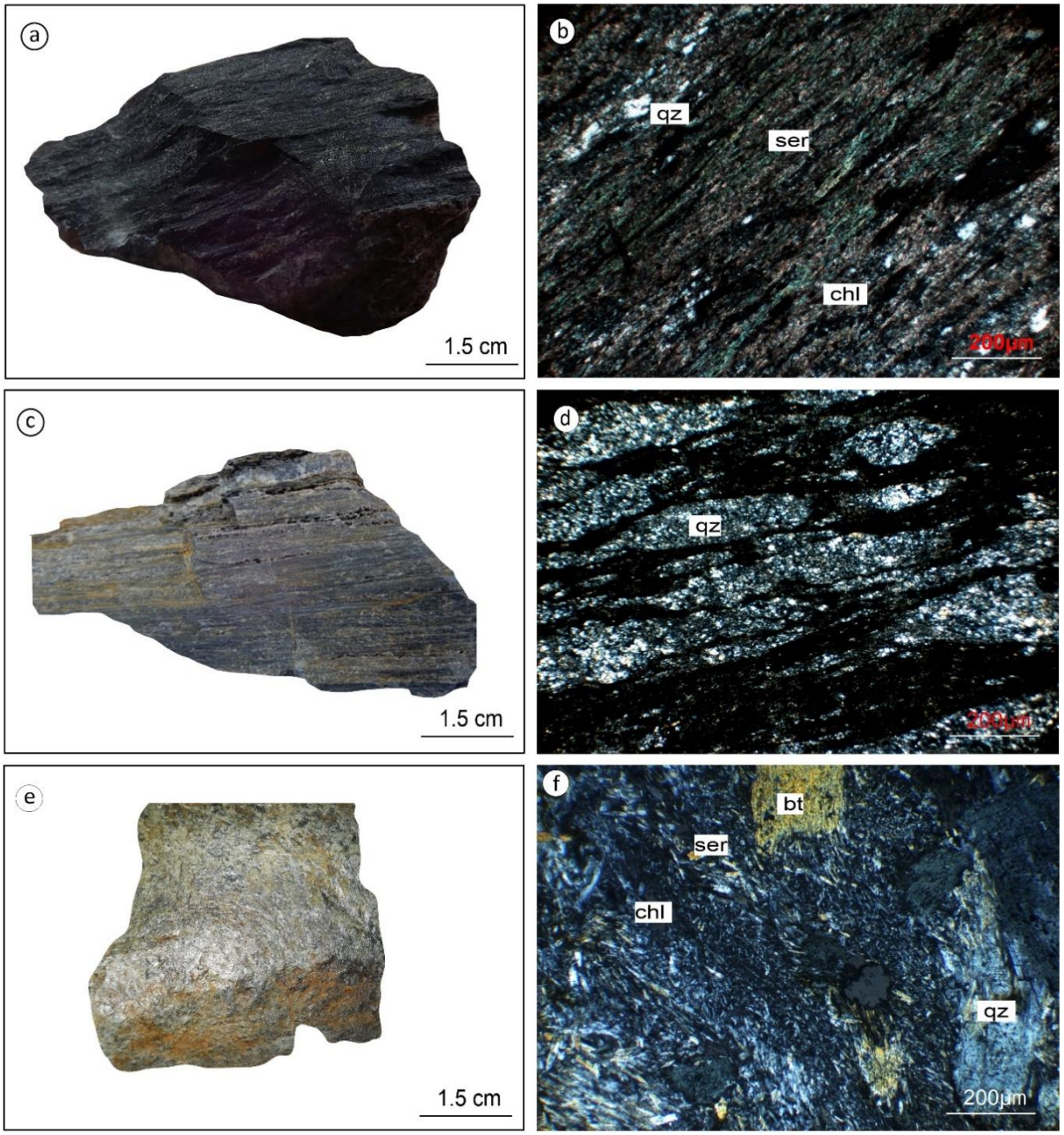

Figure 2.5. (a) Hand specimen of black slate from the Thae Phyu Chaung deposit, (b) Photomicrograph of black slate from the Thae Phyu Chaung deposit consisting of quartz (qz), chlorite (chl), sericite (ser) that show nearly parallel alignment, (c) Hand specimen of slaty phyllite from the Thae Phyu Chaung deposit, (d) Photomicrograph of slaty phyllite from the Thae Phyu Chaung deposit showing phyllitic texture, (e) Hand specimen of schist from Zibyaung deposit and (f) Photomicrograph of schist from the Zibyaung deposit consisting of quartz (qz) , chlorite (chl), biotite (bt) and sericite (ser).

2.5 Granitic rocks

On the basis of textural and mineralogical characteristics, the granitic rocks exposed in the Kyaikhto district are classified into biotite granite and biotite granodiorite.

2.5.1 Biotite granite

Biotite granite is exposed in the vicinity of Kunzeik prospect and Thae Phyu Chaung deposit. It is generally medium- to coarse-grained, massive and equigranular (Figure 2.6a). In the Kunzeik prospect, biotite granite at some exposures is highly-mineralized, containing disseminated grains of molybdenite, chalcopyrite, and pyrite. In thin section, the quartz crystals are generally anhedral, although some have wavy edges which are relatively large (2-5 mm). Petrographically, biotite granite is mainly composed of plagioclase and K-feldspar. Elongated and subhedral biotite occurs as accessory phases (Figure 2.6b). Biotite granite in the Thae Phyu Chaung deposit has textures similar to the Kyaikhtiyo granite with a zircon U–Pb age of 63.3 ± 0.6 Ma (Mitchell *et al.*, 2012) (Figure 2.4).

2.5.2 Biotite granodiorite

Biotite granodiorite is exposed at the Kunzeik prospect. It is medium- to coarse-grained with an equigranular texture (Figure 2.6c, d) and consists of quartz, plagioclase, K-feldspar and biotite. Biotite occurs as fresh vitreous flakes to highly chloritized patches. Pyrite and chalcopyrite are dispersed in the biotite granodiorite exposed in the area of Kunzeik prospect (Figure 2.6c). Plagioclase ranges from 100 to 400 μm in diameter (Figure 2.6d). The grain size of all minerals is roughly equant. Both untwined and simple contact twined orthoclase is the most common mineral in biotite granodiorite. Orthoclase, plagioclase, biotite, and quartz are major constituents of the biotite granodiorite. Quartz generally occurs as

anhedral grains and interstitial crystals among other rock-forming minerals. Some quartz grains show undulatory extinction. Euhedral to subhedral plagioclase is partially intergrown with the orthoclase.

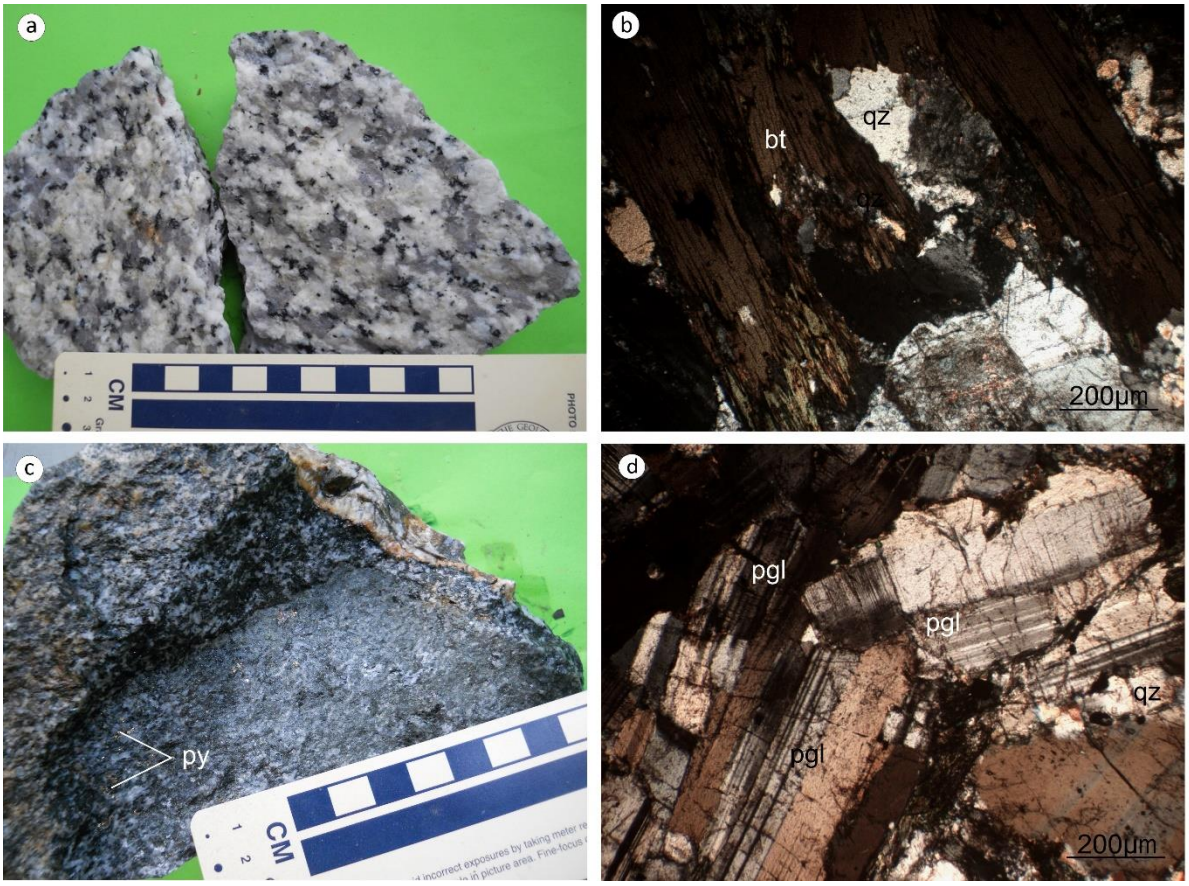

Figure 2.6.(a) Photograph of hand specimen of biotite granite at the Thae Phyu Chaung deposit, (b) Photomicrograph of biotite granite at the Thae Phyu Chaung deposit consisting of quartz (qz), orthoclase (or), and biotite (bt), (c) Hand specimen of biotite granodiorite at the Kunzeik prospect, and (d) Photomicrograph of biotite granodiorite at the Kunzeik prospect consisting of quartz (qz), orthoclase (or), plagioclase (pgl) and biotite (bt).

2.6 Modal composition

Modal percentages were obtained by point counting in thin sections (Table 2.1). Granitic rocks in the Thae Phyu Chaung deposit and from the Kunzeik prospect are mostly syeno-granites to monzogranite (Streckeisen, 1976) (Figure 2.7a).

2.7 Geochemistry

2.7.1 Major and trace element

Major element concentrations of the granitic rocks from the Kyaikhto district are listed in Table 2.2 and the trace element data are listed in Table 2.3. Loss on ignition (LOI) ranges from 0.7 to 1.1 wt% representing the low effect of hydrothermal activity. The SiO_2 abundances of biotite granite are variable (53.6- 75.9 wt%). The FeO concentrations of biotite granite are low (1.5-2.0 wt%) at the Thae Phyu Chaung deposit, but are higher at the Khunziek prospect (4.2-7.7 wt%). The MgO concentration of biotite granite ranges from 0.4 to 0.7 wt% in the Thae Phyu Chaung deposit and is 1.7 wt% at the Kunzeik prospect. The Al_2O_3 concentrations of biotite granite are similar in all deposits (12.8 - 14.7 wt%). The biotite granites in Kunziek prospect and The Phyu Chaung deposit are silicious (SiO_2 = 72.3- 75.9 wt.%) with 12.7 - 14.7 wt.% Al_2O_3, 2.6 – 3.3 wt.% Na_2O, and 1.3-4.7 wt.% K_2O. Intrusive rocks in the Kyaikhto district fall in the granite to diorite fields in the total alkali versus SiO_2 composition (Middlemost, 1985) (Figure 2.7b).

The biotite granites are classified as high-K calc-alkaline series on a SiO_2–K_2O (Maniar and Piccoli, 1989) (Figure 2.7c) and are classified as peraluminous (S-type) on an A/CNK–A/NK diagram (Peccerillo and Taylor, 1976) (Figure 2.7d). The biotite granodiorite samples from the Khunziek prospect contain 58.6 wt.% SiO_2, 16.9 wt.% Al_2O_3, 3.3 wt.%

Na_2O and 1.31wt.% K_2O. The K_2O versus SiO_2 discrimination diagram indicates that the biotite granodiorite from the Kunziek prospect is medium K calc-alkaline (Maniar and Piccoli, 1989) (Figure 2.7c). Classification of rocks based on the ASI (alumina saturation index = A/CNK [Al_2O_3/ (CaO + Na_2O + K_2O) molar]) indicates that biotite granodiorite in the Khunziek prospect is metaluminous (I-type) (Peccerillo and Taylor, 1976) (Figure 2.7d). The biotite granodiorite is enriched in Ni, Sr, and V, and depleted in Nb, Zr and Ba compared to the biotite granite. Regarding the tectonic environment, the Kyaikhto granitoids are positioned on the diagram R_1 Vs R_2 (Batchelor and Bowden,1985), forming a trend from pre-plate collision to the post-orogenic setting (Figure 2.7e).

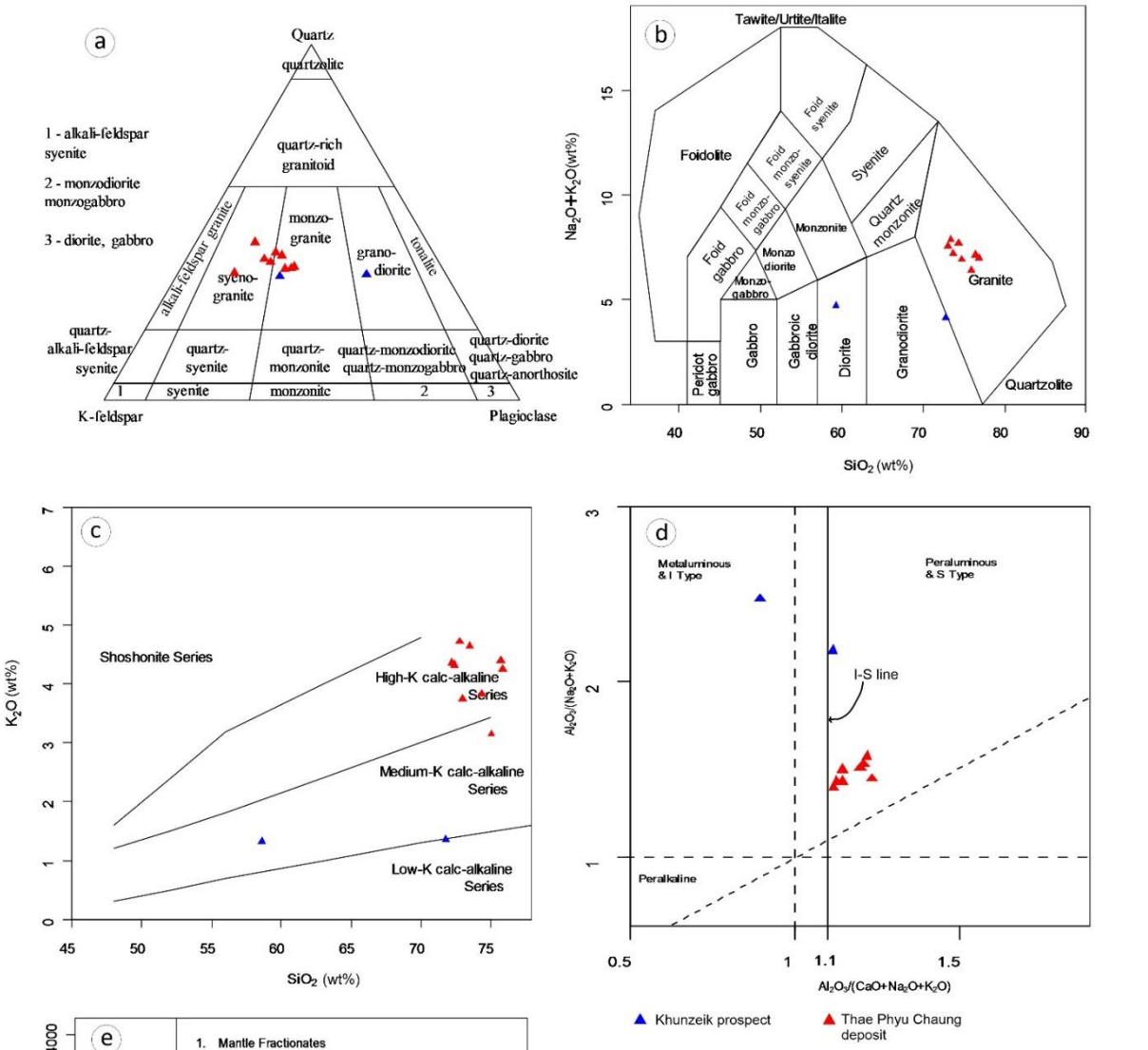

Figure 2.7. (a) Modal classification diagram of the Kyaikhto granitoids after (Streckeisen, 1976) (b) Classification diagram based on total alkali versus SiO_2 (Middlemost, 1985), (c) K_2O versus SiO_2 discrimination diagram (Maniar and Piccoli, 1989), (d) A/NK versus A/CNK (Peccerillo and Taylor, 1976) , (e) [R_1= 4Si - 11(Na + K) - 2(Fe + Ti)] Vs [R_2= 6Ca + 2Mg + Al] diagram of the Kyaikhto granitoids (Batchelor and Bowden,1985).

Table 2.1. The modal composition of the Kyaikhto granitoids

Deposit/ Prospect	Rock type	Quartz	Plagioclase	Biotite	K-feldspar vol%	Others	Total
Thae Phyu Chaung	Biotite granite	39.5	21.7	3.4	35.3	0.1	100.0
	Biotite granite	40.5	13.0	9.2	37.2	0.1	100.0
	Biotite granite	35.1	13.2	2.8	48.8	0.1	100.0
	Biotite granite	39.3	19.4	5.9	35.3	0.1	100.0
	Biotite granite	35.6	23.9	4.5	35.9	0.1	100.0
	Biotite granite	38.2	18.0	4.5	39.3	-	100.0
	Biotite granite	36.2	25.9	4.3	33.6	-	100.0
	Biotite granite	37.4	19.8	4.3	38.4	0.1	100.0
	Biotite granite	35.6	25.2	4.8	34.3	0.1	100.0
Kunzeik	Biotite granite	33.9	24.1	3.3	38.6	0.1	100.0
	Biotite granodiorite	32.4	41.1	5.2	19.0	2.3	100.0

Note: - = not detected and 'Others' refers to opaque, chlorite etc.

Table 2.2. Representative major elements analyses of intrusive rocks of Kyaikhto gold district.

Deposit/ Prospect	Rock type	SiO_2	TiO_2	Al_2O_3	FeO	MnO	MgO	CaO	Na_2O	K_2O	P_2O_5	LOI	Total
		wt%											
Thae Phyu Chaung	Biotite granite	75.9	0.18	12.7	1.50	0.14	0.54	0.80	2.60	4.25	0.03	1.12	99.9
	Biotite granite	75.1	0.19	13.5	1.71	0.09	0.63	1.36	3.16	3.14	0.04	0.97	99.8
	Biotite granite	73.0	0.22	14.5	1.88	0.14	0.65	1.36	3.36	3.74	0.04	0.87	99.8
	Biotite granite	75.8	0.17	12.6	1.47	0.08	0.57	1.21	2.64	4.40	0.03	0.84	99.8
	Biotite granite	72.8	0.20	14.4	1.70	0.12	0.60	1.46	3.06	4.72	0.05	0.70	99.8
	Biotite granite	72.3	0.21	14.6	1.82	0.16	0.62	1.61	3.12	4.35	0.04	0.97	99.8
	Biotite granite	74.4	0.21	13.6	1.74	0.09	0.62	1.54	3.03	3.82	0.44	0.75	100.3
	Biotite granite	72.4	0.23	14.7	2.04	0.20	0.68	1.33	3.13	4.32	0.04	0.72	99.8
	Biotite granite	73.5	0.17	14.0	1.53	0.12	0.57	1.32	2.93	4.64	0.04	0.96	99.7
Kunzeik	Biotite granite	71.8	0.61	12.8	4.28	0.08	1.74	3.08	2.69	1.35	0.13	1.14	99.7
	Biotite granodiorite	58.6	1.33	16.9	7.73	0.14	2.55	6.62	3.32	1.31	0.35	0.84	99.7

LOI= loss on ignition

Table 2.3. Representative trace element analyses of intrusive rocks of Kyaikhto gold district.

Deposit/ Prospect	Rock type	S	V	Co	Ni	Cu	Mo	Sn	W	Rb	Sr	Ba	Y	Zr	Nb	Th	U
										ppm							
Thae Phyu Chaung	Biotite granite	116	12	34	8	19	13	16	27	126	130	632	36	102	11	9	8
	Biotite granite	146	21	36	8	bdl	13	19	27	111	160	331	38	120	12	9	3
	Biotite granite	224	22	45	9	2	14	19	33	126	161	368	40	109	13	10	3
	Biotite granite	149	20	18	7	bdl	13	25	19	133	137	561	32	87	11	11	3
	Biotite granite	175	18	34	7	12	13	26	41	146	159	455	47	114	12	11	3
	Biotite granite	146	18	37	9	8	16	29	15	139	180	730	42	188	12	13	2
	Biotite granite	17	20	37	11	bdl	14	20	22	127	157	458	40	93	13	11	2
	Biotite granite	152	19	62	9	bdl	15	23	41	142	160	447	40	100	14	11	10
	Biotite granite	657	22	31	9	9	1	16	20	132	142	502	32	88	10	6	3
Kunzeik	Biotite granite	501	80	25	8	19	7	13	20	51	362	300	16	133	6	5	5
	Biotite granodiorite	408	221	13	9	12	8	14	40	30	912	344	12	117	3	4	5

bdl=below detection limit

2.8 Discussion and Conclusions

The Kyaikhto gold district is predominately hosted by metasedimentary rocks and intrusive rocks. Metasedimentary rocks are schist, phyllite, and slate and intrusive rocks are biotite granite and biotite granodiorite. Gold mineralization in the Kyaikhto district occurred as massive veins, network veinlets, stockworks, and dissemination. The general trend of quartz veins is NNE-SSW with some veins trending NW-SE. The granitic rocks in the Kyaikhto gold district are medium K calc-alkaline and high K calc-alkaline series. Biotite granites at the Kunziek prospect and Thae Phyu Chaung deposit are peraluminous (S-type), whereas biotite granodiorite at the Kunziek prospect is metaluminous (I-type). The granitoids in Kyaikhto show a trend from pre-plate collision to the post-orogenic setting in geochemical discrimination diagram (Figure 2.7e). Geochemical and petrographic data of the samples suggest the predominance of I-type granitoid throughout Kyaikhto gold district. I-type granitoid is closely associated with Cu-Mo mineralization at the Kunzeik prospect

References

Barber, A.J., Crow, M.J. and Zaw, K. (Eds.). (2017) Myanmar: Geology, Resources, and Tectonics. *Geology Society of London Memoir*.

Batchelor R.A. and Bowden P. (1985) Petrogenetic interpretation of granitoid rock series using multicationic parameters. *Chemical Geology,* 48, 45-55.

Mackenzie, M.J. (1999) Report on the Exploration Progress in block 3/13 for the Period January 1998 to December 1998. *Palmer Resources Ltd. Myanmar (Burma) Project, (Unpublished)*, 1-67p.

Maniar, P. D. and Piccoli, P. M. (1989) Tectonic discrimination of granitoids. *Geological Society of American Bulletin*, 101, 635-643.

Middlemost, E.A.K. (1985) Magmas, and Magmatic Rocks. An Introduction to Igneous Petrology. *Longman Group*, UK, 73-87.

Mitchell, A. H. G., Htay, N., Ausa, C., Deiparine, L., Khine, A. and Po, S. (1999) Geological settings of gold districts in Myanmar. In Weber, G. (Eds.) PACRIM 99, Proceedings International Congress on Earth Science, *Exploration and Mining around the Pacific Rim. Australasian Institute of Mining and Metallurgy, Bali, Indonesia*, 303-309.

Mitchell, A.H.G., Ausa, C., Deiparine, L., Hlaing, T., Htay, N. and Khine, A. (2004) The Modi Taung-Nankwe gold district, Slate Belt, Central Myanmar: mesothermal veins in a Mesozoic orogen. *Journal Asian Earth Science,* 23, 321-341.

Mitchell, A.H.G., Chung, S.-L., Oo, T., Lin, T.-H. and Hung, C.-H. (2012) Zircon U-Pb ages in Myanmar: Magmatic–metamorphic events and the closure of a Neo-Tethys ocean? *Journal Asian Earth Science*, 56, 1-23.

Mitchell, A.H.G. (Eds.). (2018) Geological Belts, Plate Boundaries and Mineral Deposits in Myanmar. *Myanmar Precious Resources Group, Myanmar and Oxford, United Kingdom*, 1, 3-15.

Myanmar Geosciences Society (2014). Geological Map of Myanmar (2014), 1:2,250,000. Yangon.

Oo, Z.N. and Zaw, K. (2009) Geology and mineralization characteristics of Meyon gold deposit, Mon State, Southern Myanmar. *Proceedings of 11th Regional Congress on Geology, Mineral and Energy Resources of Southeast Asia (GEOSEA), 8-10 June, Kuala Lumpur, Malaysia*, 32.

Oo, Z.N., Zaw, K. and Mernagh, T. (2010) Geological setting and nature of mineralization at Meyon gold deposit, Mon State, Myanmar. *13th Quadrennial International Association on Genesis of Ore Deposits (IAGOD) Symposium, Adelaide, 6-9 April 2010* CD-ROM.

Oo, Z.N. and Zaw, K. (2015) Geology and mineralization characteristics of Meyon gold deposit, Mon State, Southern Myanmar. *The Society of Economic Geologists Conference, Hobart, 27-30 September, CD*-ROM.

Peccerillo, R. and Taylor, S.R. (1976) Geochemistry of Eocene Calc-Alkaline Volcanic Rocks from the Kastamonu Area, Northern Turkey. *Contributions to Mineralogy and Petrology*, 58, 63-81.

Streckeisen, A. (1976) To each plutonic rock its proper name. *Earth Science Reviews,* 12, 1-33.

Zaw, K. and Meffre, S. (2014) Tectonics and metallogeny of mainland SE Asia - a review and contribution. *Special Issue on Tectonics and Metallogeny of Mainland SE Asia. Gondwana Research*, 26, 5-30.

CHAPTER III

Gold mineralization in the Kyaikhto district, Mon State, southern Myanmar

3.1 General statement

This chapter discusses the mineralization styles in the Kyaikhto gold district and fluid inclusion studies on the Kunzeik prospect and Zibyaung deposit.

3.2 Mineralization

3.2.1 Kunzeik

Gold mineralization in the Kunzeik is hosted by the biotite granite, biotite granodiorite, and metasedimentary rocks. The style of mineralization includes stockwork, dissemination and quartz-sulfide veins. Minor fine-grained pyrite and chalcopyrite are irregularly dispersed throughout the veins (Figure 3.1a, b). The biotite granodiorite and slate are composed of sericite due to intense phyllic alteration. Molybdenite occurs as disseminated grains in biotite granite (Figure 3.1c). The irregular network of small quartz veinlets cut the biotite granodiorite forming stockwork mineralization.

3.2.2 Zibyaung

In the Zibyaung, the quartz-sulfide vein strikes northwest and dips steeply to the north (Figure 3.1d). It is mainly hosted by slate and schist. The biotite granodiorite suffered from an earlier propylitic (chlorite) alteration followed by silicification and later sericitization. Electrum is present as an infill mineral in pyrite and associated with sphalerite and galena

(Figure 3.1e, f). Sphalerite forms as a fissure filling mineral within pyrite. Galena occurs as fine to medium-sized grains filling cracks in pyrite and sphalerite.

3.2.3 Thae Phyu Chaung

Gold mineralization in the Thae Phyu Chaung is characterized by white to milky sheeted quartz veins that contain Au-Ag-Te-Bi minerals (Figure 3.1g). Sphalerite-rich ores are the most common in this deposit, associated with massive chalcopyrite and galena. Pyrite ranges from medium to coarse-grained, anhedral aggregates replacing and infilling grain boundaries of chalcopyrite and, to a lesser extent, sphalerite. Native gold is mainly associated with chalcopyrite and galena or located at the boundary between chalcopyrite grains (more detail discuss and see in chapter IV) (Figure 3.1h, i).

3.2.4 Meyon

Gold mineralization in the Meyon is characterized by a shear-hosted quartz-sulfide vein (Figure 3.1j). The quartz-gold vein is hosted within an intensely deformed sedimentary sequence comprising sandstone and carbonaceous mudstones. The quartz vein strikes NNE and dips steeply to the east. It has a known strike length of 235 m and an average thickness of 1.5 m. The enclosing shear zone has an average width of 4 m. Some thin stockwork quartz veins in the sedimentary rock also carry gold. Strongly sheared and brecciated nature of the host rocks occurs adjacent to the veins. Post-mineralization deformation caused minor offsets of the vein. Brecciation and fracturing of the quartz vein have produced excellent sites for gold deposition remobilized by supergene processes. Chalcopyrite is associated with pyrite and covellite. Covellite occurs as a secondary mineral of chalcopyrite (Figure 3.1k, l).

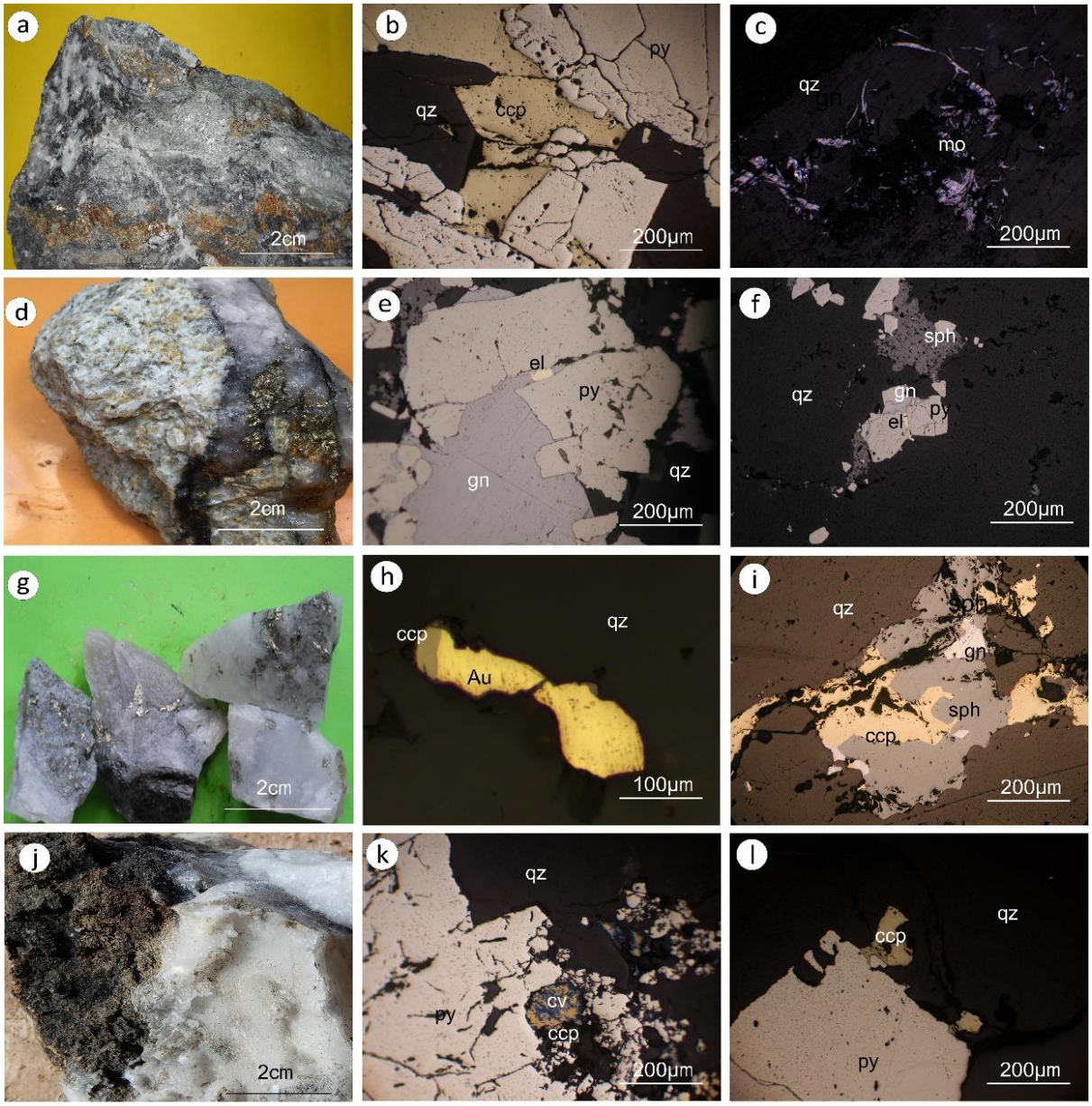

Figure 3.1. (a) Photograph (a, d, g, j) and photomicrographs (b, c, e, f, h, i, k, l) showing ore and ore minerals from the Kyaikhto gold district: (a) quartz-sulfide vein from the Kunzeik, (b) fractured pyrite replaced by chalcopyrite in quartz vein from the Kunzeik, (c) molybdenite dispersed in biotite granite from the Kunzeik, (d) quartz-sulfide vein from the Zibyaung, (e,f) electrum associated with galena, sphalerite and euhedral pyrite in the quartz-sulfide vein from the Zibyaung, (g) quartz-sulfide vein from the Thae Phyu Chaung, (h) native gold associated with chalcopyrite in the quartz-sulfide vein from the Thae Phyu Chaung, (i) sphalerite and chalcopyrite enclosed within galena in the quartz-sulfide vein from the Thae Phyu Chaung, (j) quartz-sulfide vein from the Meyon, (k) pyrite and chalcopyrite enclosed within covellite in the quartz-sulfide vein from the Meyon, and (l) pyrite associated with chalcopyrite in the quartz-sulfide vein from the Meyon. Abbreviations: py = pyrite, gn = galena, cv = covellite, ccp = chalcopyrite, sph = sphalerite, mo = molybdenite, qz = quartz, el = electrum and Au = native gold.

3.3 Fluid inclusions studies

3.3.1 Fluid inclusion petrography

Fluid inclusions in the quartz from the auriferous quartz veins of the Kunzeik and Zibyaung were examined. Fluid inclusions hosted in granular quartz crystals in veins which were distributed randomly in clusters, and in isolation, were interpreted as primary in origin. Those aligned along micro-fractures in intragranular with growth zones in granular crystals trails were interpreted as secondary or pseudo secondary inclusions based on the classification by [1]. Secondary fluid inclusions in healed fractures were avoided. Examination identified two different types of fluid inclusions: (1) Type A: aqueous carbonic fluid inclusions which have three phases with two components (liquid-liquid-vapor or L-L-V) and (2) Type B: aqueous liquid and vapor inclusions which consist of two phases (liquid-vapor or L-V) (Figure. 3.2a, b, c, d). Fluid inclusions have round to irregular shapes and contain no daughter mineral. Type A fluid inclusions coexist with Type B fluid inclusions and there is no crosscutting relation-ship between these two groups within the same quartz crystal (Figure 3.2a, b, c, d). These relationships reveal that two types of fluids were present during the precipitation of quartz-sulfide vein in the Kunzeik and Zibyaung.

Type A inclusions are exclusively found in the quartz-sulfide vein from the Kunzeik and Zibyaung. Type A fluid inclusions have ellipsoidal or irregular shapes with sizes ranging from 10 to 30 μm. The sizes of the vapor bubble are up to approximately 50–80 vol % of the inclusion (Figure 3.2a, b, c). Type B fluid inclusions are very common in quartz grains in quartz-sulfide vein at the Kunzeik and Zibyaung. The Type B fluid inclusions have a sub-rounded, small, elliptical and irregular form, and vary in size from 5 to 20 μm in diameter with most between 8 and 15μm (Figure 3.2d). Type B fluid inclusions consist of two phases (liquid-vapor or L-V) containing 10-30 vol.% vapor (average 20-25 vol.%) (Figure 3.2b).

3.4 Microthermometry

The results of fluid inclusion microthermometry are summarized in Table 3.1.

3.4.1 Kunzeik

The CO_2 phases of Type A inclusions were totally homogenized to a liquid phase at temperatures ($T_{h\text{-}CO2}$) between 28.2 and 31.3 °C, indicating the presence of NaCl. The CO_2 melting temperatures $T_{m\text{-}CO2}$ of fluid inclusions range from -58.2 to -56.8 °C similar to, or slightly lower than, the triple point of pure CO_2 (-56.6°C) [1], indicating they are mostly pure CO_2, with minor other volatile components [1]. The melting temperatures of clathrates ($T_{m\text{-}cla}$ = 7.6 - 9.2 °C) indicates that the salinity of these inclusions is low, about 1.6 to 4.6 wt.% NaCl equivalent. Total homogenization temperatures (T_h) of Type A fluid inclusions range from 296 to 376 °C (N=31) (Figure 3.3a). Homogenization temperatures (T_h) of Type B fluid inclusions in vein quartz range from 246 to 312 °C (N=53) (Figure 3.3a). Their final ice melting temperatures ($T_{m\text{-}ice}$) vary from -2.1 to -7.2 °C, which corresponds to salinities between 1.2 and 10.7 wt. % NaCl equivalent (Figure 3.3b).

3.4.2 Zibyaung

The CO_2 melting temperatures ($T_{m\text{-}CO2}$) of Type A fluid inclusions range from -57.3 to -56.8 °C similar to, or slightly lower than, the triple point of pure CO_2 (-56.6°C) [1]. The CO_2 phases were totally homogenized to a liquid phase at temperatures ($T_{h\text{-}CO2}$) between 28.3 and 30.1°C. All Type A fluid inclusion were homogenized to a liquid at temperatures (T_h) from 305 to 378 °C (N=11) (Figure 3.3c). The melting temperatures of clathrates ($T_{m\text{-}cla}$ = 4.6 – 7.6 °C) yielded salinities between 4.6 and 9.6 wt% NaCl equivalent (Figure 3.3d). Homogenization temperatures (T_h) of Type B fluid inclusions of vein quartz range from 242

to 298 °C (N=19) (Figure 3.3c). Their final ice melting temperatures ($T_{m\text{-}ice}$) range from -0.5 to -8.1 °C and correspond to salinities from 0.9 to 11.8 wt. % NaCl equivalent (Figure 3.3d).

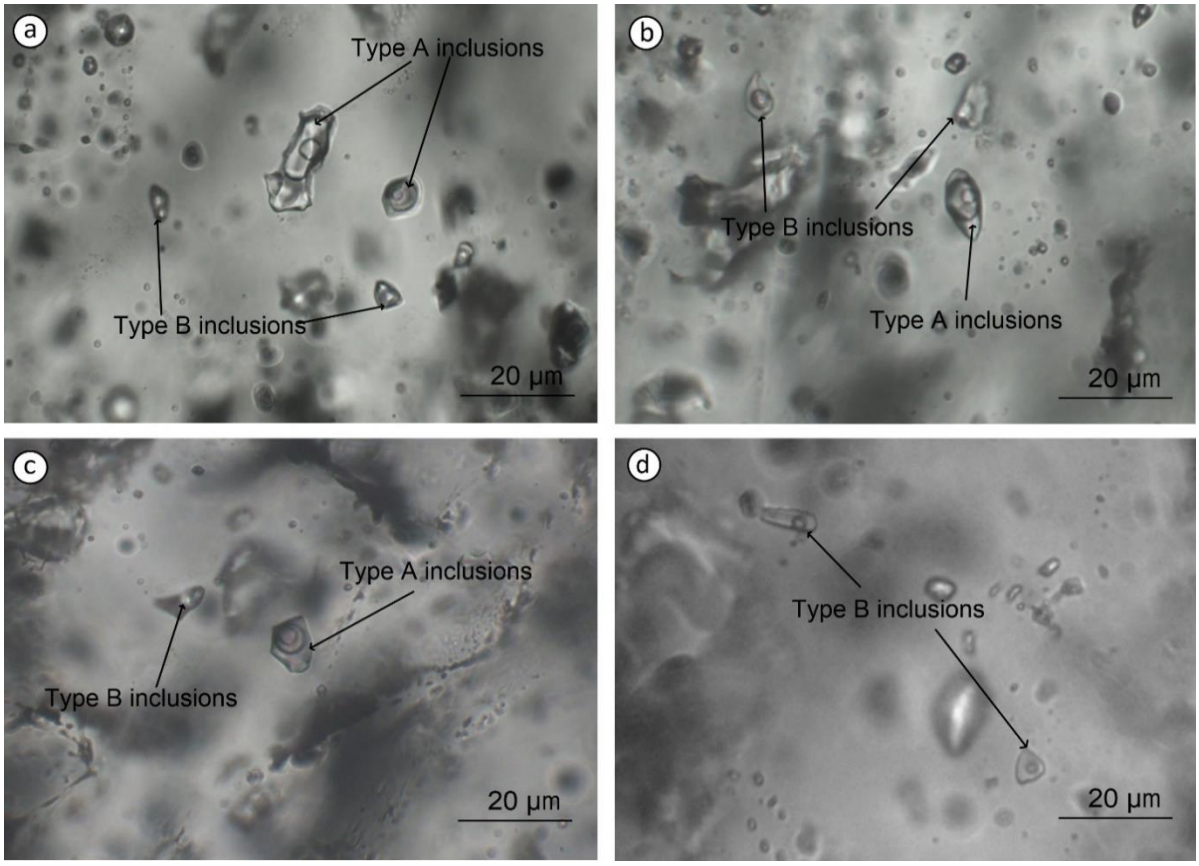

Figure 3.2. Photomicrographs of fluid inclusions in quartz-sulfide veins at room temperature in plane-polarized light. (a, b) Type A and B fluid inclusions coexisting together within same quartz gain in quartz-sulfide veins from the Kunzeik, (c) Type A and B fluid inclusions in the quartz-sulfide vein from the Zibyaung, and (d) Type B fluid inclusions in quartz-sulfide veins from the Zibyaung.

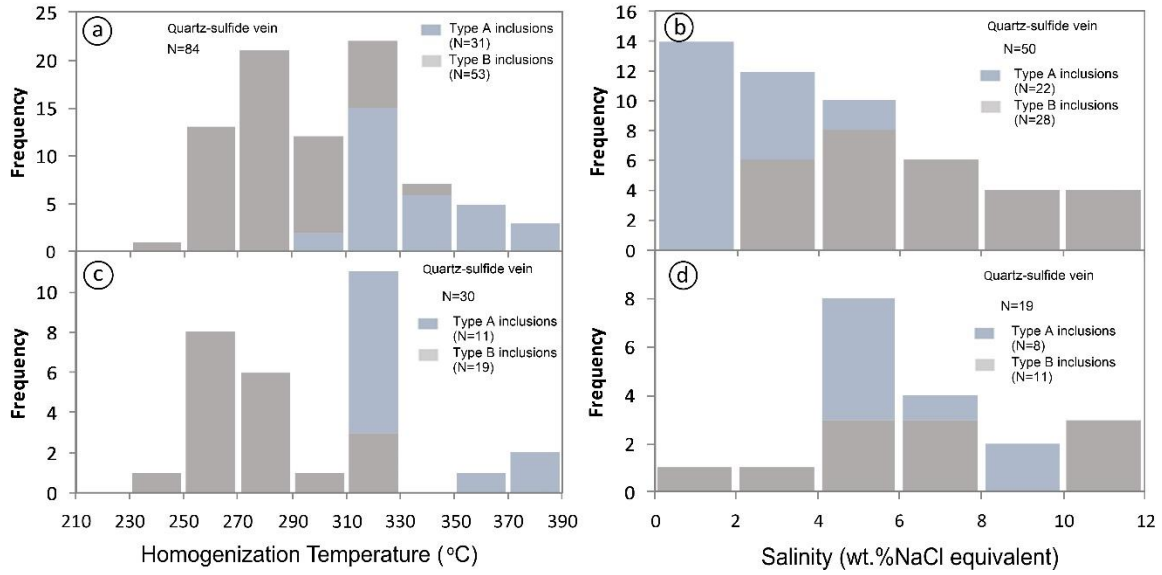

Figure 3.3. Histograms of total homogenization temperatures (T_h) of primary inclusions and salinities of fluid inclusions in quartz-sulfide vein from the Kunzeik and Zibyaung. (a) Histograms of T_h of primary inclusions in quartz-sulfide vein from the Kunzeik, (b) salinities of fluid inclusions in quartz-sulfide vein from the Kunzeik, (c) Histograms of T_h of primary inclusions in quartz-sulfide vein from the Zibyaung, and (d) salinities of fluid inclusions in quartz-sulfide vein from the Zibyaung. Note: N = total number of fluid inclusions

Table 3.1. Summary of fluid inclusion types and microthermometric data for fluid inclusions of the Kunzeik and Zibyaung.

Deposit Name	Vein Type	Type	$T_{m\text{-}CO2}$ (°C)	$T_{m\text{-}cla}$ (°C)	$T_{h\text{-}CO2}$ (°C)	T_h (°C)	$T_{m\text{-}ice}$ (°C)	Salinity (wt%NaCl eq.)
Kunzeik	Quartz-sulfide vein	Type A	-58.2 to -56.8 (N=31)	7.6 to 9.2 (N=22)	28.2 to 31.3 (N=31)	296 to 376 (N=31)		1.6 to 4.6 (N=22)
		Type B				246 to 312 (N=53)	-2.1 to -7.2 (N=28)	1.2 to 10.7 (N=28)
Zibyaung	Quartz-sulfide vein	Type A	-57.3 to -56.8 (N=11)	4.6 to 7.6 (N=7)	28.3 to 30.1 (N=11)	305 to 378 (N=11)		4.6 to 9.6 (N=8)
		Type B				242 to 298 (N=19)	-0.5 to -8.1 (N=11)	0.9 to11.8 (N=11)

Notes: $T_{m\text{-}CO2}$—melting temperature of CO_2; $T_{m\text{-}cla}$—melting temperature of CO_2 clathrate; $T_{h\text{-}CO2}$—partial homogenization temperature of CO_2 inclusions; T_h—total homogenization temperature of inclusions; $T_{m\text{-}ice}$— final ice melting temperature; wt% NaCl eq., weight percent NaCl equivalent; N= total number of fluid inclusions.

3.5 Discussion and Conclusions

The gold mineralization in the Kyaikhto district is predominately hosted by slate, slaty phyllite, and schist and biotite granite and biotite granodiorite. Gold mineralization in the Kyaikhto district occurred as sheeted veins, massive veins, network veinlets, stockworks, and dissemination. The main ore minerals are sphalerite, galena, chalco-pyrite, molybdenite, and pyrite with minor native gold and electrum. From fluid inclusion petrography and microthermometry, two different types of fluid inclusions consisting of aqueous-carbonic fluid (Type A) and aqueous fluid (Type B) are present. These two fluid types have been found to be the most common types in orogenic gold deposits worldwide [2] [3] [4] [5] [6] [7]. The factors leading to the formation of orogenic gold deposits are numerous and therefore it is difficult to identify a single responsible case for ore precipitation. According to [6] [8], metamorphic devolatilization produces low-salinity fluids that transport gold as reduced sulfur complexes. Ore deposition mechanisms in orogenic gold deposits are usually either fluid-rock re-actions, fluid phase separation or fluid mixing with meteoric waters [6] [9]. Moreover, several studies on orogenic gold deposits have perceived ore-mineralizing fluids which were low to moderate temperature, with low salinity, and fluid which was rich in CO_2 (e.g., Golden Mile and Kalgoorlie in Western Australia, Victoria in Australia, Motherlode in California and Kolar in India) [3] [4] [5]. As mentioned previously, the CO_2-bearing inclusions (Type A) are characterized by relatively higher homogenization temperatures and lower salinities, than the aqueous inclusions (Type B) in both the Kunzeik and Zibyaung. Salinities of Type A fluid inclusions in vein quartz from the Kunzeik are lower than those of gold-bearing quartz vein in the Zibyaung. The salinity of Type B fluid inclusions is the same in both the Kunzeik and Zibyaung.

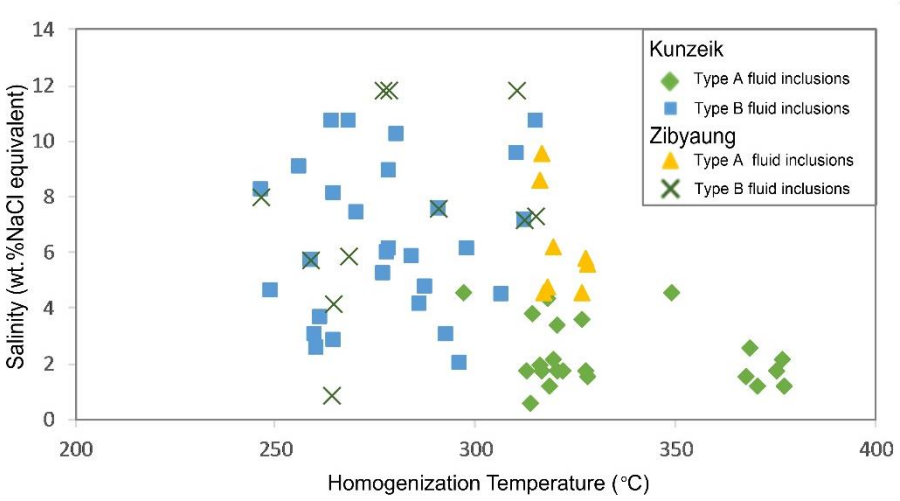

Figure 3.4. Total homogenization temperature versus salinity diagram for the fluid inclusions of in the quartz-sulfide vein from the Kunzeik and Zibyaung.

The relationship between Th and salinities of fluid inclusions is shown in (Figure 3.4). Coexistence of Type A fluid inclusions and Type B fluid inclusions in the same quartz grains has been often interpreted as evidence for fluid immiscibility [1].

Similar problems have been encountered in orogenic gold deposits where aqueous inclusions and aqueous carbonic fluid inclusions are interpreted as results of fluid unmixing, but the homogenization temperatures of the aqueous inclusions are significantly lower than the trapping temperatures estimated from other geothermometers [10] [11]. Therefore, the homogenization temperatures of Type B inclusions only represent the minimum temperature of trapping. Fluid inclusion studies in the Meyon deposit indicate that ore fluids were CO_2-rich, of moderately high temperature (240-370 °C) and salinities of <10 wt % NaCl equivalent [12] [13] [14]. The characteristics of the fluid inclusions in these three deposits are similar within the Kyaikhto gold district. The ore-forming fluids of the Kunzeik and Zibyaung which were composed of aqueous-carbonic fluid and aqueous fluid, are different from typical

magmatic fluids [3] [4] [15]. The CO_2-bearing inclusions are marked by relatively moderate homogenization temperatures (296 to 378 °C) and low salinities (1.6 to 9.6 wt% NaCl equivalent), whereas the homogenization temperatures and salinities of aqueous fluid inclusions are relatively low (242 to 312 °C) and low to moderate (0.9 to11.8 wt% NaCl equivalent). The fluid inclusion studies reveal that the ore-forming fluids responsible for the Kunzeik and Zibyaung are characterized by abundant CO_2-rich fluid inclusions, which are similar features with those of orogenic mineralization systems worldwide [2] [3] [4] [5] [6] [7]. Thus, the gold mineralization of the Kunzeik and Zibyaung are classified to be orogenic type in the Kyaikhto district.

References

[1] Roedder, E. (1984) Fluid Inclusions. Reviews in Mineralogy, 12, 644p.

[2] Diamond, L. W. (2001) Review of the systematics of CO_2-H_2O fluid inclusions. *Lithos*, 55, 69-99.

[3] Goldfarb, R. J., Baker, T., Dube, B., Groves, D. I., Hart, C. J. R., and Gosselin, P. (2005) Distribution, character, and genesis of gold deposits in metamorphic terranes. In Hedenquist, J. W., Thompson, J. F. H., Goldfarb, R. J. and Richards, J. P. (Eds.) Economic Geology 100th Anniversary Volume. *Society of Economic Geologists Inc., Littleton*, 407-450.

[4] Groves, D.I., Goldfarb, R.J., Gebre-Mariam, M., and Hagemann, S.G. (1998) Orogenic gold deposits: A proposed classification in the context of their crustal distribution and relationship to other gold deposit types. *Ore Geology Reviews*, 13, 7-27.

[5] Groves, D. I., Goldfarb, R. J., Robert, F., and Hart, C. J. R. (2003) Gold deposits in meta-morphic belts: Overview of current understanding, outstanding problems, future re-search, and exploration significance. *Economic Geology*, 98, 1-29.

[6] Ridley J.R. and Diamond L.W. (2000) Fluid chemistry of lode-gold deposits and implications for genetic models. In: Hagemann S.G. and Brown P. (Eds.), *Gold in 2000. Reviews in Economic Geology*, 13,141-162.

[7] Wilkinson, J. J. (2001) Fluid inclusions in hydrothermal ore deposits. *Lithos*, 55, 229-272.

[8] Phillips, G. N. and Powell, J. K. (1993) Link between gold provinces. *Economic Geology*, 88, 1084–1098.

[9] Hagemann, S. and Cassidy, K. (2000) Archean orogenic lode gold deposits. *Reviews in Economic Geology*, 13, 9-68.

[10] Chi, G. X. and Xue, C. J. (2011) Abundance of CO_2-rich fluid inclusions in a sedimentary basin-hosted Cu deposit at Jinman, Yunnan, China: implications for

mineralization environment and classification of the deposit. *Mineralium Deposita*, 46, 365–380

[11] Robert, F., and Kelly, W.C. (1987) Ore-forming fluids in Archean gold-bearing quartz veins at Sigma mine, Abitibi greenstone belt, Quebec, Canada. *Economic Geology*, 82, 1464-1482.

[12] Oo, Z.N. and Zaw, K. (2009) Geology and mineralization characteristics of Meyon gold deposit, Mon State, Southern Myanmar. *Proceedings of 11th Regional Congress on Geology, Mineral and Energy Resources of Southeast Asia (GEOSEA), 8-10 June, Kuala Lumpur*, Malaysia, 32.

[13] Oo, Z.N., Zaw, K. and Mernagh, T. (2010) Geological setting and nature of mineralization at Meyon gold deposit, Mon State, Myanmar. *13th Quadrennial International Association on Genesis of Ore Deposits (IAGOD) Symposium*, Adelaide, 6-9 April 2010, CD-ROM.

[14] Oo, Z.N. and Zaw, K. (2015) Geology and mineralization characteristics of Meyon gold deposit, Mon State, Southern Myanmar. *The Society of Economic Geologists Conference*, 27-30 September 2015, Hobart, CD-ROM.

[15] Audétat, A., Pettke, T., Heinrich, C.A. and Bodnar, R.J. (2008) The composition of magmatic-hydrothermal fluids in barren and mineralized intrusions. *Economic Geology*, 103, 877-908.

CHAPTER IV

Geology, mineral chemistry and fluid inclusion microthermometry of the Thae Phyu Chaung Au-Ag-Te-Bi deposit in Slate-Belt, Kyaikhto district, Mon State, Southern Myanmar

4.1 General statement

This chapter presents a detailed description of the Thae Phyu Chaung gold deposit, including the varying styles of precious and base-metal occurrences. A detailed paragenetic sequence of the mineralization and alteration is provided, together with the interpretation of fluid inclusion studies.

4.2 Deposit geology

The Thae Phyu Chaung gold deposit is hosted by black slate and slaty phyllite and is located close to the contact between the Mesozoic granitic rocks and Carboniferous to Lower Permian metasedimentary rock of Mergui Group (Fig. 4.1A, B, C). The black slate and slaty phyllite are mostly thinly laminated to thickly bedded, with foliation ranging from 2 mm to 3 cm thick (Fig. 4.2a, b, c). Black slate with a blocky form in outcrop is a very fine-grained rock with a dark grey to black in color. Altered wall rocks with pyrite disseminations are highly mineralized. The distribution of rock units in the area was partly determined by at least three episodes of faulting (e.g., F_1, F_2, and F_3) (Fig. 4.1A, C). However, the existence of almost the complete range of rock units within the area is determined largely by the zone of NNE-SSW trending normal fault.

The Thae Phyu Chaung gold deposit is characterized mainly by vein-style mineralization. The gold-bearing quartz vein is hosted in fracture system the N 10° W

trending. Quartz veins strike N-S and dip 65–80° to the east and are several meters in width and up to 100 m long along strike. Veins mostly followed normal and strike-slip faults. Gold mineralization within and adjacent to the F_1 and F_2 Fault are coincident over a strike length of 3.2 km. The most veins trend NNE-SSW and can be grouped into parallel vein systems (Fig.4.1A). The strike of veins at the Shaft II is same that at the shaft III trending a north-south (Figs.4.1B and 4.2a, b).

Vein morphologies and shapes vary across the deposit with the most common vein type being straight-walled and parallel-sided. In the Shaft III vein occurs as a series of en-echelon quartz veins that strike north-south and dip 45°-65^{o} to the east and are several meters in width and up to 100 m long along strike and was strongly faulted, pinched and swelled, brecciated (Figs. 4.1B and 4.2d). Especially, the veins at the Shaft I and II are banded and sheeted and also closely associated with argillic alteration zone (Fig.4.2a).

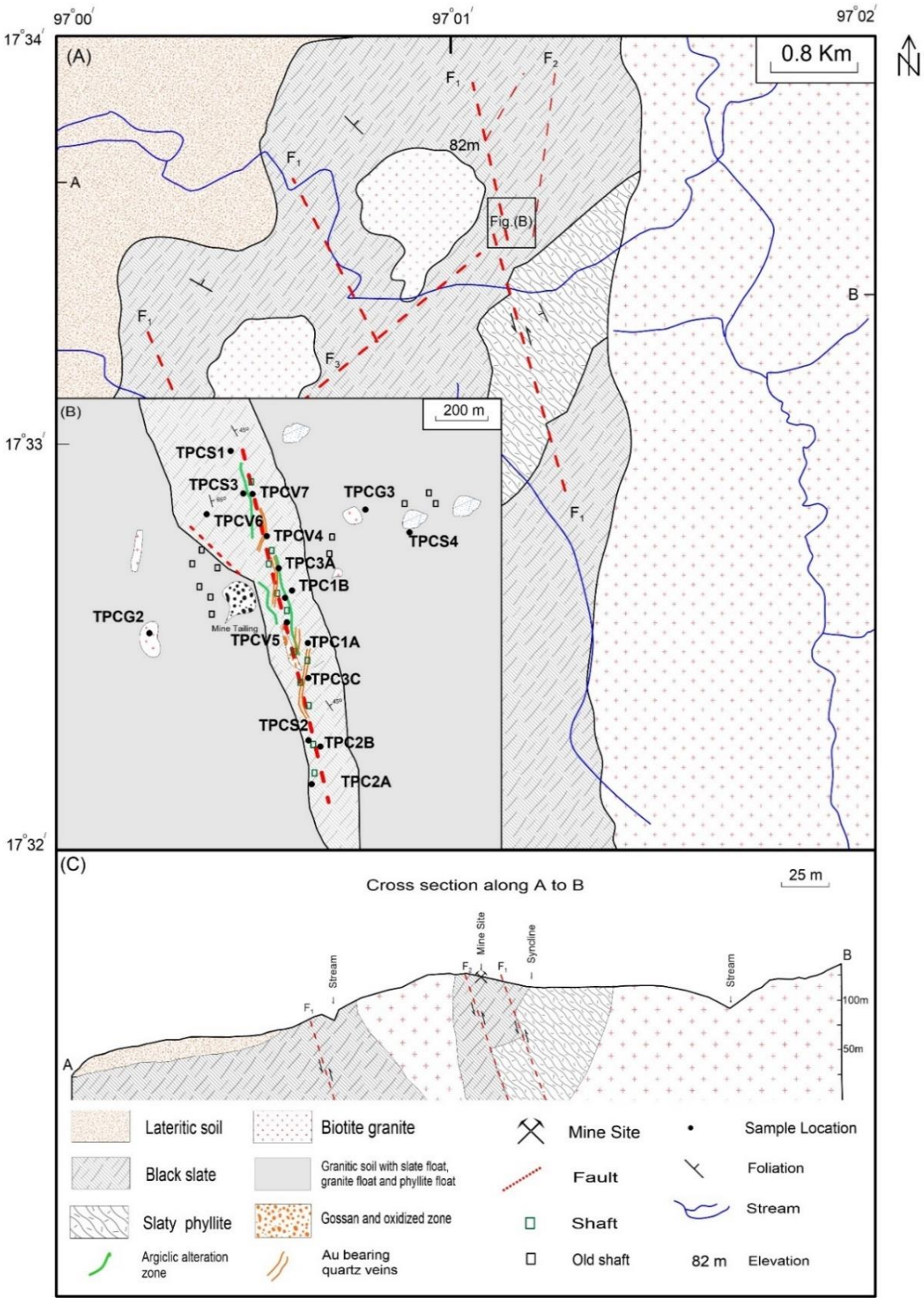

Fig.4.1 (A) Geological map of the Thae Phyu Chaung gold deposit, (B) Mineralization map of the Thae Phyu Chaung gold deposit, and (C) Cross section along the A to B of the Thae Phyu Chaung gold deposit.

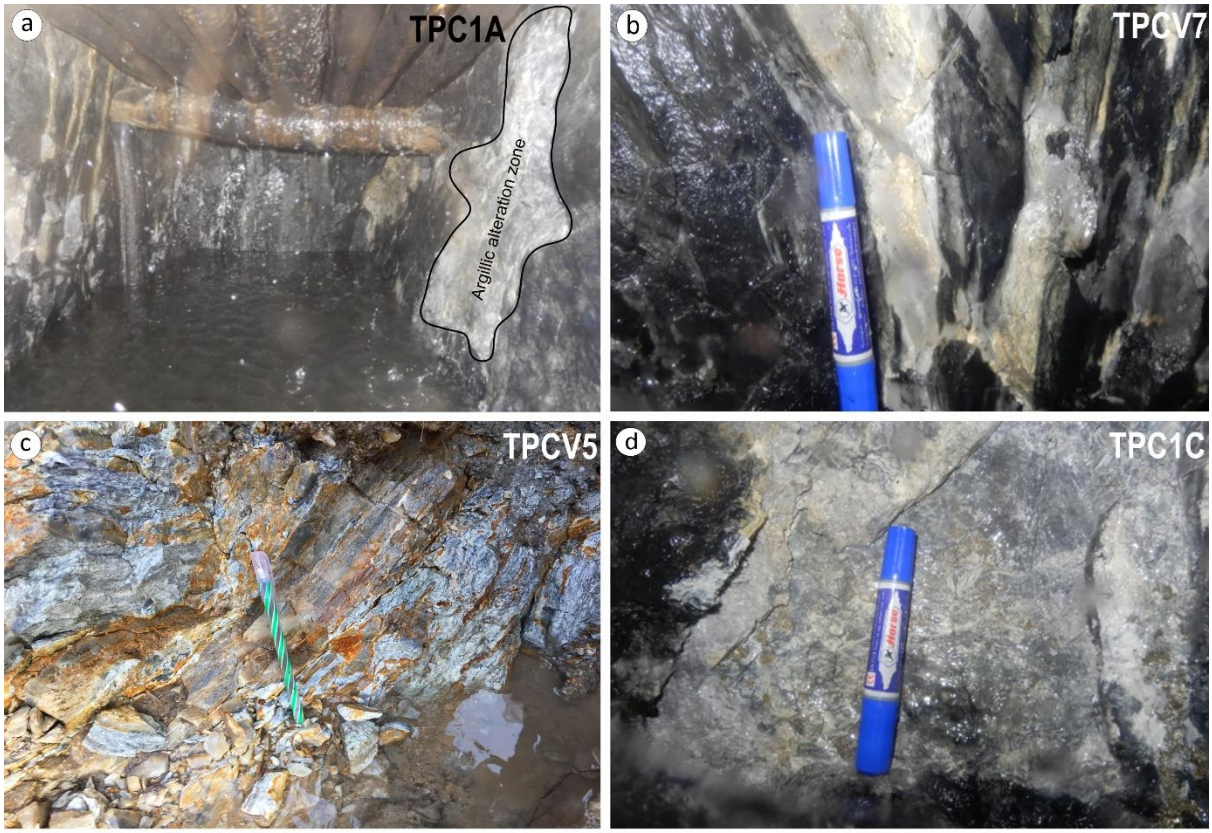

Fig. 4.2 (a) Photographs showing nature of gold-bearing quartz vein hosted by black slate with argillic alteration zone at the Shaft I of the Thae Phyu Chaung gold deposit, (b) gold-bearing quartz vein about 1m thickness at the Shaft I of the Thae Phyu Chaung gold deposit, (c) nature of bended and sheeted gold-bearing quartz vein at the Shaft III of the Thae Phyu Chaung gold deposit, (d) distorted vein by the effects of shear at the Shaft III of the Thae Phyu Chaung gold deposit.

4.3 Petrography of gold-bearing quartz veins

The major gangue minerals in the analyzed samples are quartz. The gangue minerals are composed of up to 80% quartz with sericite, chlorite and kaolinite in the gold-bearing quartz veins. Paragenetic stages of quartz veins were studied based on mineral assemblages, cross-cutting relations, and textual evidence. Petrographically, all gold-bearing quartz vein show a relatively consistent texture and paragenetic sequence, which can be organized into three stages (Fig. 4.3a, b, c). Quartz is milky to clear in color, and from microcrystalline to coarse crystalline of several micrometers in grain size in gold-bearing quartz veins. Three stages of quartz generation were recognized in gold-bearing quartz veins correspond to the paragenetic stage I, II and III, respectively. The stage I quartz is coarse-grained, anhedral, and typically exhibits undulose extinction and straight grain boundaries between the quartz grains in gold-bearing quartz veins (Fig. 4.4b).

In the mineralized vein sections stage I quartz formed was partially replaced by Stage II quartz along grain boundaries. Stage II quartz is dominantly medium-grained quartz. Both stage I and II quartz were crosscut by stage III quartz (Fig. 4.4d, e, f), which is fine-grained (microcrystalline), anhedral, and has irregular and interpenetrated grain boundaries. Stage III quartz also has very little to no internal deformation, as there is no apparent undulose extinction. Fine-grained veinlets of stage III quartz intersect stage I and II quartz. Some veins contain very fine-grained stage III quartz associated with stage II quartz (Figs. 4.4a, b,c) and sometimes sulfide minerals (e.g., chalcopyrite, pyrite, galena, and sphalerite) in gold-bearing quartz veins.

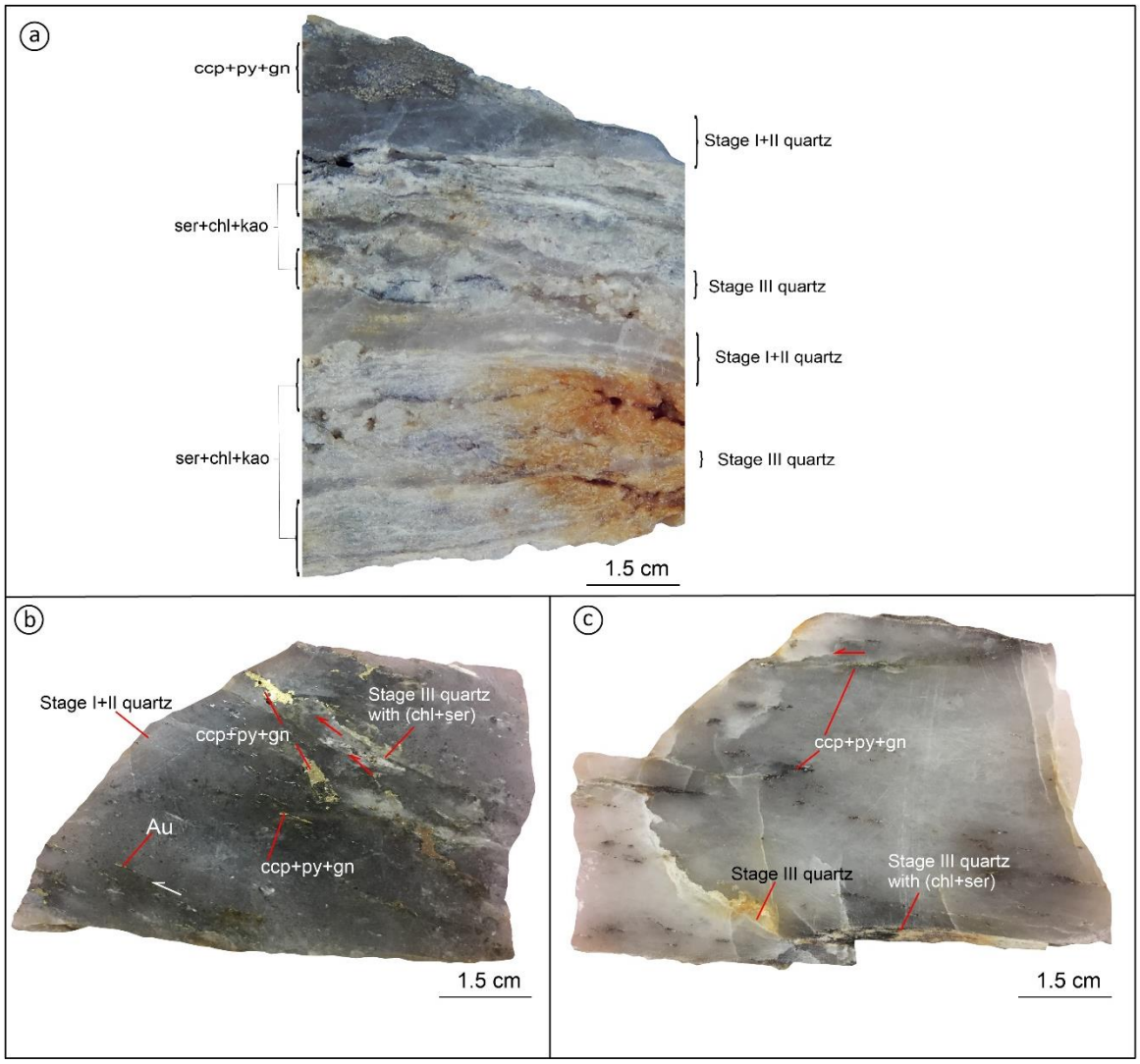

Fig.4.3 (a) Hand specimen of gold-bearing quatz veins of paragenitic stage I, II and III with chlorite (ch), kaolinite (kao) and sericite (ser) alteration, (b and c) Gold-bearing quartz veins of paragenitic stage I, II and III with sulfide and alteration minerals. Note bands enriched in gold (Au) white arrow and red arrow. ccp: chalcopyrite, py:pyrite,gn:galena, sph:sphalerite.

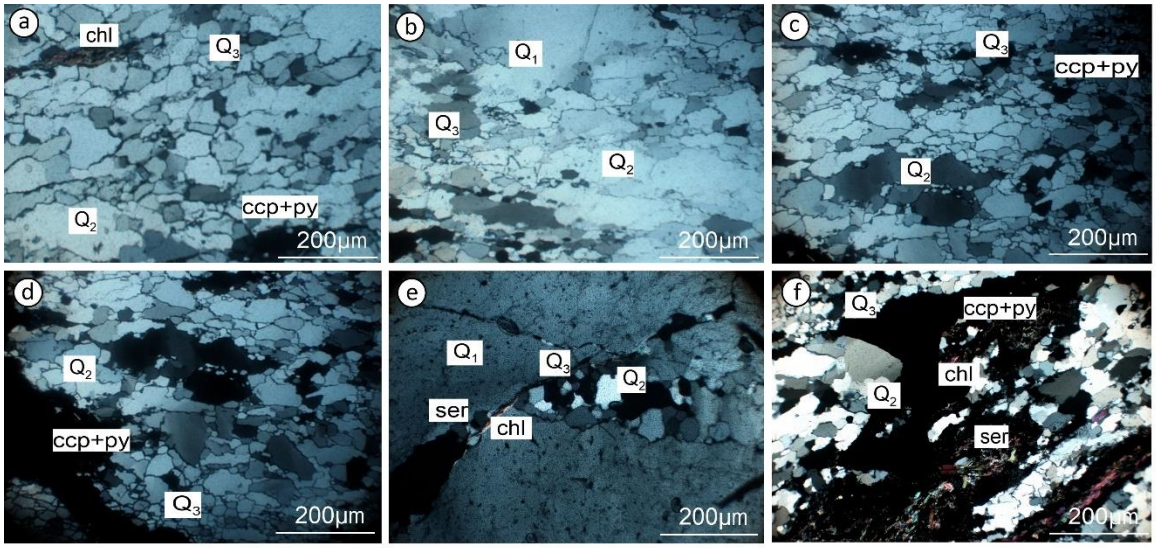

Fig.4.4 Photomicrographs of quartz under crossed polars (a) fine to medium-grained quartz formed in late stage with chlorite (chl) in gold-bearing quartz veins, (b) coarse-grained quartz formed in paragenitic stage I quartz (Q_1) with stage II quartz (Q_2) and paragenitic stage I, II and III in gold-bearing quartz veins, (c,d) fine to medium-grained paragenitic stage II quartz (Q_2) quartz associated sulfide minerals and paragenitic stage III quartz (Q_3) in the gold-bearing quartz vein, (e) different paragenitic stages I-III quartz (Q_1-Q_3) with chlorite (chl), sericite alterration in gold-bearing quartz veins and (f) paragenitic stages II-III quartz (Q_2-Q_3) which was filled by late sulfide that was formed by alteration of fine-grain sericite (ser), chlorite (chl) in the gold-bearing quartz vein.

4.4 Hydrothermal alteration

The Thae Phyu Chaung gold deposit comprises several zones of alteration with general trends of NS and NE (Figs. 4.1B and 4.5d, g). Alteration and mineralization paragenesis of the Thae Phyu Chaung gold deposit has been established through detailed observations of crosscutting and overprinting relationships, showing the trend and the shape of the various alteration zones (argillic, propylitic), as defined based on their relative content in specific minerals. Sericitization is located in the outer zone of chloritization (Fig.4.5e, f). The field observation, X-ray diffraction analysis and microscopic examination of the Thae Phyu Chaung deposit clarified that have been altered to a moderate to intensely developed pervasive magnetite–hematite-chlorite±sericite±epidote±pyrite assemblage (Table 4.1).

The presence of epidote and magnetite were confirmed by XRD and SEM-EDS analysis. The epidote alteration typically occurs as massive zones that have overprinted primary features within the black slates. The strongly altered rocks adjacent to gold-bearing quartz veins are typically rich in sulfide minerals. The following alteration characters are recognized in the Thae Phyu Chaung gold deposit. The most common alteration types in the deposit are argillic alteration and propylitic alteration which were formed close to the gold veins (Fig.4.5a, b, c). Argillic alteration is most common in the marginal zone of black slate and mostly characterized by the presence of illite + kaolinite ± smectite± sericite. Propylitic alteration also occurs in the inner zone of black slate and slaty phyllite. Hydrothermal alteration and mineralization of the areas studied are presented below and summarized in Table 4.1.

4.4.1 Propylitic alteration

Propylitic alteration is the most widespread alteration in the eastern part of the Thae Phyu Chaung deposit at the deep level (Fig. 4.18). Propylitized rocks consist of epidote, chlorite, sericite, carbonate, pyrite, Fe-oxides. Propylitic alteration is mainly related to paragenitic I, II in gold-bearing quartz veins. The altered slate consists of muscovite with sericite and chlorite microaggregates, carbonate and fine-grained pyrite. Some of the altered slaty phyllite consist of interlocking crystals of equigranular anhedral quartz, acicular crystals and radiating aggregates of pale green to green chlorite (Fig. 4.5d, e,f). Sulfides are sparsely disseminated throughout the altered slate and totally altered to limonite.

4.4.2 Argillic alteration

This alteration zone is mainly characterized by the presence of illite + kaolinite ± smectite and pyrite. Argillic alteration is closely associated with paragenetic stage II, III quartz in gold-bearing quartz veins (Fig. 4.5g, h, i). Illite and kaolinite were initially logged as ‘sericite’. This alteration is observed in metasediments and oxidization zone. Fine-grained anhedral to subhedral quartz + sericite and sulfides filled in fractures. Residual cavities are infilled by kaolinite (Fig. 4.5g, h, i). Locally the sericite forms hairline veinlets within the quartz. The altered slate consists of illite, kaolinite, and quartz. Scarce biotite has been completely replaced by fine chlorite. Within this alteration zone, kaolinite is generally more widely distributed towards the transition to propylitic alteration zone.

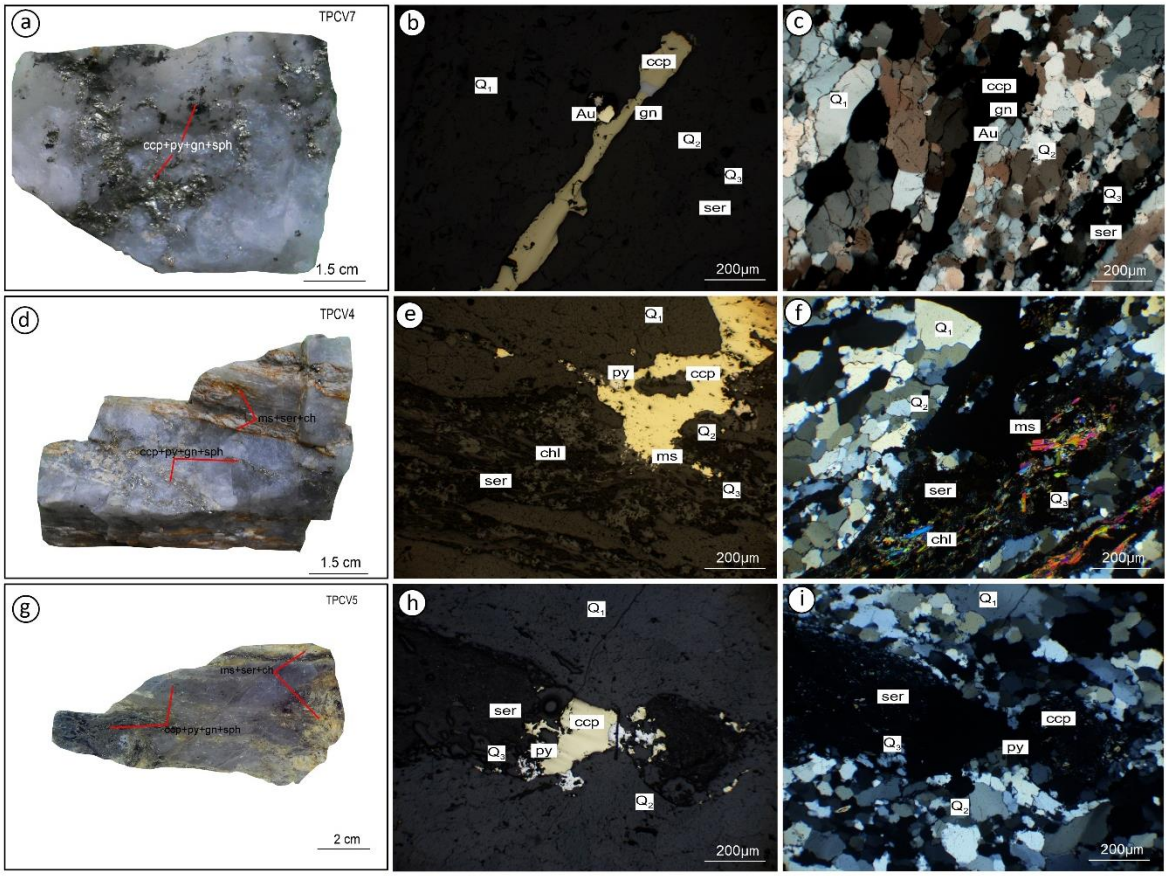

Fig. 4.5. (a,d and g) hand specimen in paragenetic stage I-III of gold-bearing quartz veins. Photomicrograph showing (b and c) native gold (Au) associated with paragenetic stage I (Q_1),II (Q_2) and III (Q_3) quartz, galena (gn), chalcopyrite (ccp) ,chlorite (chl) and sericite(ser) of gold-bearing quartz vein, (e and f) chalcopyrite (ccp) associated with paragenetic stage I (Q_1),II (Q_2) and III (Q_3) quartz, pyrite (py), chlorite (chl) and sericite(ser) in gold-bearing quartz vein, (h and i) chalcopyrite (ccp) associated with paragenetic stage I (Q_1),II (Q_2) and III (Q_3) quartz, pyrite (py) chlorite (chl) and sericite(ser) of gold-bearing quartz vein.

Table 4.1. Summary of hydrothermal alteration from orientated samples analyzed by XRD and thin section

Sample No & Depth	Rock Name	Kaolinite	Smectite	Illite or Sericite	Epidote	Chlorite	Chlorite/smectite mixed layer	Carbonate
TPC1A (70m)	Silicified slate	+++		+++			+	
TPC1B (70m)	Altered slate		+	+++		+		
TPC1C (70m)	Altered slate			+++		+	+	
TPC3C (70m)	Altered slate	++	+	+++				+
TPC2B (70m)	Altered slate	+++		+++		+++		
TPC2A (70m)	Altered slate			+++		++		
TPCS4 (70m)	Black Slate	+++		+++			+	
TPCS7 (80m)	Black Slate	++		+++			+	+
TPCS4 (85m)	Black Slate	+	+	+++			+	+
TPCS5 (85m)	Black Slate	+		+++			+	
TPCS15 (85m)	Slaty phyllite	+		+++				
TPCS2 (80m)	Slaty phyllite			+++	+	+		+
TPCS3 (85m)	Slaty phyllite			+++	+	+		+
TPCS4 (85m)	Slaty phyllite			+++		+		+

Notes: +++ Common, ++ Few, + Rare

4.5 Mineral parageneses

The hydrothermal mineralization in the Thae Phyu Chaung deposit can be divided into four paragenetic stages based on crosscutting and overgrowth (Fig.4.6). The paragenetic stages are as follows:

4.5.1 Stage I (Fe-As)

Stage I (Fe-As) is the first mineral assemblage to fill fissures, and this early event is commonly accompanied by propylitic alteration of adjacent wall rock. It consists of of pyrite I, arsenopyrite and coarse-grained Stage I quartz of gold-bearing quartz veins (Fig. 4.8a, f). Clear coarse-grained euhedral Stage I quartz is very common along vein margins with wall rocks during this stage. Pyrrhotite also occurs with chalcopyrite. Euhedral arsenopyrite and pyrite up to few micrometers in size are finely disseminated in the wall rocks. Pyrite I is more abundant than arsenopyrite and pyrrhotite.

4.5.2 Stage II (Cu-Pb-Zn)

Stage II (Cu-Pb-Zn) was deposition of base metal sulfides (e.g., galena, sphalerite, and chalcopyrite). Ore minerals in Stage II quartz include Type I and II of telluride minerals assemblages with native gold (Type I gold), electrum (Type III gold) galena, sphalerite, pyrite, famatinite, and chalcopyrite in this stage. Chalcopyrite is commonly partially replaced by later sulfides (e.g., galena, sphalerite and pyrite II). It is characterized by coarse-grained sphalerite, galena and chalcopyrite intergrown with medium-grained Stage II quartz (Figs. 4.8c, d, h).

A pervasive fine-grained quartz-sericite-pyrite alteration of proximal wall rock is associated with this stage. Minor, fine- to medium-grained pyrite II and hematite are found within sphalerite. Chalcopyrite is commonly only several microns in scale but can be several

millimeters in scale when replacing pyrite II grains or pyrite II aggregates. Coarse-grained chalcopyrite accompanies sphalerite.

Type I of native gold and electrum (Type III gold) also accompanies this stage and occurs as fine-medium grains in chalcopyrite. Sphalerite appears to selectively replace and fill fractures within chalcopyrite grains (Fig. 4.8c). Galena is found as large anhedral aggregates of finer grained crystals. Stage II quartz is often enclosed in galena, sphalerite, and chalcopyrite, indicating that fracturing took place during their deposition.

4.5.3 Stage III (Au-Ag-Te-Bi-Sb)

Stage III (Au-Ag-Te-Bi-Sb) was the main ore stage. Stage III quartz is commonly accompanied with argillic alteration in gold-bearing quartz veins during this stage. Type I and II of native gold occurred with pyrite as inclusions, or along the fissure veins of pyrite and chalcopyrite, galena, sphalerite and also associated with Type I, II and III telluride minerals assemblages in Stage III quartz of gold-bearing quartz veins (Fig. 4.7a, b,c). Stage III quartz is distinguished from Stage II quartz by lacking associated pyrite II. Mineralization is found as late overgrowths on earlier minerals or as infill. Stage III quartz is transparent subhedral to euhedral and commonly lines vugs.

Electrum (Type III gold) was also found in grain boundaries between sphalerite, galena and Type I, II and III telluride minerals assemblages with Stage III quartz of gold-bearing quartz veins. The tellurides are included either in galena, chalcopyrite, and sphalerite, or they always occur at the grain boundaries between sphalerite and galena. The native bismuth and silver minerals replaced in arsenopyrite and galena. Hedleyite occur along grain boundaries between arsenopyrite, galena, and chalcopyrite. Gudmundite also occurs as

inclusions in chalcopyrite and famatinite (Fig. 4.8g). Type I and II native gold and electrum (type III gold) were mostly deposited in this stage.

4.5.4 Stage IV (Fe-O)

Stage IV (Fe-O) includes unnamed mineral (Au+Sb), covellite, hematite, magnetite, and kaolinite as a gangue. Hematite occurs as a replacement of chalcopyrite and sphalerite. There are a few samples where pyrrhotite and pyrite are altered to hematite and magnetite. In most cases, hematite is secondary after pyrite and magnetite, which indicates that the system is oxidizing, because hematite is a common dissolution product of pyrite. Unnamed mineral (Au+Sb) could be decomposed form petzite and native gold (Fig.4.9b).

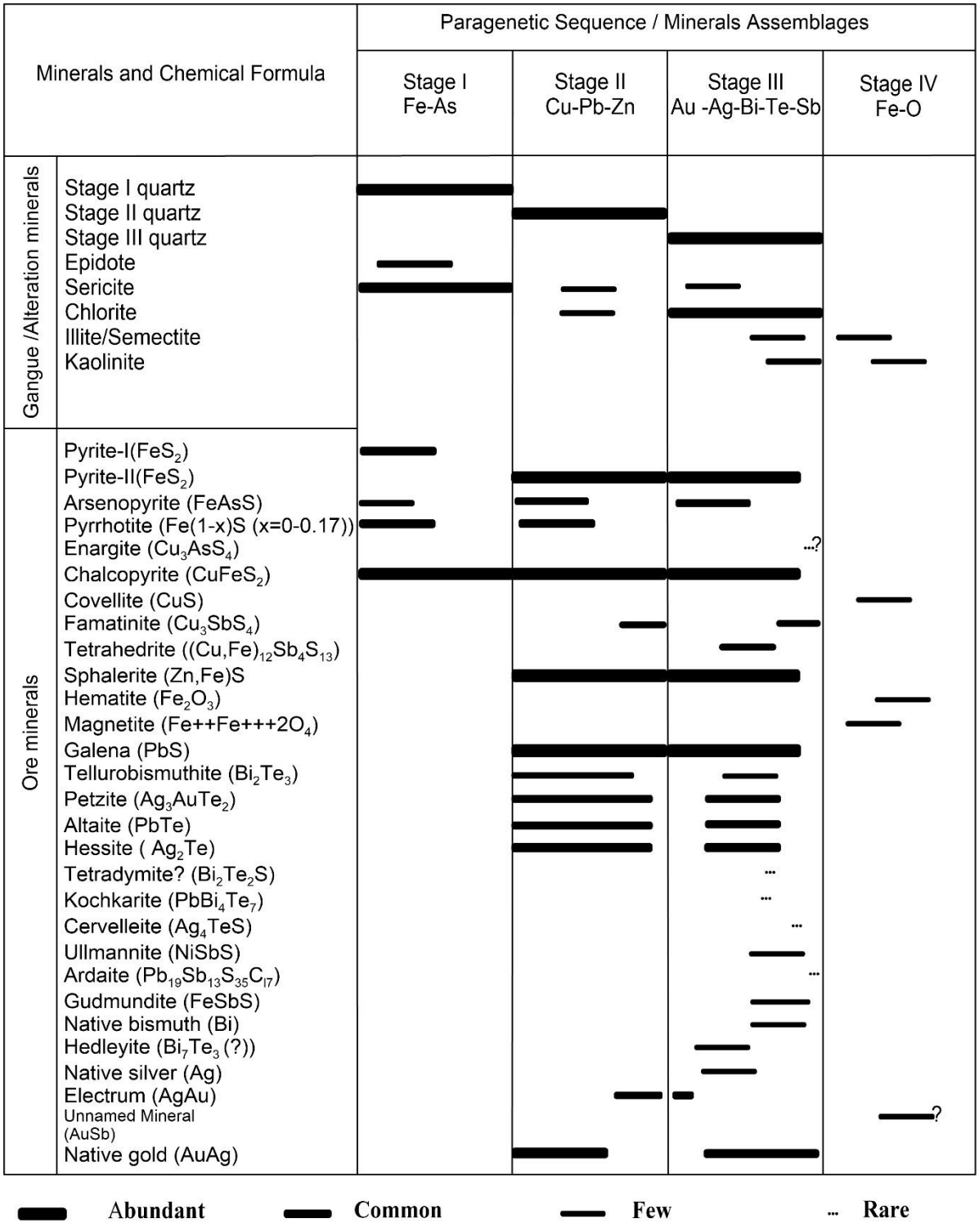

Fig. 4.6 Paragenetic sequence of mineral deposition in the Thae Phyu Chaung gold deposit.

4.6 Ore mineralogy and mineral chemistry

4.6.1 Sulfide minerals

The sulfide minerals are enclosed almost exclusively in paragenetic stage II and III quartz of gold-bearing quartz veins, or they form veinlets in the paragenetic stage I grain boundaries and in fractures. Pyrite of both first and second generations are the dominant ore mineral in the Thae Phyu Chaung gold deposit. Pyrite I is found in the paragenetic Stage I dispersed in host rocks or are aggregated coarse-grained euhedral (idiomorphic) crystals and aggregates of numerous intergrown crystals in veins (Fig.4.9a).

The pyrite I crystals commonly range in size between 50 μm and 2-3 mm. Pyrite I is closely related with chalcopyrite of the paragenetic stage I of gold-bearing quartz veins. Almost always pyrite II forms subhedral strongly fractured grains. Pyrite II associated with galena, sphalerite, chalcopyrite and native gold inclusion in the quartz of paragenetic Stage II of gold-bearing quartz veins (Figs. 4.7, 4.8 and 4.9).

Pyrrhotite is subhedral to elongated with chalcopyrite of the paragenetic stage I (Fig. 3.8f). Arsenopyrite is closely related with chalcopyrite, galena and Bi-Te minerals (Fig.4.9a, b). Pyrrhotite crystals exhibit platy or isometric shapes. Chalcopyrite is rimmed or crosscut by pyrite II and/or sphalerite (Fig. 4.8c, d). Both pyrite and sphalerite frequently form grain aggregates several cm in size (or locally millimeter-sized subhedral crystals). Galena form subhedral to anhedral grains, which accompany chalcopyrite, sphalerite, pyrite, telluride minerals, electrum, and native gold. Chalcopyrite was rimmed and crosscut by pyrite II of the paragenetic stage II.

Gudmundite occurred as inclusions in famatinite and chalcopyrite (Fig.4.8g). The Fe content of sphalerite varies from 9.5 to 11.2at % for the sphalerite of the paragenetic stage I, from 6.8 to 8.7 at % for the sphalerite of the paragenetic stage II, from 3.7 to 4.8 at % for the sphalerite of the paragenetic stage III and correspond to 9 to 12 mol % for Stage I, 6 to 9 mol % for stage II and 3 to 5 FeS mol % for stage III, respectively (Table 4.2).

4.6.2 Telluride minerals

Telluride minerals occur in the paragenetic Stage II and III of gold-bearing quartz veins. Three types of telluride minerals assemblage can occur as Bi-telluride (hedleyite, tellurobismuthite), Pb-telluride (altaite) and Ag+Au tellurides (petzite, hessite) in paragenetic stage II and III. Tellurobismuthite (Bi-telluride) is commonly found in contact with galena and altaite and bladed intergrowth texture (Fig. 4.7). Altaite occurs in contact with hessite, petzite, electrum, and native gold. Hessite (Ag_2Te) is by far the most common telluride mineral found in the samples. It is almost always found in contact with or very near petzite (Ag_3AuTe_2). Petzite is present as minute grains within blebs of hessite or as coarser inclusions surrounded by hessite (Fig. 4.7a, b, c). The subhedral shape of some petzite inclusions, suggests co-crystallization of hessite and petzite. Petzite occurs also as skeletal flakes in hessite or as inclusions. Hessite mainly occurs as composite blebs within galena (Fig. 4.7a, c), altaite and chalcopyrite. Most hessite is closely associated with petzite, electrum and/or native gold and altaite.

Bi+Te minerals occur as fine subhedral to bladed grains intergrown with and disseminated in arsenopyrite, galena, and chalcopyrite. Native Bismuth occurs as inclusions in bismuth telluride and arsenopyrite (Fig.4.10a, b). The telluride minerals identified include petzite (Ag_3AuTe_2), altaite (PbTe), hessite (Ag_2Te), cervelleite? (Ag_4TeS), hedleyite?

(Bi_7Te_3), tetradymite? (Bi_2Te_2S). The composition of the telluride minerals is listed in Table 4.3.

Three types of coexisting tellurides minerals are distinguished when plotted in the Au–Ag–Te ternary system (Fig.4.12) (Afifi *et al.,* 1988). Type-I is coexistence of hessite, pezite, native gold and electrum in paragenetic stage II and III of gold-bearing quartz veins, suggesting that chemical composition of native gold had been controlled by the Au–Ag–Te system (eg., Nakata *et al.,* 2011). Type II includes hessite, pezite, electrum and native silver (up to 68.9 wt. % Ag), silver-rich assemblage in the paragenetic stage II and III of gold-bearing quartz veins. The mineralization of this type would not be Au- rich as compared to Type I. The Type-III consists of various Pb-Te-Bi minerals such as altiate, kochkarite, tellurobismuthite, hedleyite, native bismuth, in the paragenetic stage III.

4.6.3 Gold-silver minerals

Native gold is the only economically important ore mineral in the Thae Phyu Chaung gold deposit. It is present in almost all the investigated polished sections. Three distinct types of gold were distinguished according to the mode of occurrences. The first type is deposited in veinlets and voids in chalcopyrite, galena, sphalerite, pyrite II and telluride minerals in paragenetic stage II and III of gold-bearing quartz veins. (Figs. 4.8b and 4.9a, c, e,g). This native gold is located only inside the grains of the above-mentioned host minerals (Fig. 4.6a, b,c).

The second type of native gold is courser (up to 100 μm) and was deposited both in chalcopyrite, galena, unnamed mineral (Au+Sb) in paragenetic stage II and III of gold-bearing quartz veins and also occurs as free grains (Figs. 4.9b, h and 4.11a, b,c). Native gold is genetically associated with chalcopyrite galena, sphalerite and native gold inclusions in pyrite

II (Fig.4.9a). The type three of gold is electrum which is mainly associated with sphalerite, famatinite, galena, chalcopyrite and native bismuth in paragenetic Stage II and III of gold-bearing quartz veins. (Fig. 4.9d, f). Silver contents of the native gold range between 4.4 and 16.9 at % Ag. The Ag of electrum contains vary from 21.1 to 79.6 at% Au (Table 4.3).

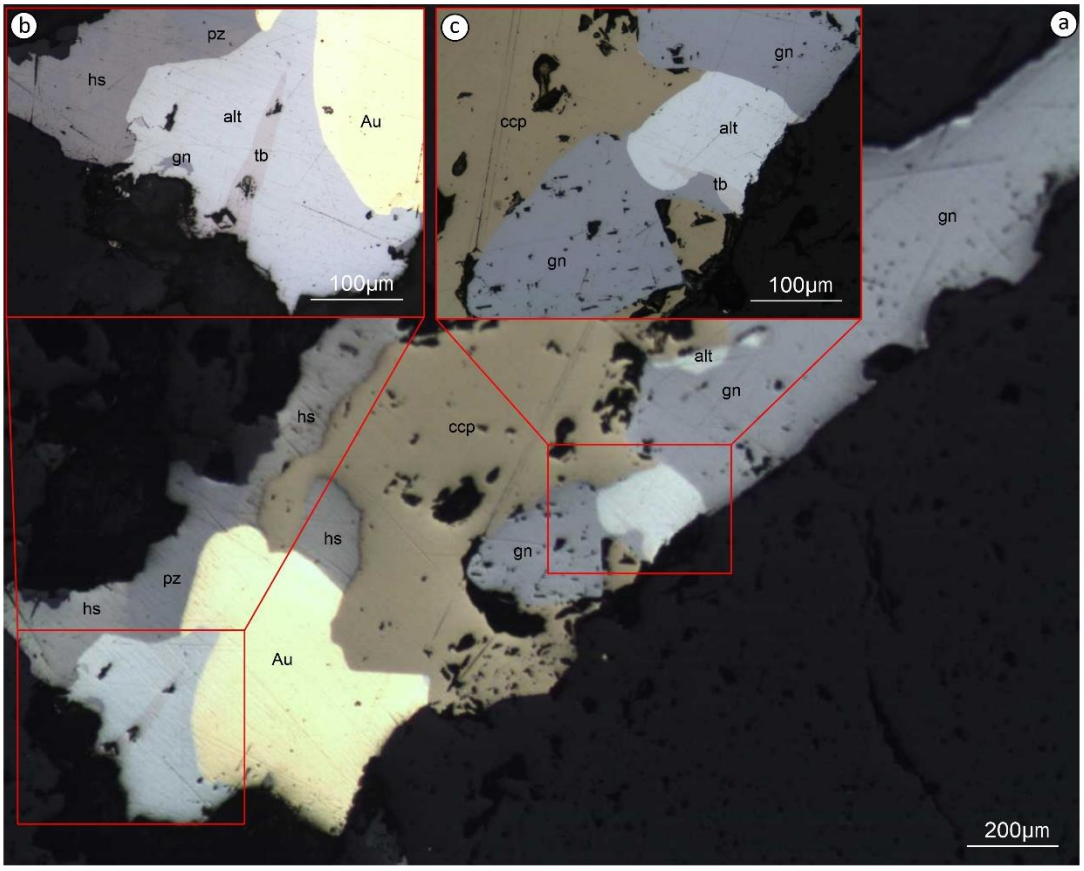

Fig. 4.7(a) Photomicrographs showing native gold (Au) associated with galena(gn), tellurobismuthite (tb), hessite (hs), pezite (pz) and chalcopyrite (ccp) in paragenetic stage II and III of the gold bearing quartz vein, (b) native gold (au) associated with altaite (alt) (PbTe), tellurobismuthite (tb) (Bi_2Te_3), galena (gn), hessite (hs), pezite (pz) in paragenetic stage II and III of the gold bearing quartz vein, (c) chalcopyrite associated with altaite (alt) (PbTe), tellurobismuthite (tb) (Bi_2Te_3) and galena (gn) in paragenetic stage II and III of the gold bearing quartz vein.

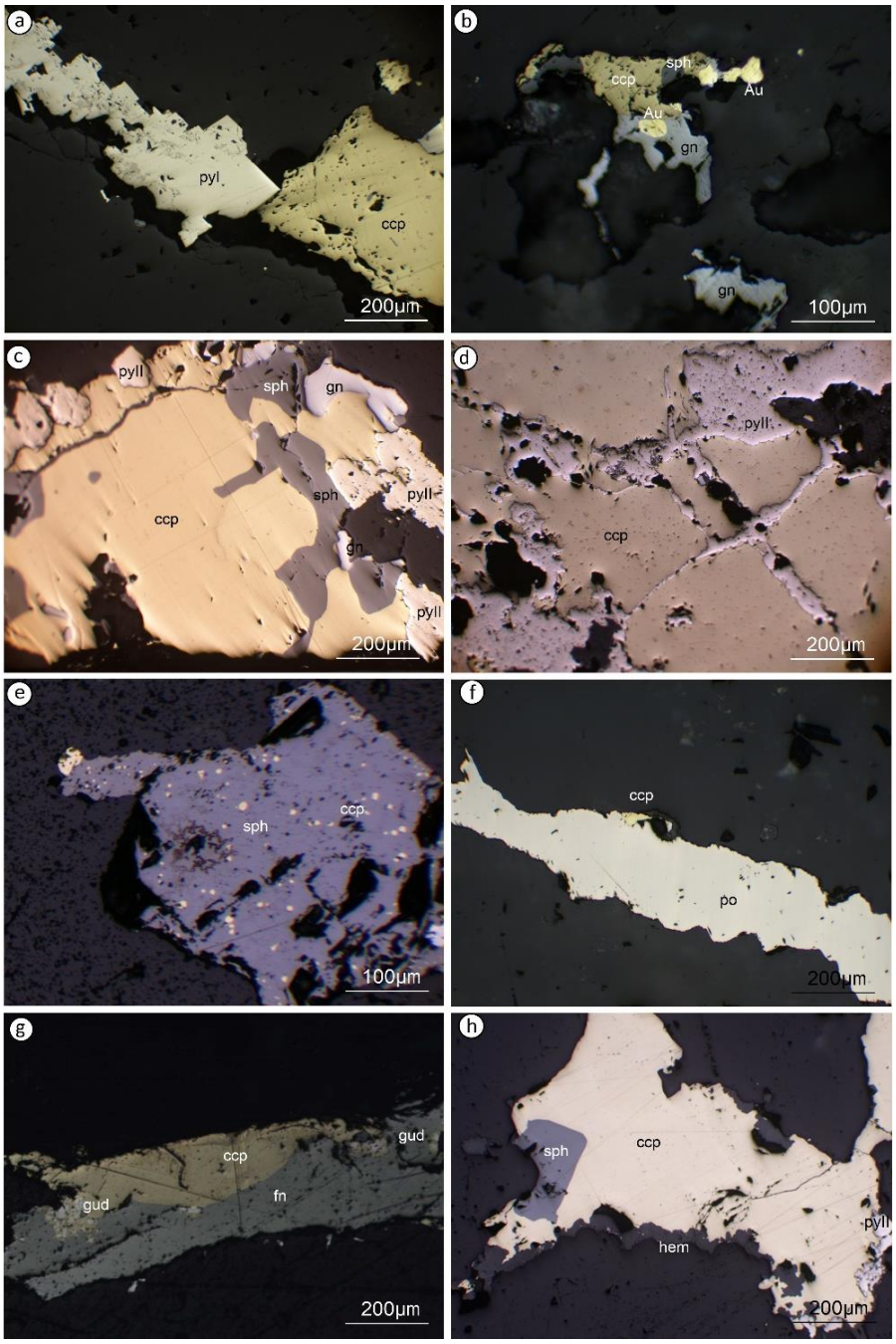

Fig. 4.8(a) Photomicrographs of chalcopyrite (ccp) associated with early pyrite (py I) in paragenetic stage I of the gold bearing quartz vein, (b) native gold (Au) inclusions in galena (gn) associated with chalcopyrite (ccp) and sphalerite (sph) in paragenetic stage II and III of the gold bearing quartz vein, (c) sphalerite (sph) associated with late pyrite (py II), early chalcopyrite (ccp) and galena (gn) in paragenetic stage II and III of the gold bearing quartz vein, (d) pyrite (py II) fracture fillings within chalcopyrite (ccp), (e) chalcopyrite (ccp) inclusions in sphalerite (sph) filling cracks, (f) pyrrhotite (po) associated with chalcopyrite, (g) the famatinite (fn) associated with gudmundite (gud) and chalcopyrite in paragenetic stage II and III of the gold bearing quartz vein, (h) chalcopyrite is also in contact to sphalerite (sph) and pyrite (pyII) and it is surrounded by hematite (hem) in paragenetic stage III and IV of the gold bearing quartz vein.

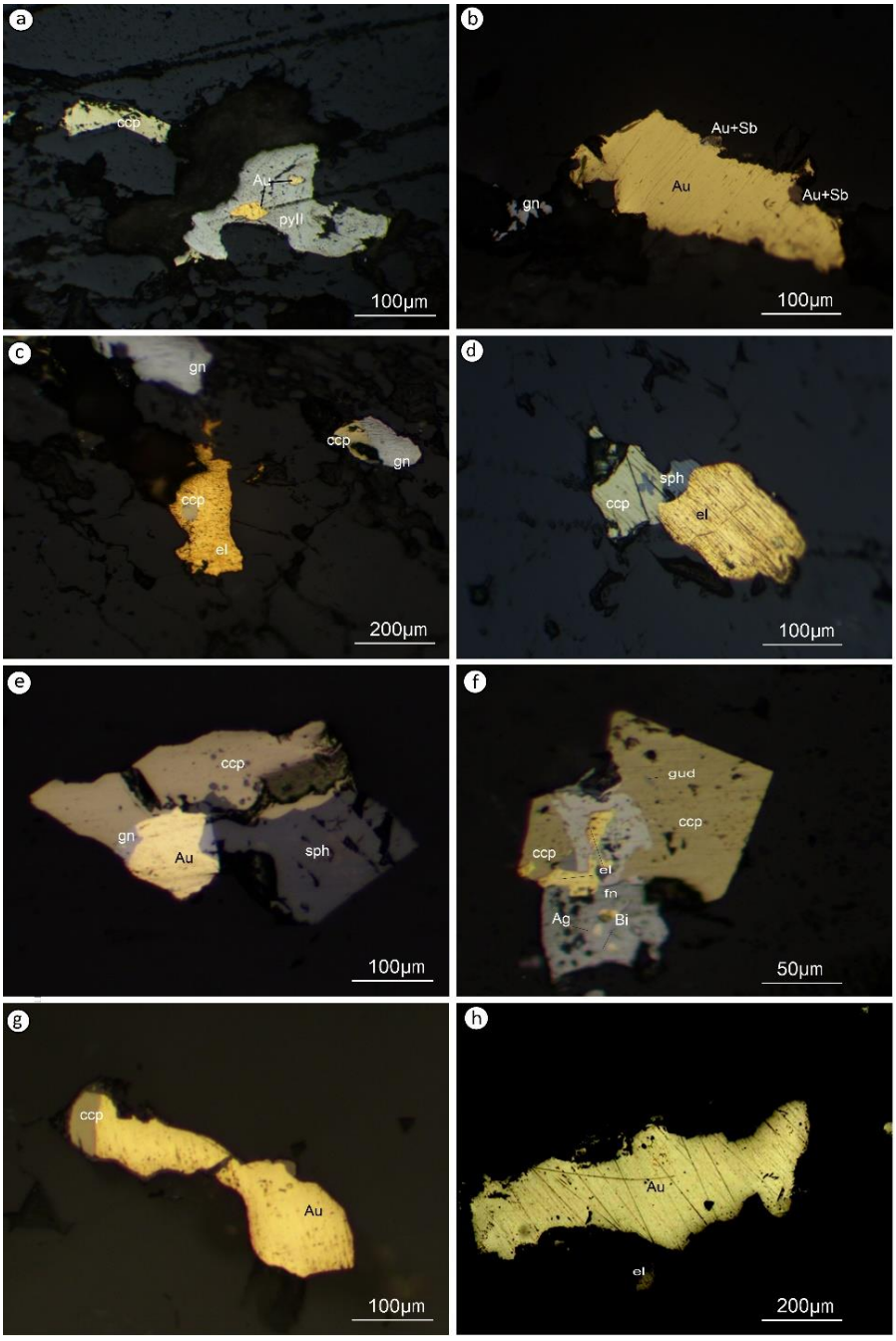

Fig.4.9(a) Photomicrographs showing native gold (Au) in late pyrite (py II) in paragenetic stage II and III of the gold bearing quartz vein, (b) native gold (Au) associated with (Au+Sb) unnamed mineral in paragenetic stage II and III of the gold bearing quartz vein, (c) chalcopyrite (ccp) in native gold (Au) in paragenetic stage III and IV of the gold bearing quartz vein, (d) electrum (el) associated with sphalerite (sph) and chalcopyrite (ccp) in paragenetic stage II and III of the gold bearing quartz vein, (e) native gold (Au) associated with galena (gn), sphalerite (sph) and chalcopyrite (ccp) in paragenetic stage II and III of the gold bearing quartz vein, (f) electrum (el) associated with native silver (Ag), native bismuth (Bi) and chalcopyrite (ccp), famatinite (fn) and gudmundite (gud) in paragenetic stage II and III of the gold bearing quartz vein, and (g) native gold (Au) associated with chalcopyrite (ccp), (h) free native gold (Au) in paragenetic stage II and III of the gold bearing quartz vein.

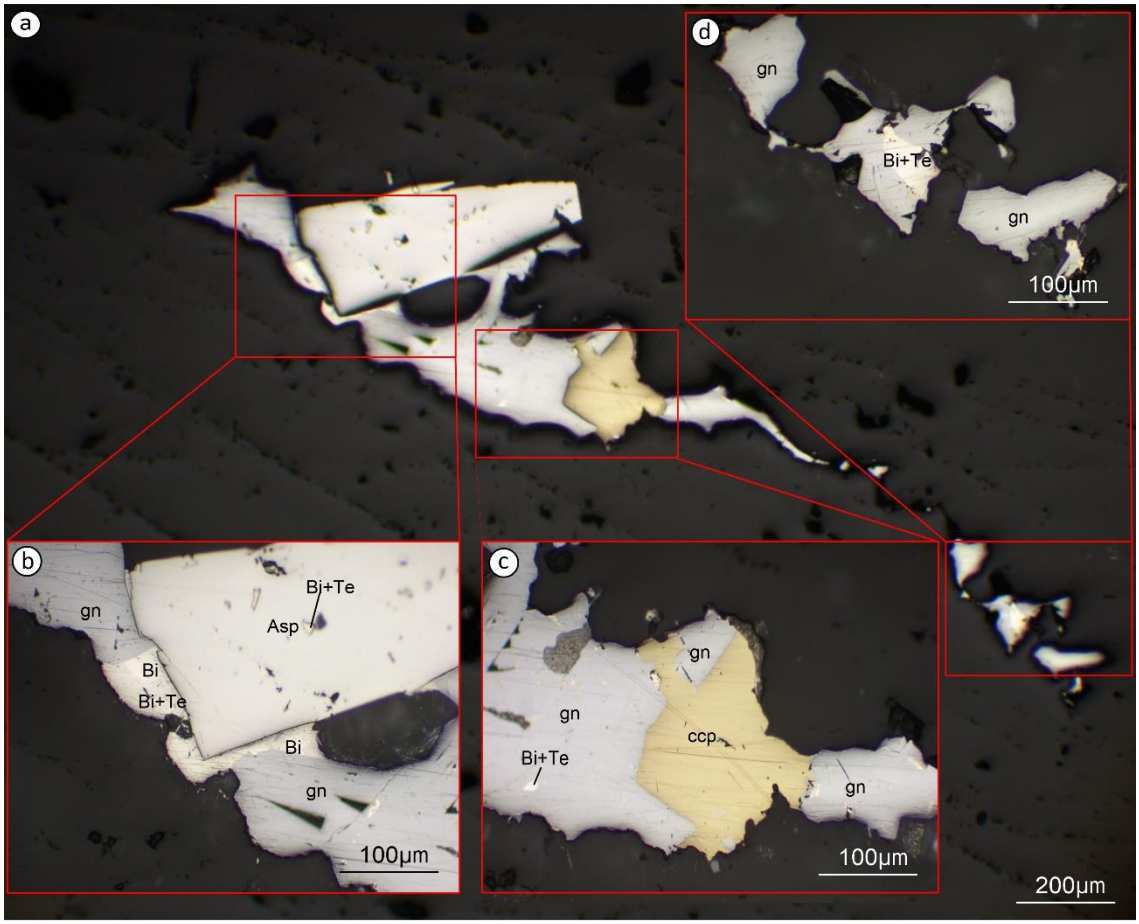

Fig. 4.10(a) Photomicrographs showing native bismuth (Bi) associated with galena (gn), arsenopyrite (Asp) and Bi+Te minerals in paragenetic stage II and III of the gold bearing quartz vein (b) arsenopyrite associated with galena (gn), native bismuth (Bi) and Bi+Te minerals in paragenetic stage II and III of the gold bearing quartz vein (c) chalcopyrite (ccp) associated with galena (gn) and Bi+Te minerals in paragenetic stage II and III of the gold bearing quartz vein.

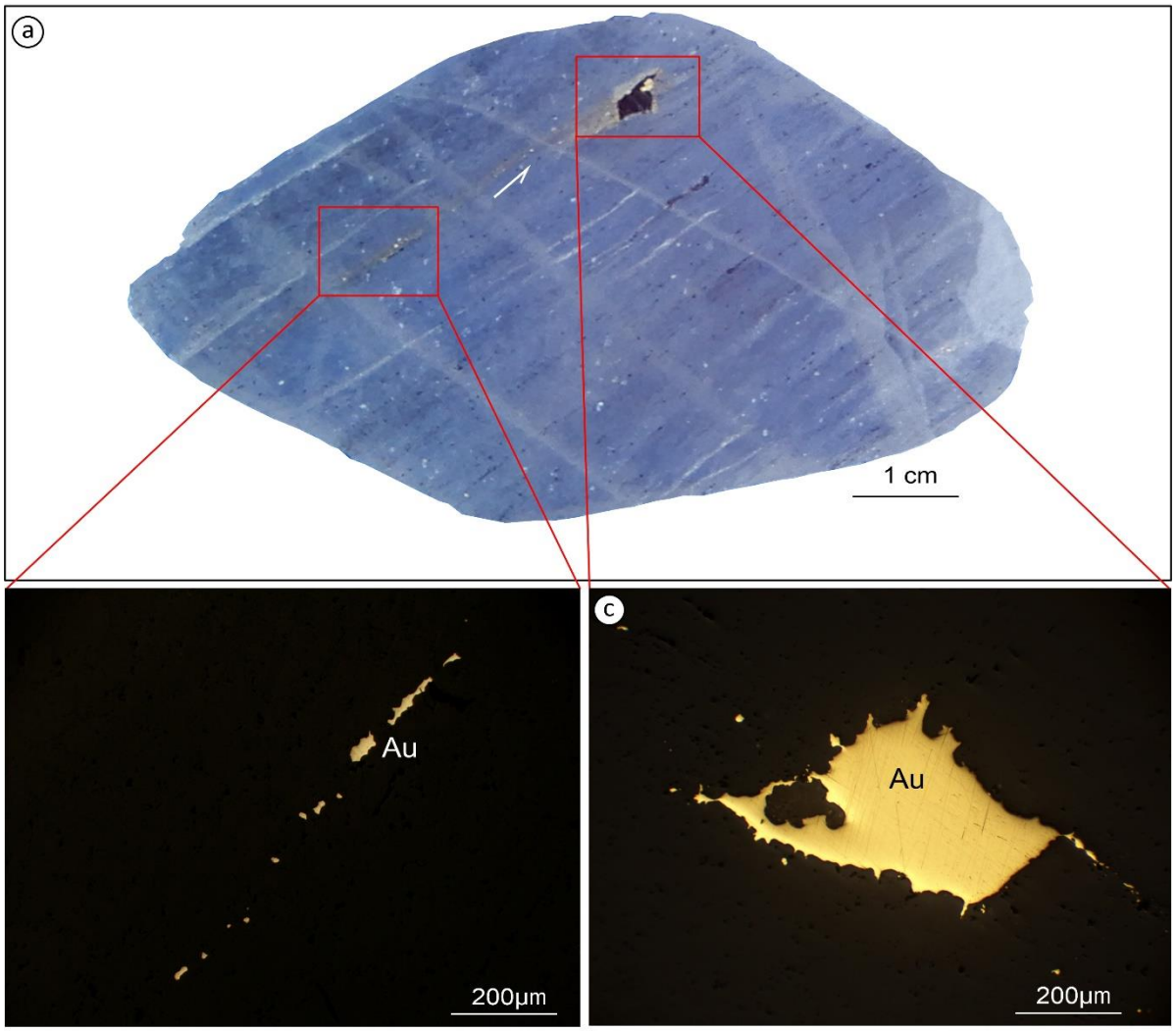

Fig. 4.11(a) Hand specimen of native free gold (Au) in paragenetic stage II and III of the gold-bearing quartz vein, (b) Photomicrographs showing free grains of native gold (Au) in paragenetic stage II and III of the gold bearing quartz vein (c) free grains of native gold (Au) in paragenetic stage II and III of gold-bearing quartz vein.

Table 4.2. Representative chemical compositions of sulfide minerals from the Thae Phyu Chaung gold deposit.

Mineral name &Formula	Samples ID& Depth	Stages	Zn	Fe	As	S	Total (wt%)	Zn	Fe	As	S	Total (at%)
			(wt%)					(at%)				
Sphalerite (ZnS)	TPCV7(85m)	Stage I	57.22	12.77	0.00	30.01	100.00	42.91	11.21	0.00	45.88	100.00
			58.79	10.88	0.00	30.33	100.00	44.09	9.55	0.00	46.36	100.00
	TPCV7(85m)	Stage II	62.25	8.76	0.00	28.99	100.00	47.30	7.79	0.00	44.91	100.00
			57.27	9.03	0.00	33.7	100.00	41.94	7.74	0.00	50.32	100.00
			57.04	8.00	0.00	34.96	100.00	41.43	6.80	0.00	51.77	100.00
	TPCV6(80m)	Stage II	56.63	10.18	0.00	33.19	100.00	41.58	8.75	0.00	49.67	100.00
			57.46	9.76	0.00	32.79	100.00	42.33	8.42	0.00	49.25	100.00
			57.29	9.47	0.00	33.24	100.00	42.08	8.15	0.00	49.77	100.00
			58.98	8.48	0.00	32.54	100.00	43.61	7.34	0.00	49.05	100.00
	TPCV5(80m)	Stage III	64.30	4.23	0.00	31.46	100.00	48.20	3.72	0.00	48.08	100.00
			61.90	4.32	0.00	33.78	100.00	45.57	3.72	0.00	50.71	100.00
	TPC047(70m)	Stage III	61.58	5.15	0.00	33.27	100.00	45.47	4.45	0.00	50.08	100.00
			60.83	5.65	0.00	33.51	100.00	0.00	4.87	0.00	50.32	100.00
Pyrite (FeS_2)	TPCV7(85m)	Stage I	0.00	46.70	0.00	53.30	100.00	0.00	33.47	0.00	66.53	100.00
			0.00	47.04	0.00	52.96	100.00	0.00	33.77	0.00	66.23	100.00
	TPCV6(80m)	Stage II	0.00	46.20	0.00	53.80	100.00	0.00	33.03	0.00	66.97	100.00
			0.00	46.35	0.00	53.65	100.00	0.00	33.16	0.00	66.84	100.00
			0.00	46.64	0.00	53.36	100.00	0.00	33.41	0.00	66.59	100.00
			0.00	46.63	0.00	53.37	100.00	0.00	33.40	0.00	66.60	100.00
			0.00	46.98	0.00	53.02	100.00	0.00	33.72	0.00	66.28	100.00
Pyrrhotite	TPCV7(85m)	Stage I	0.00	63.63	0.00	36.37	100.00	0.00	50.11	0.00	49.89	100.00
			0.00	62.62	0.00	37.38	100.00	0.00	49.02	0.00	50.98	100.00
			0.00	63.42	0.00	36.58	100.00	0.00	49.89	0.00	50.11	100.00
	TPC047(70m)	Stage I	0.00	60.70	0.00	39.30	100.00	0.00	47.00	0.00	53.00	100.00
			0.00	61.17	0.00	38.83	100.00	0.00	47.49	0.00	52.51	100.00
			0.00	61.76	0.00	38.24	100.00	0.00	48.11	0.00	51.89	100.00
Arsenopyrite (FeAsS)	TPC047(70m)	Stage I	0.00	34.73	48.97	16.30	100.00	0.00	33.20	32.01	34.80	100.00
			0.00	34.54	44.67	20.79	100.00	0.00	28.91	30.07	41.02	100.00

Determined by EDS

Normalized to 100%

Table 4.3. Representative chemical compositions of Au-Ag-Te-Bi bearing minerals from the Thae Phyu Chaung gold deposit.

Mineral name &Formula	Samples ID & Depth	Stages	Au	Ag	Te	Bi	Sb	S	Fe	Pb	Total	Au	Ag	Te	Bi	Sb	S	Fe	Pb	Total
			(wt%)								(wt%)	(at%)								(at%)
Petzite (Ag_3AuTe_2)	TPCV7(85m)	Stage II	28.43	41.3.0	30.27	0.00	0.00	0.00	0.00	0.00	100.00	18.88	50.08	31.03	0.00	0.00	0.00	0.00	0.00	100.00
			29.60	40.20	30.20	0.00	0.00	0.00	0.00	0.00	100.00	19.78	49.06	31.16	0.00	0.00	0.00	0.00	0.00	100.00
	TPCV4(75m)	Stage II	29.87	40.12	30.00	0.00	0.00	0.00	0.00	0.00	100.00	19.99	49.02	30.99	0.00	0.00	0.00	0.00	0.00	100.00
	TPCV5(80m)	Stage II	29.8	40.25	29.94	0.00	0.00	0.00	0.00	0.00	100.00	19.93	49.16	30.91	0.00	0.00	0.00	0.00	0.00	100.00
	TPCV6(80m)	Stage II	29.38	40.43	30.18	0.00	0.00	0.00	0.00	0.00	100.00	19.61	49.29	31.10	0.00	0.00	0.00	0.00	0.00	100.00
			28.60	40.80	30.60	0.00	0.00	0.00	0.00	0.00	100.00	19.02	49.55	31.42	0.00	0.00	0.00	0.00	0.00	100.00
Altaite (PbTe)	TPCV7(85m)	Stage II	0.00	0.00	39.37	0.00	0.00	0.00	0.00	60.63	100.00	0.00	0.00	51.32	0.00	0.00	0.00	0.00	48.68	100.00
			0.00	0.00	39.07	0.00	0.00	0.00	0.00	60.93	100.00	0.00	0.00	51.01	0.00	0.00	0.00	0.00	48.99	100.00
	TPCV6(80m)	Stage II	0.00	0.00	39.14	0.00	0.00	0.00	0.00	60.86	100.00	0.00	0.00	51.08	0.00	0.00	0.00	0.00	48.92	100.00
			0.00	0.00	38.82	0.00	0.00	0.00	0.00	61.18	100.00	0.00	0.00	50.75	0.00	0.00	0.00	0.00	49.25	100.00
Hessite (Ag_2Te)	TPCV7(85m)	Stage II	0.00	63.72	36.28	0.00	0.00	0.00	0.00	0.00	100.00	0.00	67.51	32.49	0.00	0.00	0.00	0.00	0.00	100.00
			0.00	63.98	36.02	0.00	0.00	0.00	0.00	0.00	100.00	0.00	67.75	32.25	0.00	0.00	0.00	0.00	0.00	100.00
	TPCV6(80m)	Stage II	0.00	63.82	36.18	0.00	0.00	0.00	0.00	0.00	100.00	0.00	67.6	32.4	0.00	0.00	0.00	0.00	0.00	100.00
			0.00	63.83	36.17	0.00	0.00	0.00	0.00	0.00	100.00	0.00	67.61	32.39	0.00	0.00	0.00	0.00	0.00	100.00
Native Gold	TPCV7(85m)	Stage II	97.54	2.46	0.00	0.00	0.00	0.00	0.00	0.00	100.00	95.60	4.40	0.00	0.00	0.00	0.00	0.00	0.00	100.00
			89 .41	10.59	0.00	0.00	0.00	0.00	0.00	0.00	100.00	82.22	17.78	0.00	0.00	0.00	0.00	0.00	0.00	100.00
	TPCV6(80m)	Stage II	90.88	9.12	0.00	0.00	0.00	0.00	0.00	0.00	100.00	84.51	15.49	0.00	0.00	0.00	0.00	0.00	0.00	100.00
			89 .96	10.04	0.00	0.00	0.00	0.00	0.00	0.00	100.00	83.07	16.93	0.00	0.00	0.00	0.00	0.00	0.00	100.00
	TPCV5(80m)	Stage II	93.13	6.87	0.00	0.00	0.00	0.00	0.00	0.00	100.00	88.12	11.88	0.00	0.00	0.00	0.00	0.00	0.00	100.00
			93.04	6.96	0.00	0.00	0.00	0.00	0.00	0.00	100.00	87.99	12.01	0.00	0.00	0.00	0.00	0.00	0.00	100.00
	TPCV4(75m)	Stage II	94.61	5.39	0.00	0.00	0.00	0.00	0.00	0.00	100.00	90.58	9.42	0.00	0.00	0.00	0.00	0.00	0.00	100.00
			95.87	4.13	0.00	0.00	0.00	0.00	0.00	0.00	100.00	92.71	7.29	0.00	0.00	0.00	0.00	0.00	0.00	100.00
	TPC047(70m)	Stage III	95.70	4.30	0.00	0.00	0.00	0.00	0.00	0.00	100.00	92.42	7.58	0.00	0.00	0.00	0.00	0.00	0.00	100.00
			96.14	3.86	0.00	0.00	0.00	0.00	0.00	0.00	100.00	93.17	6.83	0.00	0.00	0.00	0.00	0.00	0.00	100.00
	TPCV4(75m)	Stage III	96.00	4.00	0.00	0.00	0.00	0.00	0.00	0.00	100.00	92.93	7.07	0.00	0.00	0.00	0.00	0.00	0.00	100.00
			90.68	9.32	0.00	0.00	0.00	0.00	0.00	0.00	100.00	84.19	15.81	0.00	0.00	0.00	0.00	0.00	0.00	100.00
	TPC048(70m)	Stage III	94.50	5.50	0.00	0.00	0.00	0.00	0.00	0.00	100.00	90.39	9.61	0.00	0.00	0.00	0.00	0.00	0.00	100.00
			96.05	3.95	0.00	0.00	0.00	0.00	0.00	0.00	100.00	93.02	6.98	0.00	0.00	0.00	0.00	0.00	0.00	100.00
			94.66	5.34	0.00	0.00	0.00	0.00	0.00	0.00	100.00	90.66	9.34	0.00	0.00	0.00	0.00	0.00	0.00	100.00
	TPC050(70m)	Stage III	95.51	4.49	0.00	0.00	0.00	0.00	0.00	0.00	100.00	92.10	7.90	0.00	0.00	0.00	0.00	0.00	0.00	100.00
			94.73	5.27	0.00	0.00	0.00	0.00	0.00	0.00	100.00	90.79	9.21	0.00	0.00	0.00	0.00	0.00	0.00	100.00
			96.54	3.46	0.00	0.00	0.00	0.00	0.00	0.00	100.00	93.86	6.14	0.00	0.00	0.00	0.00	0.00	0.00	100.00
Electrum	TPCV7(85m)	Stage II	87.68	12.32	0.00	0.00	0.00	0.00	0.00	0.00	100.00	79.57	20.43	0.00	0.00	0.00	0.00	0.00	0.00	100.00
			84.16	15.84	0.00	0.00	0.00	0.00	0.00	0.00	100.00	74.42	25.58	0.00	0.00	0.00	0.00	0.00	0.00	100.00
			84.30	15.70	0.00	0.00	0.00	0.00	0.00	0.00	100.00	74.62	25.38	0.00	0.00	0.00	0.00	0.00	0.00	100.00
	TPCV6(80m)	Stage II	87.25	12.75	0.00	0.00	0.00	0.00	0.00	0.00	100.00	78.94	21.06	0.00	0.00	0.00	0.00	0.00	0.00	100.00
			82.17	17.83	0.00	0.00	0.00	0.00	0.00	0.00	100.00	71.62	28.38	0.00	0.00	0.00	0.00	0.00	0.00	100.00
	TPCV5(80m)	Stage II	87.54	12.46	0.00	0.00	0.00	0.00	0.00	0.00	100.00	79.38	20.62	0.00	0.00	0.00	0.00	0.00	0.00	100.00
			86.11	13.89	0.00	0.00	0.00	0.00	0.00	0.00	100.00	77.25	22.75	0.00	0.00	0.00	0.00	0.00	0.00	100.00
			87.05	12.95	0.00	0.00	0.00	0.00	0.00	0.00	100.00	78.64	21.36	0.00	0.00	0.00	0.00	0.00	0.00	100.00
			86.40	13.60	0.00	0.00	0.00	0.00	0.00	0.00	100.00	77.67	22.33	0.00	0.00	0.00	0.00	0.00	0.00	100.00
	TPC047(70m)	Stage III	31.07	68.93	0.00	0.00	0.00	0.00	0.00	0.00	100.00	19.79	80.21	0.00	0.00	0.00	0.00	0.00	0.00	100.00
			32.77	67.23	0.00	0.00	0.00	0.00	0.00	0.00	100.00	21.07	78.93	0.00	0.00	0.00	0.00	0.00	0.00	100.00
			33.67	66.33	0.00	0.00	0.00	0.00	0.00	0.00	100.00	21.75	78.25	0.00	0.00	0.00	0.00	0.00	0.00	100.00
Native Silver (AgAu)	TPC047(70m)	Stage III	25.48	74.52	0.00	0.00	0.00	0.00	0.00	0.00	100.00	15.77	84.23	0.00	0.00	0.00	0.00	0.00	0.00	100.00
Native Bismuth	TPC047(70m)	Stage III	0.00	0.00	0.00	100.00	0.00	0.00	0.00	0.00	100.00	0.0.0	0.00	0.00	100.00	0.00	0.00	0.00	0.00	100.00
			0.00	0.00	0.00	100.00	0.00	0.00	0.00	0.00	100.00	0.00	0.00	0.00	100.00	0.00	0.00	0.00	0.00	100.00
	TPCV5(80m)	Stage III	0.00	0.00	0.00	100.00	0.00	0.00	0.00	0.00	100.00	0.00	0.00	0.00	100.00	0.00	0.00	0.00	0.00	100.00
			0.00	0.00	0.00	100.00	0.00	0.00	0.00	0.00	100.00	0.00	0.00	0.00	100.00	0.00	0.00	0.00	0.00	100.00
Hedleyite (Bi_7Te_3)	TPC047(70m)	Stage III	0.00	0.00	22.42	77.58	0.00	0.00	0.00	0.00	100.00	0.00	0.00	32.12	67.88	0.00	0.00	0.00	0.00	100.00
			0.00	0.00	22.12	77.88	0.00	0.00	0.00	0.00	100.00	0.00	0.00	31.75	68.25	0.00	0.00	0.00	0.00	100.00
			0.00	0.00	21.62	78.38	0.00	0.00	0.00	0.00	100.00	0.00	0.00	31.12	68.88	0.00	0.00	0.00	0.00	100.00
			0.00	0.00	21.00	79.00	0.00	0.00	0.00	0.00	100.00	0.00	0.00	30.33	69.67	0.00	0.00	0.00	0.00	100.00
			0.00	0.00	20.07	79.93	0.00	0.00	0.00	0.00	100.00	0.00	0.00	29.14	70.86	0.00	0.00	0.00	0.00	100.00
Ardaite	TPC047(70m)	Stage III	0.00	0.00	0.00	0.00	24.50	17.26	0.00	58.24	100.00	0.00	0.00	0.00	0.00	19.72	52.74	0.00	27.74	100.00
			0.00	0.00	0.00	0.00	24.28	16.95	0.00	58.77	100.00	0.00	0.00	0.00	0.00	20.12	51.56	0.00	28.32	100.00
Gudmundite(Fe_3+SbS)	TPCV5(80m)	Stage III	0.00	0.00	0.00	0.00	58.61	14.57	26.81	0.00	100.00	0.00	0.00	0.00	0.00	34.0	32.10	33.90	0.00	100.00
			0.00	0.00	0.00	0.00	56.87	16.30	26.83	0.00	100.00	0.00	0.00	0.00	0.00	32.09	34.92	32.99	0.00	100.00
			0.00	0.00	0.00	0.00	57.86	14.85	27.29	0.00	100.00	0.00	0.00	0.00	0.00	33.3	32.45	34.25	0.00	100.00
			0.00	0.00	0.00	0.00	58.03	14.68	27.29	0.00	100.00	0.00	0.00	0.00	0.00	33.49	32.16	34.34	0.00	100.00
			0.00	0.00	0.00	0.00	59.3	15.49	25.22	0.00	100.00	0.00	0 .00	0.00	0.00	34.26	33.98	31.76	0.00	100.00
Cervelleite? (Ag_4TeS)	TPCV7(85m)	Stage III	0.00	69.54	21.45	0.00	0.00	9.02	0.00	0.00	100.00	0.00	58.93	15.37	0.00	0.00	25.70	0.00	0.00	100.00
Tetradymite (Bi_2Te_2S)	TPC047(70m)	Stage III	0.00	0.00	17.74	60.30	11.68	4.79	5.48	0.00	100.00	0.00	0.00	18.03	37.41	12.45	19.37	12.75	0.00	100.00
Tellurobismuthite (Bi_2Te_3)	TPCV7(85m)	Stage II	0.00	0.00	47.99	52.01	0.00	0.00	0.00	0.00	100.00	0.00	0.00	60.18	39.82	0.00	0.00	0.00	0.00	100.00
			0.00	0.00	48.25	51 .75	0.00	0.00	0.00	0.00	100.00	0.00	0.00	60.43	39 .57	0.00	0.00	0.00	0.00	100.00
Kochkarite? ($PbBi_4Te_7$)	TPCV7(85m)	Stage III	0.00	0.00	46.13	37.90	0.00	0.00	0.00	15.98	100.00	0.00	0.00	58.31	29.25	0.00	0.00	0.00	12.44	100.00
			0.00	1.79	46.07	36.21	0.00	0.00	0.00	15.92	100.00	0.00	2.64	57.51	27.60	0.00	0.00	0.00	12.24	100.00
Unnamed Mineral (AuSb)	TPCV5(80m)	Stage IV	73.77	0.00	0.00	0.00	26.23	0.00	0.00	0.00	100.00	63.48	0.00	36.52	0.00	0.00	0.00	0.00	0.00	100.00
			85.80	0.00	0.00	0.00	14.20	0.00	0.00	0.00	100.00	78.87	0.00	21.13	0.00	0.00	0.00	0.00	0.00	100.00
Unnamed Mineral (BiTeSb)	TPC047(70m)	Stage III	0.00	0.00	16.01	81.84	2.15	0.00	0.00	0.00	100.00	0.00	0.00	23.46	73.24	3.30	0.00	0.00	0.00	100.00

Determined by EDS

Normalized to 100%

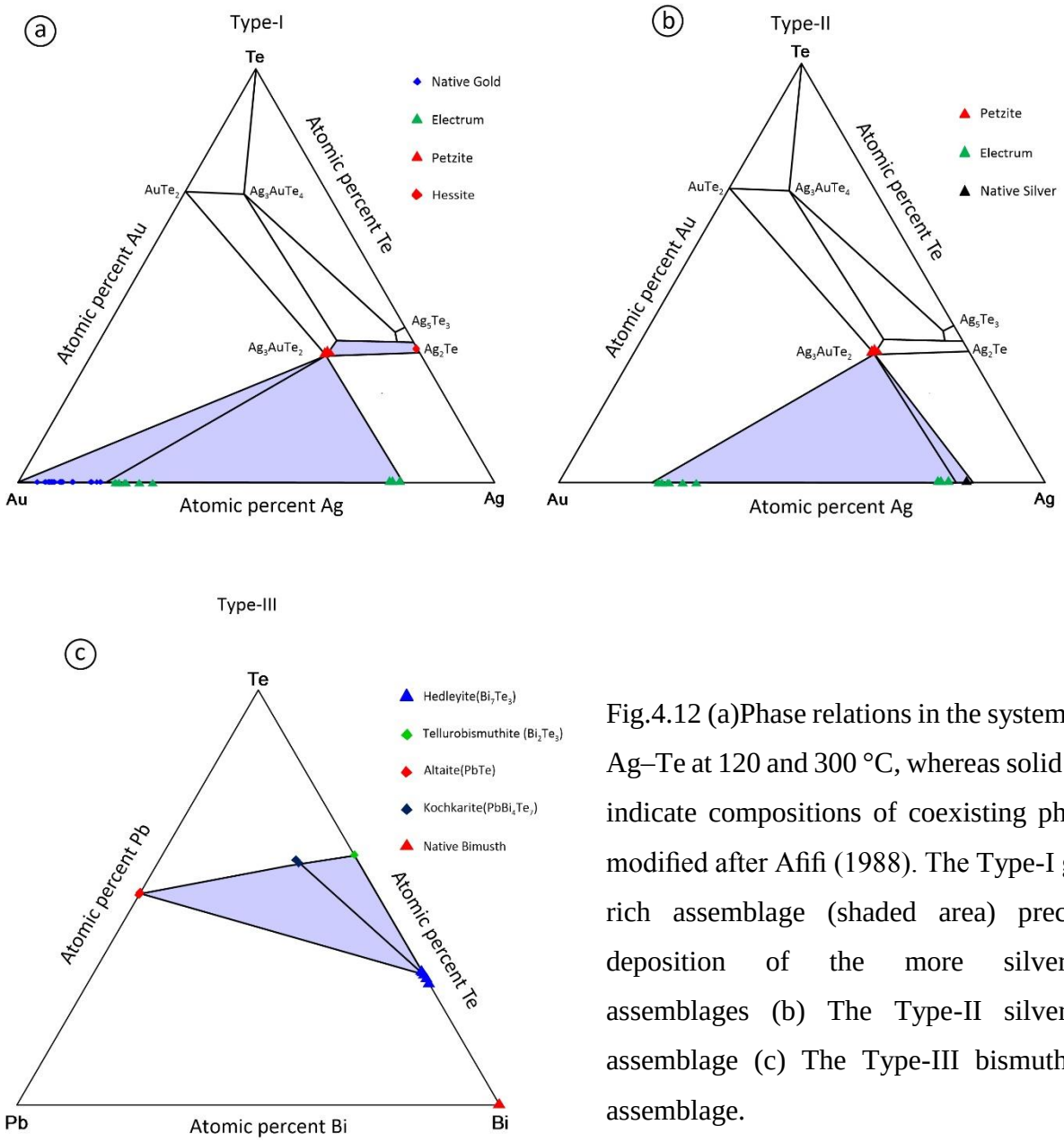

Fig.4.12 (a)Phase relations in the system Au–Ag–Te at 120 and 300 °C, whereas solid lines indicate compositions of coexisting phases, modified after Afifi (1988). The Type-I gold-rich assemblage (shaded area) preceded deposition of the more silver-rich assemblages (b) The Type-II silver-rich assemblage (c) The Type-III bismuth-rich assemblage.

4.7 Fluid inclusions studies

4.7.1 Fluid inclusions petrography

This study focused on primary fluid inclusions hosted in Stage I, II and III quartz of gold-bearing quartz veins. Fluid inclusions for paragenetic Stage IV were not studied in this study. 30 samples of gold-bearing quartz vein samples were selected from various depths and locations from all stages of mineralization within the Thae Phyu Chaung gold deposit.

Fluid inclusions hosted in quartz crystals were randomly distributed in the cluster, in isolation and interpreted as primary in origin. Those aligned along growth zones in intragranular crystals trails were interpreted as secondary or pseudo secondary inclusions based on the classification of Roedder (1984) (Fig. 4.13a). The secondary fluid inclusions in healed fractures was avoided in this study. The fluid inclusions have round to very irregular shapes and no daughter minerals were observed.

Three types of workable fluid inclusions in quartz were reorganized based on fluid morphology, relative location and phases present at room temperature (25^{o}C) and combined with their behavior on cooling to about -100°C and heating up to total homogenization: (1) aqueous-carbonic fluid inclusions (Type I), (2) aqueous fluid inclusions (Type II) and (3) carbonic fluid inclusions (Type III) (Fig. 4.13a-e).

1. Aqueous-carbonic fluid inclusions (Type I)

The Type I inclusions which have three phases with two components (liquid+liquid+ vapor or V_{CO2} + L_{CO2}+ L_{H2O}). The Type I inclusions are exclusively found in Stage I quartz. They are not most common as Type II inclusions. The presence of three phases with two liquids and one vapor is the distinguishing feature of this type (Fig. 4.13b). The Type I fluid inclusions have ellipsoidal or irregular shapes and size ranging from 10 to 30 μm with the vapor bubble taking up approximately 40-80% of the inclusion (Fig. 4.14a). The Type I inclusions in quartz are interpreted to represent Stage I quartz.

2. Aqueous fluid inclusions (Type II)

The Type II fluid inclusions are very common in quartz grains formed in the all Stage quartz. Type II fluid inclusions can be subdivided into the two groups: (1) vapor-rich (Type IIa) and (2) liquid-rich (Type IIb). They tend to be found in primary randomly oriented clusters or as isolated large inclusions in quartz. These fluid inclusions which have two phases (vapor-rich or V_{CO2} + L_{H2O} and liquid-rich or L_{H2O} + V_{CO2}) and they contain 10-90 vol.% vapor (average 20-60 vol.%) (Fig. 4.13a, c,d). The Type II fluid inclusions have sub-rounded, small, elliptical, and vary in size from 5 to 25 μm in diameter with most between 5 and 15μm (Fig. 4.14b-f). They commonly occur in an assemblage with Type I and III inclusions in the Stage I quartz (Fig. 4.14b-f).

3. Carbonic fluid inclusions (Type III)

Type III fluid inclusions consist of almost pure carbonic fluid that contains little or no water and comprises two-phase CO_2 (V_{CO2} + L_{CO2}) at room temperature or Single-phase CO_2 (vapor or liquid) that formed a CO_2-rich vapor bubble during cooling. The Type III fluid

inclusions account for 6% of the total fluid inclusion population and are generally 5-20 μm in size. They are distributed in clusters with Type I and Type II fluid inclusions in quartz grains from the Stage I quartz (Figs. 4.13e, 4.14b).

4.8. Microthermometry

The microthermometrc data are summarized in Table 4.4. The Type I, Type II and Type III inclusions are presented to represent Stage I, II and III of quartz gold-bearing quartz veins (Fig. 4.15).

4.8.1. Stage I (Fe-As)

Stage I quartz crystals contain commonly Type I associated with Type IIa, Type IIb and Type III fluid inclusions in this stage. The CO_2 melting temperatures ($T_{m\text{-}CO2}$) of the Type I fluid inclusions range from -57.8 °C to -56.7 °C. These values are slightly lower than the triple point (melting temperature) of pure CO_2 at –56.6 °C (Roedder, 1984), suggesting the presence of minor components of other volatiles. The melting temperatures of clathrates ($T_{m\text{-}cla}$ = 8.6 to 9.8 °C) indicates that the salinity of these inclusions is quite low, about 0.4 to 2.8 wt.%.

The partial homogenization temperatures ($T_{h\text{-}CO2}$) of the CO_2 phase homogenizing into a liquid phase, range from -28.6 to -31.5 °C. The total homogenization temperatures (T_h) of Type I of stage I quartz range from 345°C to 384°C (Fig. 4.15). The homogenization temperatures (T_h) of Type IIa and IIb of stage I quartz range from 313 ^oC to 371 ^oC, (peak at 330 – 350^oC) (Fig. 4.15). Their final ice melting temperatures ($T_{m\text{-}ice}$) range from -1.1 to -5.3^oC, and the salinities of fluid inclusions in Stage I quartz, based on freezing point depression, ranging from 1.9 to 8.3 wt. % NaCl equivalent (Fig. 4.15). The melting

temperatures ($T_{m\text{-}CO2}$) for CO_2 of Type III fluid inclusion range from -57.4 to -56.6°C. The partial homogenization temperatures ($T_{h\text{-}CO2}$) of CO_2 range from 26.6 to 31.1°C.

4.8.2 Stage II (Cu-Pb-Zn)

The Type IIa and Type IIb fluid inclusion dominantly occurred in this stage. The final ice-melting temperature of fluid inclusions in stage II quartz range from - 0.8 to - 4.5 (average: -2.5). Homogenization temperatures of fluid inclusions in Stage II quartz the liquid range from 250 ^{o}C to 335 ^{o}C (peak at 290-310^{o}C), (Fig.4.15). Salinities calculated from melting temperatures range from 1.4 to 7.2 wt. % NaCl equivalent.

4.8.3 Stage III (Au-Ag-Bi-Te-Sb)

The Type IIb fluid inclusions only occur in this stage III quartz crystal. They have mostly subrounded in shapes, small, irregular shapes, and range from 5 to 10 μm in size in this stage. The final ice-melting temperature of fluid inclusions in stage III quartz ranges from -0.3 to -3.3 (average: -1.3). Homogenization temperatures of Stage III quartz range from 213^{o}C to 280^{o}C (peak at 230-250^{o}C) (Fig.4.15). Salinities of stage III quartz fluid inclusions range from 0.5 to 5.4 wt. % NaCl equivalent (Fig.4.15).

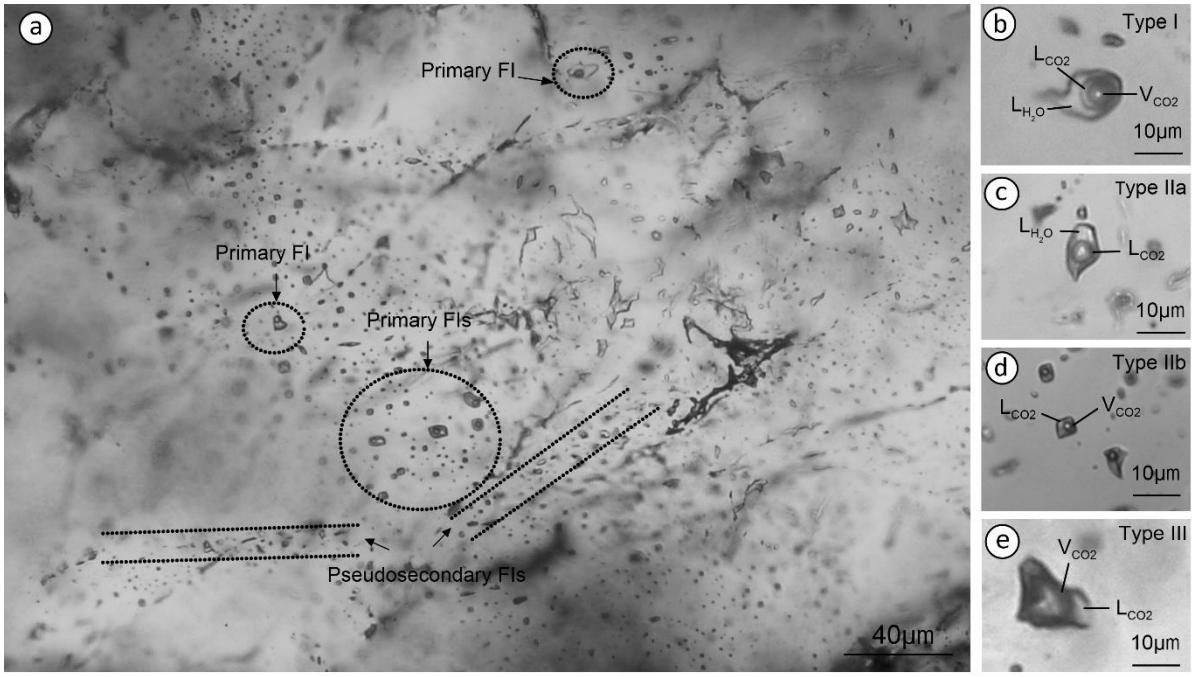

Fig.4.13 Photomicrographs of typical fluid inclusion assemblage from different mineralization stages at the Thae Phyu Chaung gold deposit. (a) Primary, pseudosecondary and secondary fluid inclusions in same sample; (b) Aqueous-carbonic fluid inclusions (Type I) (liquid+liquid+vapor) fluid inclusions in Stage I quartz , (c) Aqueous fluid inclusions (Type IIa) (vapor-rich) fluid inclusions in Stage II quartz , (d) Aqueous fluid inclusions (Type IIb) (liquid-rich) fluid inclusions in Stage III quartz, and (e) Carbonic fluid (Type III) (vapor or liqiud) fluid inclusions in Stage I quartz of gold-bearing quartz vein.

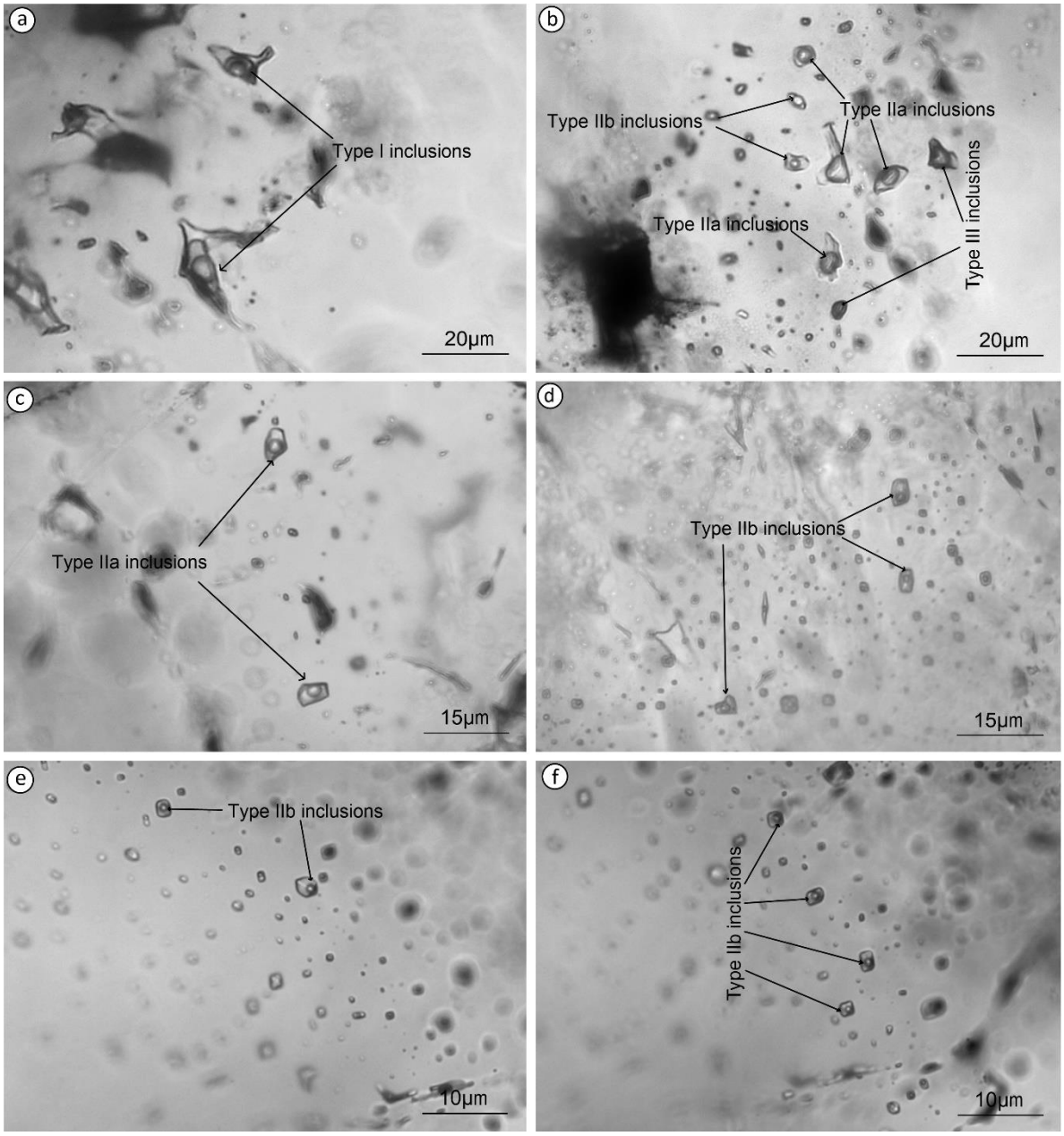

Fig.4.14 Photomicrographs of fluid inclusion assemblage from different mineralization stages at the Thae Phyu Chaung gold deposit. (a , b) Primary Type I and Type IIa, IIb, and Type III fluid inclusions in Stage I quartz of gold-bearing quartz veins from different samples; (c ,d) Primary Type IIa and IIb fluid inclusions in Stage II quartz of gold-bearing quartz veins from different samples; (e , f) Primary Type IIb fluid inclusions in Stage III quartz of gold-bearing quartz veins from different samples.

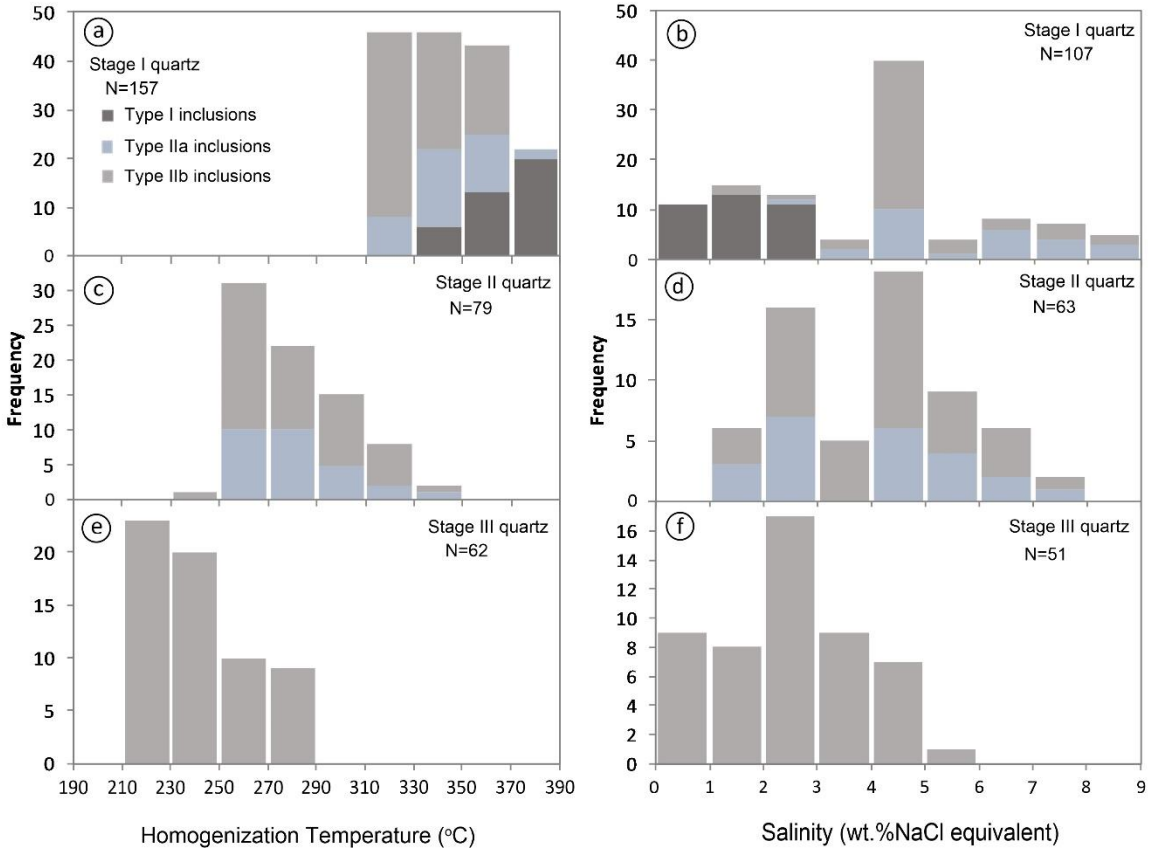

Fig.4.15 Histograms of total homogenization temperatures (T_h) of primary inclusions and salinities of fluid inclusions in different stages at the Thae Phyu Chaung deposit.

Note: N= total number of fluid inclusions

Table 4.4. Summary of fluid inclusion types and microthermometric data for fluid inclusions of the different stage in the Thae Phyu Chaung deposit.

Paragenetic Stage	Type	$T_{m\text{-}CO2}$ (°C)	$T_{m\text{-}cla}$ (°C)	$T_{h\text{-}CO2}$ (°C)	T_h (°C)	$T_{m\text{-}ice}$ (°C)	Salinity (wt%NaCl eq.)
Stage I	Type I	-57.8 to -56.7	8.6 to 9.8	28.6 to 31.5	345 to 384 (N=39)		0.4 to 2.8 (N=35)
	Type IIa				315 to 371 (N=38)	-1.2 to -5.3	2.1 to 8.3 (N=27)
	Type IIb				313 to 367 (N=80)	-1.1 to -5.3	1.9 to 8.3 (N=45)
	Type III	-57.4 to -56.6 (N=9)		26.6 to 31.1			
Stage II	Type IIa				256 to 335 (N=28)	-0.8 to -3.9	1.4 to 6.3 (N=23)
	Type IIb				251 to 335 (N=51)	-0.8 to -4.5	1.4 to 7.2 (N=40)
Stage III	Type IIb				213 to 280 (N=62)	-0.3 to -3.3	0.5 to 5.4 (N=51)

Notes: $T_{m\text{-}CO2}$—melting temperature of CO_2; $T_{m\text{-}cla}$—melting temperature of CO_2 clathrate; $T_{h\text{-}CO2}$—partial homogenization temperature of CO_2 inclusions; T_h—total homogenization temperature of inclusions; $T_{m\text{-}ice}$—final ice melting temperature; wt% NaCl eq., weight percent NaCl equivalent, N= total number of fluid inclusions.

4.9 Discussion

As mentioned earlier, the mineralizing hydrothermal fluids in Stage I, II and III quartz are composed of three types: (1) aqueous-carbonic fluid inclusions were low salinity (Type I), (2) aqueous fluid inclusions of moderate to low salinity (Type II) and (3) carbonic fluid inclusions (Type III). The CO_2-rich Type I inclusions in Stage I quartz homogenized at nearly the same temperatures as H_2O-rich Type II inclusions in Stage I quartz. These fluid inclusions indicate that trapping of immiscible H_2O-CO_2 fluids (Fig.4.16).

The abundance of CO_2 in the Stage I mineralization fluids may have played a critical role in gold transportation (Hagemann and Cassidy, 2000); because it can buffer the pH of the solution (Phillips & Evans, 2004), providing favorable conditions for the migration of gold, tellurides and other sulfides. The relationship between homogenization temperature and salinity for gold-depositing stage fluids is shown in Figure 4.16.

The entire range of CO_2 concentration is observed within single quartz grains in Stage I quartz. Total homogenization temperatures of Type I and Type IIa, Type IIb inclusions are similar (313-384ºC), with the peak at 330-370°C in their distribution in Stage I quartz (Fig.4.16). These observations likely indicate CO_2 phase separation of hydrothermal fluids during deposition of vein quartz. The wide range of total homogenization temperatures (213 to 384°C) is thought to reflect several episodes of CO_2 phase separation during vein formation, as indicated by textural evidence of repeated fracturing and filling of the veins.

All of these trends can be interpreted to indicate CO_2 phase separation, because phase separation of a relatively low-salinity, H_2O-CO_2 fluid produces both a high-salinity H_2O-rich fluid and a low-salinity CO_2-rich fluid into the H_2O rich liquid phase (Bowers and Helgeson,

1983, Phillips and Powell, 1993, Hagemann and Cassidy, 2000 Goldfarb *et al.*, 2001,2004 Dubé, and Gosselin, 2007).

The H_2O-rich fluids became after the extensive escape of CO_2 gas were probably trapped at temperatures between 250 and 335°C (Fig. 4.16). Type IIa and Type IIb fluid inclusions in Stage II quartz. Salinity of Type IIa and Type IIb fluid inclusions tend to increases from 1.9 to 8.3 wt% equiv. NaCl with decreasing temperature, indicating the continued trapping of remain fluids evolved through CO_2 separation into as CO_2-absent fluid inclusions in Stage III quartz (Figure 4.16). Type IIb (liquid-rich) inclusions in Stage III quartz represent cooling of the hydrothermal fluids. Following the complete loss of CO_2 from Stage II quartz fluids which reflect a further decline in temperature, the residual fluids were trapped as in Stage III quartz liquid-rich (Type IIb) fluid inclusions at temperatures between 213 and 280°C.

According to Phillips and Powell (1993), metamorphic devolatilization produces low-salinity fluids that transport gold as reduced sulfur complexes. The decrease in temperature and pressure may lead to fluid immiscibility and the fluid is separated into CO_2-rich and H_2O-rich fluid phases and this separation causes partitioning of gold and H_2S (Phillips and Powell 1993). The physical separation of the immiscible fluid phases results in them to follow different evolution trends which may lead to changes in gold solubility (Phillips and Powell 1993).

The fluid types present in the Thae Phyu Chaung gold deposit are similar to the fluid types in the other orogenic gold deposits in the Kyaikhto gold district.

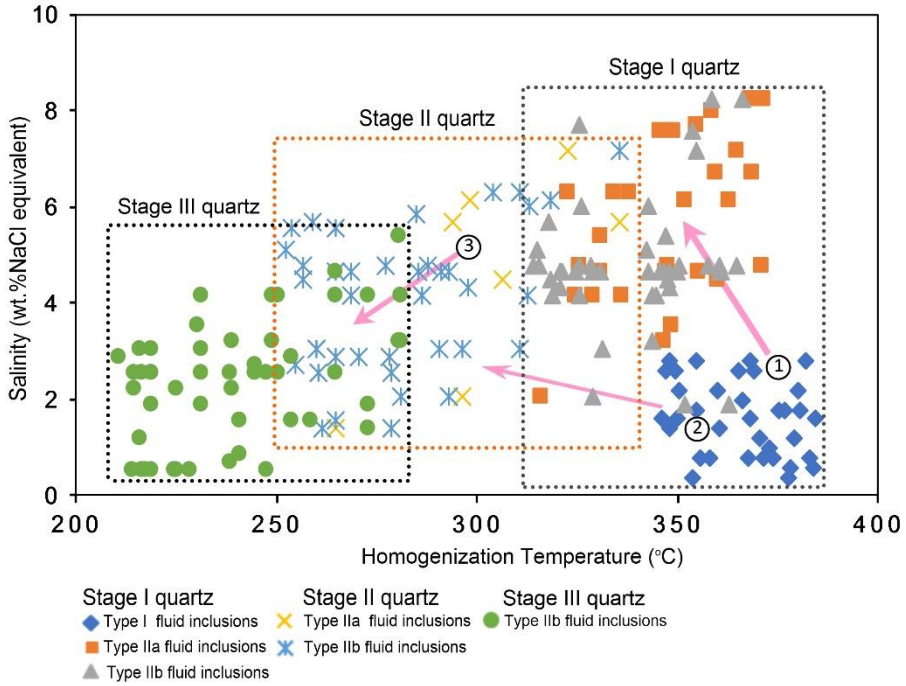

Fig.4.16 Plots of total homogenization temperatures (T_h) vs salinities of fluid inclusions in different stages quartz in the Thae Phyu Chaung deposit. Three pink arrows marked as ①, ② and ③ represent the fluid evolution from Stage I quartz to Stage III quartz. The arrows ① and ② mean that the fluids have wider salinities range from Stage I quartz to Stage II quartz due to the fluid immiscibility. The arrow ③ represents that the temperature and salinities both decrease from Stage II quartz to Stage III quartz.

4.10 Conclusions

The conclusions from this study are summarized as follows:

1. Thae Phyu Chaung gold deposit is mainly hosted by Carboniferous to Lower Permian age of Metasedimentary rocks and is structurally controlled by the NNE or NNW-trending faults system.
2. Hydrothermal alterations are propylitic alteration in early Stage I, followed by argillic alterations in Stage II, Stage III and Stage IV.
3. Thae Phyu Chaung gold deposit is an Au-Ag-Te-Bi deposit, comprising an early stage I (Fe-As), middle stage II (Cu-Pb-Zn), main ore stage III (Bi-Te-Sb-Ag-Au) and late stage IV (Fe-O).
4. The mineralogy of the vein system is complex. At least 30 minerals, including telluride (hessite, petzite, tetradymite, tellurobismuthite, hedleyite, cervelleite, and altaite), gudmundite and ullmannite, the first occurrence in Myanmar, have been identified from the Thae Phyu Chaung gold deposit. In addition, one unidentified mineral is reported.
5. Three types of primary fluid inclusions are identified: the aqueous-carbonic fluid inclusions (Type I), aqueous fluid inclusions (Type II), and carbonic fluid inclusions (Type III). The early Stage I quartz crystals contain all three types of primary fluid inclusions, and the middle Stage II quartz composes vapor-rich (Type IIa) and liquid-rich (Type IIb) inclusions and Stage III quartz contain only liquid-rich (Type IIb) inclusions.
6. Fluid inclusions petrography and microthermometric data indicate the ore fluids were moderate temperature, CO_2-rich, and low salinities.
7. The characteristics of fluid inclusion studies reveal that the ore-forming fluid transformed from a CO_2-rich mesothermal fluid into a CO_2-poor fluid.

8. A general sequence of mineral formation at the Thae Phyu Chaung gold deposit was Fe-As-Cu-Zn-Pb-sulfide precipitation, followed by Bi+Sb+Ag+Au tellurides.
9. CO_2-rich and H_2O-rich fluid was the key factor in the precipitation of gold, tellurides and other metal sulfides of the Thae Phyu Chaung gold deposit.

References

Afifi, A. M., Kelly, W. C. and Essene, E. J. (1988) Phase relations among tellurides, sulfides, and oxides: I. Thermochemical data and calculated equilibria. *Econ. Geol.*, 83, 377–394.

Cabri, L.J. (1965) Phase relations in the Au–Ag–Te systems and their mineralogical significance. *Econ. Geol.*, 60, 1569–1606.

Diamond, L. W. (2001) Review of the systematics of CO_2-H_2O fluid inclusions. *Lithos*, 55, 69–99.

Dubé, B. and Gosselin, P. (2007) Greenstone-hosted quartz-carbonate vein deposits: in Good fellow, W.D., ed., Mineral Deposits of Canada: A Synthesis of Major Deposit-Types, District Metallogeny, the Evolution of Geological Provinces, and Exploration Methods: *Geological Association of Canada, Mineral Deposits Division, Spec. Publ*., 5, 49-73.

Goldfarb, R. J., Groves, D. I., and Gardoll, S. (2001) Orogenic gold and geologic time: A global synthesis. *Ore Geol. Rev.*, 18,1 - 75.

Goldfarb, R. J., Ayuso, R., Miller, M. L., Ebert, S. W., Marsh, E. E., Petsel, S. A., Miller, L. D., Bradley, D., Johnson, C. and McClelland, W. (2004) The late Cretaceous Donlin Creek gold deposit, Southwestern Alaska: Controls on epizonal ore-forming. *Econ. Geol*., 99, 643- 671.

Groves, D. I., Goldfarb, R. J., Gebre-Mariam, M., Hagemann, S. G. and Robert, F. (1998) Orogenic gold deposits: A proposed classification in the context of their crustal distribution and relationship to other gold deposit types. *Ore Geol. Rev*., 13,7 - 27.

Hagemann, S. and Cassidy, K. (2000) Archean orogenic lode gold deposits. *Reviews in Econ. Geol*, 13, 9-68.

Mitchell, A.H.G., Ausa, C., Deiparine, L., Hlaing, T., Htay, N. and Khine, A. (2004) The Modi Taung-Nankwe gold district, Slate Belt, Central Myanmar: mesothermal veins in a Mesozoic orogen. J. *Asian Earth Sci*., 23, 321–341.

Nakata, M. and Komuro, K. (2011) Chemistry and occurrences of native tellurium from epithermal gold deposits in Japan. *Resour. Geol*., 61, 211–223.

Phillips, G. N., and Powell, J. K. (1993) Link between gold provinces. *Econ. Geol*., 88, 1084–1098.117–132.

Phillips, G. N., and Evans, K. A. (2004) Role of CO_2 in the formation of gold deposits. *Nature*, 429, 60–863.

Robert, F., and Kelly, W.C. (1987) Ore-forming fluids in Archean gold-bearing quartz veins at Sigma mine, Abitibi greenstone belt, Quebec, Canada. *Econ. Geol*., 82, 1464-1482.

Roedder, E. (1984) Fluid inclusions. Rev. Miner., 12, 644p.

White N.C. and Hedenquist J.W. (1995) Epithermal gold deposits: Styles, characteristics and exploration. *SEG Newsletter.*, 23, p. 9-13.

CHAPTER V

GENERAL CONCLUSIONS

5.1 General statement

This chapter concludes this thesis by comparisons with worldwide, general conclusions, and recommendations for further research of the Kyaikhto gold district.

5.2 Comparison of orogenic gold deposits worldwide

As mentioned previously, many geological and geochemical features of the Kyaikhto gold district are consistent with typical orogenic gold deposits worldwide (Groves *et al.,* 1998, 2003, Goldfarb *et al.*,2001 2005) (Fig 5.1).

Similarities include the followings (see Table 4.1): (1) The orebodies which are mainly hosted in the Archean to Paleozoic age metasedimentary rocks and are structurally controlled (2) Multiple stages of mineralization of the disseminated and quartz vein and veinlet/stockworks ores. (3) Sulfide mineral associations of dominantly pyrite, sphalerite, galena, chalcopyrite with Au, Ag, Bi+Te minerals. (4) Hydrothermal alteration characterized by sericite, chlorite, and carbonate alterations. (5) The ore-forming fluids which were low to moderate temperature, H_2O-CO_2-NaCl system with low salinity, and the fluid which was rich in CO_2. (6) The fluids transformed from CO_2-rich ore-forming fluids to CO_2-poor during fluid evolution (e.g., Golden Mile and Kalgoorlie in Western Australia, Western Lachlan Orogen in Victoria, SE Australia, Buller Terrane in Western South Island, New Zealand and Meguma Terrane in Nova Scotia, Canada, Modi Taung in Myanmar) (Table 5.1).

Although hosted in the Carboniferous age of metasedimentary rocks, the gold mineralization in the Kyaikhto gold district is most likely Lower Jurassic to Cretaceous in age

(Mitchell *et al.,* 2004). The Slate Belt or Mergui Group became part of the India–Burma Plate collision tectonic during Lower Jurassic to Cretaceous when the major tectonic transformation from N-S compression to NNE-SSW shearing was gradually completed. Mitchell *et al.,* (2004) considered this region as a continental margin orogenic belt, and its landward boundary was the NNE-trending N-S Gravity Lineament. The gold veins deposited during the ascent of metamorphic fluids into the Slate Belt, accompanied with Lower Jurassic metamorphism and dehydration at depth of 5–12 km (Figs 2.3 and 5.2). Thus, although far from the eastern margin of Slate Belt or Mergui Group, the region could be affected by the subduction of the Paleo- Burma Plate, and large-scale fluid circulation, granitic magmatism, and metallogenesis took place during the Early Jurassic to Cretaceous in the Kyaikhto gold district.

These features support the fact that the Kyaikhto gold district could be classified as an orogenic type gold deposit in Myanmar.

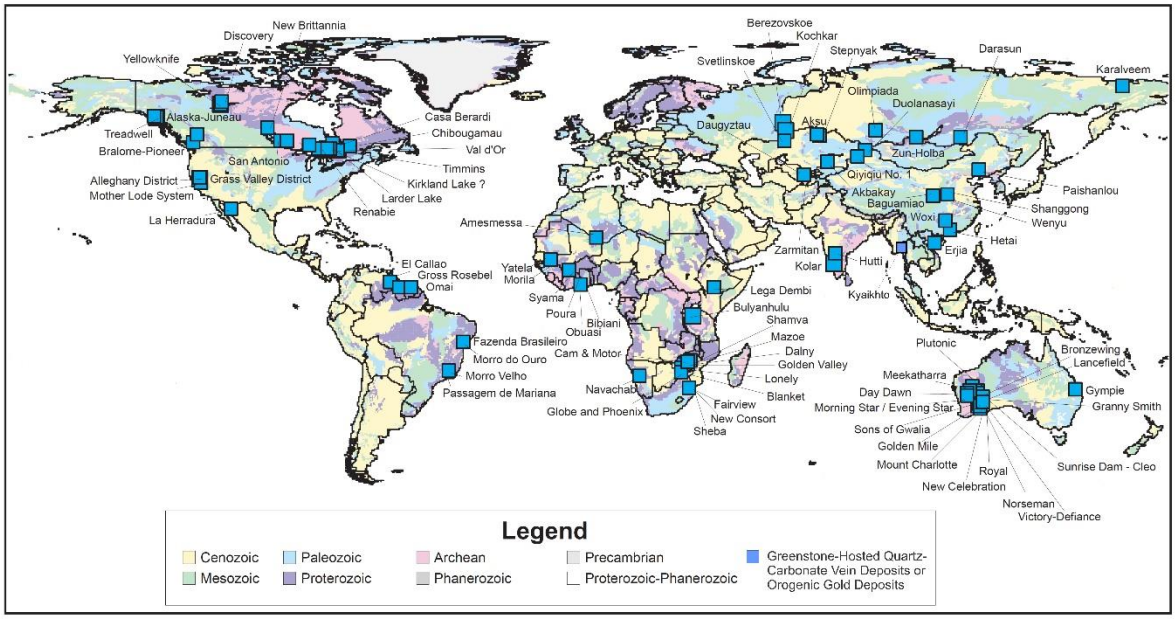

Fig 5.1. World distribution of greenstone-hosted quartz-carbonate vein deposits or orogenic gold deposits containing at least 30 tons of Au. (from Dubé *et al.*, 2007)

Table 5.1 Comparative table with other orogenic gold deposits Myanmar and worldwide

Name of deposit/ prospect	Location and geologic setting	Host rocks	Mineralization style	Alteration	Metal associations	Ore fluid system, temperature and Salinity	Regional peak Metamorphism events	Age of host terranes	References
Golden Mile	Kalgoorlie, Western Australia	Black shale, slate, basalts, and dolerite	Quartz vein and stockwork	Carbonation, sericitization, sulfidation;	Cu, Fe, As, Pb, Zn, Bi, Sb, Mo, Te, Ag, Au	H_2O-CO_2±CH_4-NaCl 200–400 (0.5–10 wt% eqiv. NaCl)	lower greenschist Archean	Archean	Shackleton et al., 2003, Groves et al., 1998, 2003, Goldfarb et al., 2001,2005
Western Lachlan Orogen	Victoria, SE Australia	Slates, massive sandstone	Laminated or ribbon banded quartz vein disseminated – stockwork-breccia systems	Carbonation, sericitization, sulfidation;	Cu, Fe, As, Pb, Zn, Sb, Mo, Ag, Au	H_2O-CO_2±CH_4-NaCl 200-400 (2 – 10 wt% eqiv. NaCl)	zeolite– lower amphibolite Devonian	Late Cambrian–Early Devonian	Groves et al., 1998, 2003 Goldfarb et al., 2001, 2005, Bierlein et al., 2004
Buller Terrane	Western South Island, New Zealand	massive siltstone and sandstone	Ribbon texture banded vein shear-zone-related quartz lodes gold.	Carbonation, sericitization, sulfidation	Cu, Fe, As, Ag, Au	H_2O-CO_2±CH_4-NaCl 152-293 (3.5–7.2 wt% eqiv. NaCl)	lower greenschist Devonian	Late Cambrian–Middle Ordovician	Bierlein et al., 2004, Groves et al., 1998,2003, Goldfarb et al., 2001, 2005
Meguma Terrane	Nova Scotia, Canada	slate, argillite or meta-sandstones.	Laminated bedding-parallel veins	carbonate Sericite Chlorite,Sulphidation	Cu, Fe, As, Pb, Sn, Ag, Au	H_2O-CO_2±CH_4-NaCl 300-400 (< 10 wt% eqiv. NaCl	lower greenschist –upper amphibolite Devonian	Late Cambrian–Late Ordovician	Groves et al., 1998, 2003 Goldfarb et al., 2001, 2005., Bierlein et al., 2004
Phayaung Taung	Slate belt, Central Myanmar	Phyllite, schist, and quartzite	Sulfide quartz vein	Silicification, Phyllic/sericitic, chloritization, Oxidation	Cu, Fe, As, Pb, Zn, Bi, Te, Ag, Au	NaCl-H_2O 243-426 (0.4-8.4 wt% eqiv. NaCl)	lower greenschist –upper Amphibolite Early Jurassic-Cretaceous	Carboniferous to Early Permian	Swe et al., 2017 Phyo et al., 2016
Modi Taung	Slate belt, Central Myanmar	Mudstone, graywacke, and slate	Book and Ribbon, Laminated vein	Argillic, Propylitic	Cu, Fe, As, Pb, Zn, Ag, Au	NaCl-H_2O 240-360 (<12 wt% eqiv. NaCl)	lower greenschist Early Jurassic-Cretaceous	Carboniferous to Early Permian	Hlaing et al., 2013, 2016 Mitchell et al., 2004
Shwe Kyin	Slate belt, Southern Myanmar	Slate, phyllite, schist, and quartzite	Sulfide quartz vein	Argillic, Propylitic	Cu, Fe, As, Pb, Zn, Ag, Au	H_2O-CO_2±CH_4-NaCl 245-411 (1.5-7.0 wt% eqiv. NaCl)	lower greenschist –upper Amphibolite Early Jurassic-Cretaceous	Carboniferous to Early Permian	Aye et al., 2017
Kunzeik	Slate belt, Southern Myanmar	Slate, biotite granite, granodiorite	Sulfide quartz vein, stockwork	Argillic, Propylitic	Cu, Fe, Mo, Ag, Au	H_2O-CO_2 –NaCl *a 246 ~ 312 (1.2 ~ 10.7 wt% eqiv. NaCl) *b 296 ~ 376 (1.6 ~ 4.6 wt% eqiv. NaCl)	lower greenschist Early Jurassic-Cretaceous	Carboniferous to Early Permian	This study
Zibyaung	Slate belt, Southern Myanmar	Slate and schist	Sulfide quartz vein	Propylitic, Silicification, sericitization	Cu, Fe, Pb, Zn, Ag, Au	H_2O-CO_2-NaCl *a 246 ~ 312 (1.2 ~ 10.7 wt% eqiv. NaCl) *b 296 ~ 376 (1.6 ~ 4.6 wt% eqiv. NaCl)	lower greenschist –upper Amphibolite Early Jurassic-Cretaceous	Carboniferous to Early Permian	This study
Thae Phyu Chaung	Slate belt, Southern Myanmar	Slate and slaty phyllite	Sheeted quartz vein	Argillic, Propylitic alteration	Cu, Fe, As, Pb, Zn, Bi, Sb, Te, Ag, Au	H_2O-CO_2 -NaCl *a 345 ~ 384 (0.4 ~ 4.6 wt% eqiv. NaCl) *b 213 ~ 371 (0.5 ~ 8.3 wt% eqiv. NaCl)	lower greenschist Early Jurassic-Cretaceous	Carboniferous to Early Permian	This study
Meyon	Slate belt, Southern Myanmar	Greywacke and slate	Stratabound, Sulfide quartz vein	Silicification, Argillic, Propylitic	Cu, Fe, As, Zn, Ag, Au	H_2O-CO_2±CH_4-NaCl 240-370 (5~12 wt% eqiv. NaCl)	lower greenschist Early Jurassic-Cretaceous	Carboniferous to Early Permian	Oo et al., 2010 This study

Notes: *a= Aqueous-carbonic fluid inclusions, *b= Aqueous fluid inclusions

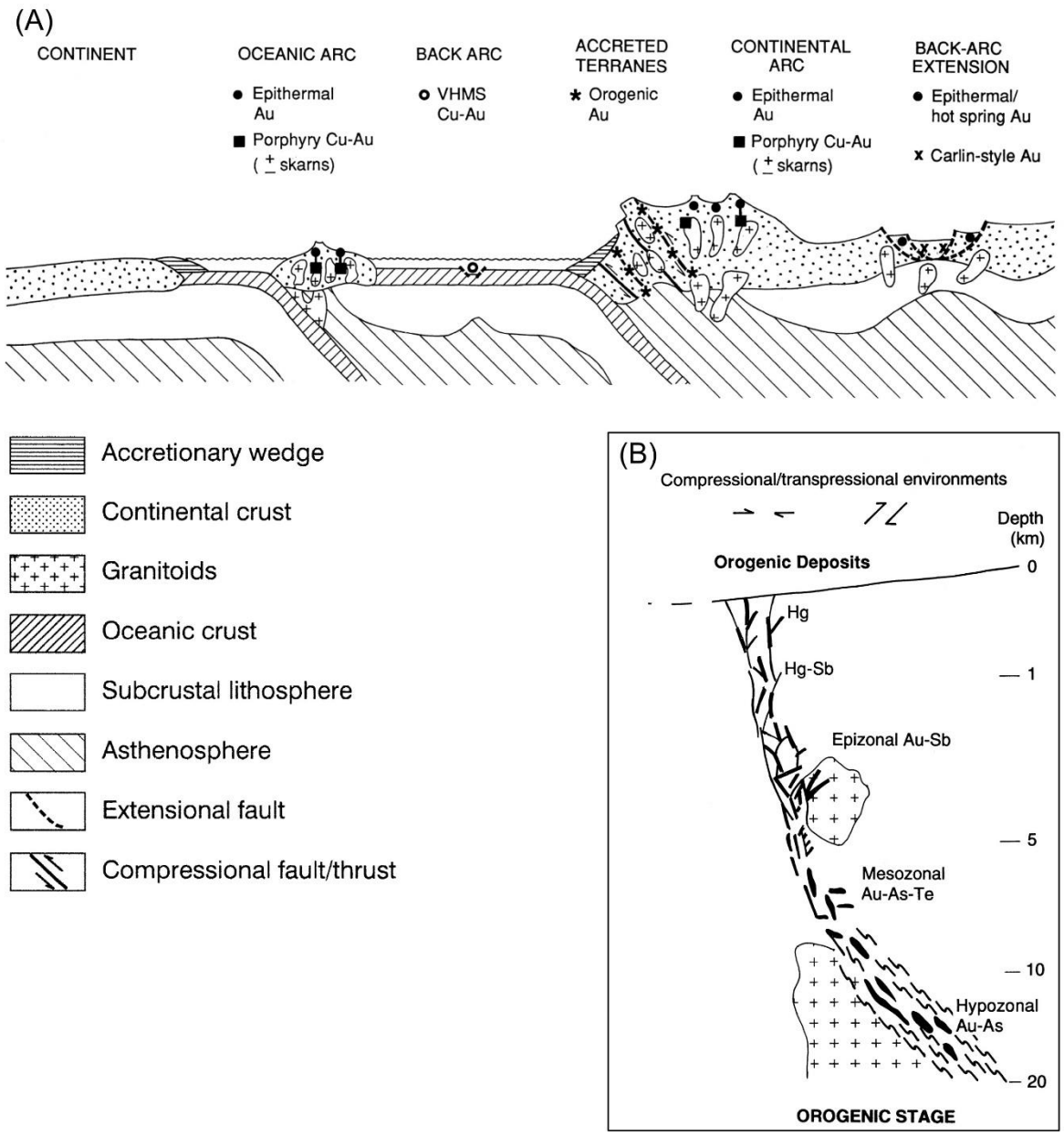

Fig. 5.2. Schematic diagram showing the setting and nature of orogenic lode–gold deposits. (A). Plate tectonic environments of formation of orogenic lode–gold deposits and other largely syn-volcanic or syn-intrusive gold-rich deposit styles. (B). Depth profile of orogenic lode–gold deposit (from Groves *et al.*,1998).

5.3 General Conclusions

Major conclusions from this study are:

1. The Kyaikhto gold district is predominately hosted by slate, slaty phyllite, and schist and biotite granite and biotite granodiorite and is structurally controlled by the NNE-NNW trending faults system. The main ore minerals are sphalerite, galena, chalcopyrite, pyrite and arsenopyrite with native gold, electrum, native silver, native bismuth, and telluride minerals.
2. Hydrothermal alteration is characterized by argillic and propylitic alterations.
3. The ore-forming fluids of Kyaikhto gold district belong to the H_2O-CO_2-NaCl system.
4. These features of the gold mineralization in the Kyaikhto district are consistent with orogenic gold deposits worldwide.

5.4 Recommendations for further research

This study provides a starting point for future studies into the genesis of the Kyaikhto district and of orogenic mineralization systems in the Slate Belt. Recommendations for future research include:

- Geochronological analyses of quartz-muscovite vein should be undertaken in order to establish the timing of gold mineralization.
- A district-scale geologic long section through Kyaikhto district should be constructed to help better understand the intrusive history and spatial and temporal relationships between the four gold-mineralized centers.

- Systematic sampling and analyses of sulfur isotopic compositions throughout the district would supplement alteration facies and help with tracing magmatic fluid pathways.
- Additional analyses of hydrogen, carbon and oxygen isotopes can be used to elucidate the origin and evolution of hydrothermal fluids, and to determine conditions of ore formation.
- Raman spectroscopy analyses of the CO_2 bearing inclusions could be used to determine the compositions of the presence of the CH_4, N_2, and salts of the mineralizing hydrothermal fluids and would help to confirm the author's classification of the Kyaikhto gold district as orogenic gold mineralization systems.
- Detailed structural analysis of vein arrays, dikes and faults in the Kyaikhto gold district to better understand structural controls on mineralization.

References

Aye, M.T., Hlaing, M.K., Yonezu, K. and Watanabe, K. (2017) Fluid Inclusion Study of Shwegyin Gold Deposit, Bago Region, Myanmar, *7th Asia Africa Mineral Resources Conference*, 157-160.

Berlin, F.P., Christieb, A.B. and Smith., P.K. (2004) A comparison of orogenic gold mineralization in central Victoria (AUS), western South Island (NZ) and Nova Scotia (CAN) implications for variations in the endowment of Palaeozoic metamorphic terrains. *Ore Geology Reviews*, 25, 125–168

Dubé, B. and Gosselin, P. (2007) Greenstone-hosted quartz-carbonate vein deposits: in Good fellow, W.D., ed., Mineral Deposits of Canada: A Synthesis of Major Deposit-Types, District Metallogeny, the Evolution of Geological Provinces, and Exploration Methods: *Geological Association*

Goldfarb, R. J., Groves, D. I., and Gardoll, S. (2001) Orogenic gold and geologic time: A global synthesis. *Ore Geol. Rev., 18,1 - 75. of Canada, Mineral Deposits Division, Spec. Publ.*, 5, 49-73.

Goldfarb, R. J., Baker, T., Dube, B., Groves, D. I., Hart, C. J. R. and Gosselin, P. (2005) Distribution, character, and genesis of gold deposits in metamorphic terranes. In Hedenquist, J. W., Thompson, J. F. H., Goldfarb, R. J. and Richards, J. P. (eds.) *Economic Geology 100th Anniversary Volume. Society of Economic Geologists Inc., Littleton*, 407–450.

Groves, D. I., Goldfarb, R. J., Gebre-Mariam, M., Hagemann, S. G. and Robert, F. (1998) Orogenic gold deposits: A proposed classification in the context of their crustal distribution and relationship to other gold deposit types. *Ore Geol. Rev.,* 13,7 - 27.

Groves, D. I., Goldfarb, R. J., Robert, F. and Hart, C. J. R. (2003) "Gold deposits in metamorphic belts: Overview of current under- standing, outstanding problems, future research, and exploration significance," *Economic Geology*, 98, 1–29.

Hlaing, M.K., Yonezu, K., Aye, M.T., Myint, A.Z. and Watanabe, K. (2016) Geology and Geochemical Characteristics of Gold Mineralization at Shwetagun Area, Yemethin Township, Mandalay Region, Myanmar, *Poster no. 19, presented at the Society of Resources Geology Conference, Tokyo., Japan*, 71.

Hlaing, M.K., Yonezu, K., Aye, M.T., Myint, A.Z. and Watanabe, K. (2016) Geology and Mineralogical characteristics of Zibyaung Gold Deposit at Kyaikhto area, Southern Myanmar. *Proceedings of International Symposium on Earth Science and Technology*, 403-407.

Mitchell, A.H.G., Ausa, C., Deiparine, L., Hlaing, T., Htay, N. and Khine, A. (2004) The Modi Taung-Nankwe gold district, Slate Belt, Central Myanmar: mesothermal veins in a Mesozoic orogen. *Journal of Asian Earth Society.*, 23, 321–341.

Phyo, W. Yonezu, K. and Watanabe, K. (2016) Ore-forming conditions of metasedimentary rock-hosted gold mineralization, Phayaung Taung area, Mandalay Region, central Myanmar. *Proceedings of International Symposium on Earth Science and Technology*, 314-319.

Swe, Y.M., Aye, C.C. and Zaw, K. (2017) Gold deposits of Myanmar. In: Barber, A.J., Zaw, K. and Crow, M.J. (Eds.) Myanmar: Geology, Resources, and Tectonics. *Geological Society, London, Memoirs*, 48, 557–572.

Shackleton J.M., Spry P.G. and Bateman R. (2003) Telluride mineralogy of the Golden Mile Deposit, Kalgoorlie, Western Australia. *The Canadian Mineralogist*, 41, 1503-1524